Complete Electroweak $\mathcal{O}(\alpha)$ Corrections to Charged-Current $e^+e^- \to 4$ Fermion Processes

Dissertation
zur
Erlangung der naturwissenschaftlichen Doktorwürde
(Dr. sc. nat.)

vorgelegt der
Mathematisch-naturwissenschaftlichen Fakultät
der
Universität Zürich
von
Lars H. Wieders
aus Deutschland

Promotionskomitee

Prof. Dr. Daniel Wyler	(Vorsitz)
PD. Dr. Ansgar Denner	(Leitung der Dissertation)
Prof. Dr. Thomas Gehrmann	

Zürich 2005

Zusammenfassung

Die vollständigen elektroschwachen $\mathcal{O}(\alpha)$ Korrekturen für Vier-Fermionen-Produktionsprozesse mit geladenen Strömen $e^+e^- \to \nu_\tau\tau^+\mu^-\bar{\nu}_\mu$, $u\bar{d}\mu^-\bar{\nu}_\mu$, und $u\bar{d}s\bar{c}$ wurden berechnet. Die Berechnung wurde mittels algebraischer Reduktion von Spinorketten auf wenige Standardstrukturen und konsistenter Implementierung der W-Boson Breite durchgeführt. Für das letztere wurde ein auf das Einschleifenniveau verallgemeinertes Komplexes-Massen-Schema benutzt, das wir in seiner praktischen Anwendung beschreiben.

Explizite numerische Ergebnisse werden für totale Wirkungsquerschnitte im Energiebereich von der W-Paarproduktionsschwelle bis zu Streuenergien von 2 TeV gegeben. Ein Vergleich mit Vorhersagen, die auf der "Doppelpolapproximation" (DPA) basieren und mit dem Generator RacoonWW erzeugt wurden, macht Korrekturen deutlich, die im Energiebereich 170−300 GeV mit $\lesssim 0.5\%$ über die DPA hinausgehen, was mit früheren Abschätzungen über die intrinsische Genauigkeit der DPA übereinstimmt. Der Unterschied zur DPA wächst auf 1−2% für $\sqrt{s} \sim 1{-}2$ TeV an. An der Schwelle wird die DPA unzuverlässig und die $\mathcal{O}(\alpha)$ Rechnung korrigiert eine verbesserte Bornapproximation (IBA) um etwa 1.6%, was ebenfalls mit einer Fehlerabschätzung der IBA übereinstimmt.

Zum Schluss werden Effekte der vollständigen $\mathcal{O}(\alpha)$ Korrekturen zu differentiellen Wirkungsquerschnitten von physikalischem Interesse besprochen und mit Vorhersagen der DPA verglichen, was zeigt, daß die DPA nicht ausreicht, um das Potential eines zukünftigen Linearbeschleunigers bei der Analyse von W-Bosonpaaren bei hohen Energien auszuschöpfen.

Abstract

The complete electroweak $\mathcal{O}(\alpha)$ corrections have been calculated for the charged-current four-fermion production processes $e^+e^- \to \nu_\tau\tau^+\mu^-\bar{\nu}_\mu$, $u\bar{d}\mu^-\bar{\nu}_\mu$, and $u\bar{d}s\bar{c}$. The calculation is performed by the algebraic reduction of spinor chains to a few standard structures and the consistent implementation of the finite width of the W boson. For the latter, a generalization of the complex-mass scheme to the one-loop level is used, and the practical application of this method is described.

Explicit numerical results are presented for total cross sections in the energy range from the W-pair-production threshold region up to a scattering energy of 2 TeV. A comparison with the predictions based on the "double-pole approximation" (DPA) provided by the generator RacoonWW reveals corrections beyond DPA of $\lesssim 0.5\%$ in the energy range $170-300$ GeV, in agreement with previous estimates for the intrinsic DPA uncertainty. The difference to the DPA increases to $1-2\%$ for $\sqrt{s} \sim 1-2$ TeV. At threshold, where the DPA becomes unreliable, the full $\mathcal{O}(\alpha)$ calculation corrects an improved Born approximation (IBA) by about 1.6%, also consistent with an error estimate of the IBA.

Finally, the effects of the complete $\mathcal{O}(\alpha)$ corrections to various differential cross sections of physical interest are discussed and compared to predictions of the DPA, revealing that the latter approximation is not sufficient to fully exploit the potential of a future linear collider in an analysis of W-boson pairs at high energies.

Contents

Chapter 1

Introduction

1.1 The electroweak Standard Model

Since this thesis is embedded in the context of the electroweak Standard Model (SM, see Refs. [1–3]) we briefly resume its important facts. The SM incorporates all fundamental interactions, except for the gravitation, i.e. the strong, the weak and the electromagnetic forces. For energies that are small compared to the electroweak scale it reproduces quantum electrodynamics (QED). Despite its success, the SM is considered to be only an effective theory, which should be incorporated in a larger model structure. Further experiments will help to decide on possible extensions of the SM and therefore adequate precision calculations are necessary to be able to see deviations from the SM.

From the theoretical point of view the electroweak SM is a non-Abelian locally gauge-invariant theory based on the symmetry group $\mathrm{SU(2)_W} \otimes \mathrm{U(1)_Y}$ with four associated gauge bosons, which are written in their mass eigenstate representation as $W^{\pm}$, Z and γ. Further, the SM is a consistent, renormalizable quantum field theory, as was proven by 't Hooft [4], which allows to calculate unambiguous quantum corrections order by order in perturbation theory.

By introducing in the formally massless gauge theory a scalar field with non-vanishing vacuum expectation value, the so-called Higgs field*, the gauge symmetry of $\mathrm{SU(2)_W} \otimes \mathrm{U(1)_Y}$ is spontaneously broken to the electromagnetic subgroup $\mathrm{U(1)_Q}$. This is known as the Higgs mechanism and satisfies the experimental fact that the $W^{\pm}$ and Z gauge bosons are massive. On the level of the Lagrangian this mechanism introduces mass terms for the Yang-Mills part $\mathcal{L}_{\mathrm{YM}}$.

*The corresponding Higgs particle is the last missing piece of the experimental confirmation for the SM.

The (classical) Lagrangian $\mathcal{L}_{\rm C}$ of the electroweak SM is composed of the Yang-Mills, the Higgs and the fermion part

$$\mathcal{L}_{\rm C} = \mathcal{L}_{\rm YM} + \mathcal{L}_{\rm H} + \mathcal{L}_{\rm F}, \tag{1.1.1}$$

each of them being separately gauge-invariant. The pure gauge-field Lagrangian with the isotriplet W^a_μ, $a = 1, 2, 3$, associated with the generator I^a_W of the weak isospin group $\mathrm{SU(2)_W}$, and the isosinglet B_μ, associated with the weak hypercharge $Y_{\rm W}$ of the group $U(1)$, reads

$$\mathcal{L}_{\rm YM} = -\frac{1}{4}\Big(\partial_\mu W^a_\nu - \partial_\nu W^a_\mu + g_2\epsilon^{abc}W^b_\mu W^c_\nu\Big)^2 - \frac{1}{4}\Big(\partial_\mu B_\nu - \partial_\nu B_\mu\Big)^2, \tag{1.1.2}$$

where ϵ^{abc} are the totally antisymmetric structure constants of SU(2). The Higgs part of the Lagrangian $\mathcal{L}_{\rm C}$ has the form

$$\mathcal{L}_{\rm H} = \Big(D_\mu\Phi^\dagger\Big)\Big(D^\mu\Phi\Big) - V(\Phi)\,, \tag{1.1.3}$$

with the Higgs potential

$$V(\Phi) = \frac{\lambda}{4}\Big(\Phi^\dagger\Phi\Big)^2 - \mu^2\Phi^\dagger\Phi\,, \tag{1.1.4}$$

with the parameters λ and μ[†], the Higgs field Φ and the covariant derivative

$$D_\mu = \partial_\mu - \mathrm{i}g_2 I^a_W W^a_\mu + \mathrm{i}\frac{1}{2}g_1 Y_W B_\mu. \tag{1.1.5}$$

The gauge couplings are denoted as $g_{1,2}$. The fermionic part of the Lagrangian $\mathcal{L}_{\rm C}$ reads

$$\begin{aligned}\mathcal{L}_{\rm F} = &\sum_i \Big(\mathrm{i}\bar{L'}^L_i\gamma^\mu D_\mu L'^L_i + \mathrm{i}\bar{Q'}^L_i\gamma^\mu D_\mu Q'^L_i\Big)\\ &+\sum_i \Big(\mathrm{i}\bar{l'}^R_i\gamma^\mu D_\mu l'^R_i + \mathrm{i}\bar{u'}^R_i\gamma^\mu D_\mu u'^R_i + \mathrm{i}\bar{d'}^R_i\gamma^\mu D_\mu d'^R_i\Big)\\ &-\sum_{i,j}\Big(\bar{L'}^L_i G^l_{ij} l'^R_i\Phi + \bar{Q'}^L_i G^u_{ij} u'^R_i\tilde{\Phi} + \bar{Q'}^L_i G^d_{ij} d'^R_i\Phi + h.c.\Big)\,,\end{aligned} \tag{1.1.6}$$

where the left-handed fermions of each lepton (L) and quark (Q) generation are grouped into $\mathrm{SU(2)_W}$ doublets (the colour index is suppressed)

$$L'^L_i = \omega_- L'_i = \begin{pmatrix}\nu'^L_i\\ l'^L_i\end{pmatrix}, \quad Q'^L_i = \omega_- Q'_i = \begin{pmatrix}u'^L_i\\ d'^L_i\end{pmatrix}, \tag{1.1.7}$$

[†]The Higgs potential is constructed in such a way that it gives rise to spontaneous symmetry breaking. This means that the parameters λ and μ are chosen such that the potential $V(\Phi)$ takes its minimum for a non-vanishing Higgs field, i.e. the vacuum expectation value $\langle\Phi\rangle$ of the Higgs field is nonzero.

and the right-handed fermions into singlets

$$l_i'^R = \omega_+ l_i', \quad u_i'^R = \omega_+ u_i', \quad d_i'^R = \omega_+ d_i', \tag{1.1.8}$$

where $\omega_\pm$ is the projector on right- and left-handed fields, respectively, i is the generation index and ν, l, u and d stand for neutrinos, charged leptons, up-type quarks and down-type quarks, respectively. Further, $G_{ij}^{l,u,d}$ are the Yukawa coupling matrices and $\tilde{\Phi}$ is the charge conjugated Higgs field. The fermion masses are generated through spontaneous symmetry breaking from the Yukawa couplings. The diagonalization of the fermion mass matrices introduces a quark mixing in the coupling to the $W^\pm$ and Z bosons, given in the elements of the Cabbibo-Kobayashi-Maskawa (CKM) matrix.

The quantized Lagrangian of the electroweak SM carries gauge fixing terms $\mathcal{L}_{\text{fix}}$ and involves unphysical components of the gauge-fields, which are compensated by introducing a Faddeev-Popov ghost Lagrangian $\mathcal{L}_{\text{FP}}$. These additional terms destroy the former gauge symmetry in order to eliminate unphysical bosonic degrees of freedom, but the effective Lagrangian is still invariant under so called BRS transformations and fulfills Slavnov-Taylor identities, which have to be satisfied in consistent perturbative calculations. The complete renormalizable Lagrangian for the electroweak SM reads therefore

$$\mathcal{L}_{\text{SM}} = \mathcal{L}_{\text{C}} + \mathcal{L}_{\text{fix}} + \mathcal{L}_{\text{FP}}. \tag{1.1.9}$$

The explicit representation of the SM Lagrangian is given in Ref. [52]. The SM is in agreement with all experimental results of electroweak phenomena.[‡]

1.2 W-pair production

W-pair production is an important process for testing the SM. On the one hand, it allows to measure precisely the mass of the W boson, a fundamental parameter of the SM. On the other hand, it is sensitive to the triple non-abelian gauge couplings (γW^+W^-, ZW^+W^-, see (1.1.2)), and, in particular at high energies, allows to test the non-abelian structure of the SM accurately, owing to the delicate gauge cancellations in its lowest-order matrix elements.

1.3 Experimental precision at LEP and a future ILC

Experimentally, W-pair production has been studied intensively at LEP2 with quite high precision [5]. The total cross section was measured from threshold up to a centre-of-mass (CM) energy of 207 GeV leading to a combined

[‡]Right-handed neutrinos could be easily added to the SM, in order to agree with recent experimental results which give evidence for massive neutrinos indicated by neutrino oscillations.

experimental accuracy of $\sim 1\%$. While the W-boson mass M_{W} was determined from the threshold cross section with an error of $\sim 200\,\mathrm{MeV}$ and by reconstructing the W bosons from their decay products within $\sim 40\,\mathrm{MeV}$, deviations from the SM triple gauge-boson couplings, usually quantified in the parameters Δg_1^Z, $\Delta\kappa_\gamma$, and λ_γ, were constrained within a few per cent.

More precise experimental investigations of W-pair production will be possible at a future International $\mathrm{e^+e^-}$ Linear Collider (ILC) [6–8]. Owing to the high luminosity of such a collider, the accuracy of the cross section measurement will be at the per-mille level, and the precision of the W-mass determination is expected to be $\sim 10\,\mathrm{MeV}$ [9] by direct reconstruction and $\sim 7\,\mathrm{MeV}$ from a threshold scan of the total W-pair-production cross section [6,7].

1.4 Developments in the calculation of W-pair production

Because of its theoretical importance, W-pair production found early interest. The lowest-order amplitudes for on-shell W-pair production were already considered at the end of the 1970's [10]. The electroweak corrections to on-shell W-pair production have been calculated by four different groups [11,12] shortly after and supplemented by hard photon radiation [13]. Already at that time, these calculations were at the forefront of the technical developments in higher-order calculations. Later, the structure of these corrections has been investigated by constructing improved Born approximations [14] and high-energy approximations [15]. With the advent of LEP2 it became quickly clear that the decays of the W bosons into fermion pairs had to be included. The electroweak corrections to the on-shell W-boson decay were given in Ref. [16]. Different types of programs (ranging from semianalytical codes to Monte Carlo generators) for lowest-order predictions for $\mathrm{e^+e^-} \to 4f$ were developed [17] (see also Refs. [18–20] and references therein) and subsequently supplemented by universal corrections thus reaching an accuracy of about 2%. The universal corrections included running couplings, leading-logarithmic corrections from initial-state radiation (ISR), and also the effects of the Coulomb singularity for off-shell W-pair production [21]. These corrections can be combined with the lowest-order matrix elements easily. The remaining corrections are called non-universal, since they depend on the process under investigation. Since the accuracy of 2% was not sufficient for LEP2, the $\mathcal{O}(\alpha)$ corrections to $\mathrm{e^+e^-} \to \mathrm{WW} \to 4f$ were calculated in the double-pole approximation (DPA), where only the leading terms in an expansion about the resonance poles of the two W-boson propagators were taken into account [22,23,25,27,28]. These corrections were implemented into the event generators YFSWW [23] and RacoonWW [25,27,29].

In the DPA approach, the W-pair cross section can be predicted within $\sim 0.5\%$ (0.7%) in the energy range between 180 GeV (170 GeV) and ~ 500 GeV, which was sufficient for the LEP2 accuracy of $\sim 1\%$ for energies 170−207 GeV. In the threshold region ($\sqrt{s} \lesssim 170$ GeV) where singly- or non-resonant contributions become important, the DPA is not reliable, and the best available prediction results from an improved Born approximation (IBA) based on leading universal corrections only, and thus possesses an intrinsic uncertainty of $\sim 2\%$. At energies above 500 GeV effects beyond $\mathcal{O}(\alpha)$, such as Sudakov logarithms at higher orders, become important and should be included in predictions at per-cent accuracy.

The theoretical uncertainty (TU) for the direct mass reconstruction at LEP2 is estimated to be of the order of ~ 5 MeV to $\lesssim 10$ MeV [30], based on results of YFSWW and RacoonWW; thus theoretical improvements are desirable for an ILC. For the cross-section prediction at threshold the TU is only $\sim 2\%$, because it is based on an IBA, and thus is definitely insufficient for the planned precision measurement of M_{W} in a threshold scan. The main sensitivity of all observables to anomalous couplings in the triple gauge-boson vertices is provided by the W-pair production angle distribution. The TU in constraining the parameter λ_γ was estimated to be ~ 0.005 [31] for the LEP2 analysis.

Since the higher energy at a future ILC will improve the sensitive to (anomalous) gauge-boson couplings more than an order of magnitude compared to LEP2, a further reduction of the uncertainties resulting from missing radiative corrections is necessary. In summary, these considerations demonstrate the necessity of a full one-loop calculation for the $\mathrm{e^+e^-} \to 4f$ process and of further improvements by leading higher-order corrections.

1.5 Improvements in the calculation beyond DPA

In view of the improved precision of the ILC, a further reduction of the uncertainties from missing radiative corrections is necessary. This requires, in particular, the calculation of the full one-loop corrections for W-pair-mediated $\mathrm{e^+e^-} \to 4f$ processes. Such a calculation poses a number of theoretical challenges.[§] Neglecting diagrams involving couplings of Higgs bosons to light fermions, which are proportional to the fermion masses, already for the simplest final states $\mathrm{e^+e^-} \to \nu_\tau\tau^+\mu^-\bar{\nu}_\mu$, $\mathrm{u\bar{d}}\mu^-\bar{\nu}_\mu$, and $\mathrm{u\bar{d}s\bar{c}}$ about 1200 Feynman

[§]Some of the problems appearing in a first attempt of such a calculation were already described in Ref. [32]. Recently the authors of the GRACE/1-LOOP system reported on progress towards a full one-loop calculation for $\mathrm{e^+e^-} \to \mu^-\bar{\nu}_\mu\mathrm{u\bar{d}}$ in Ref. [43] so that one can expect that the system will be able to deal with $\mathrm{e^+e^-} \to 4f$ processes at one loop in the near future.

diagrams contribute (counting the contributions of the three fermion generations in the loops only once), and for the most complicated final state $\nu_e e^+ e^- \bar{\nu}_e$, there are about 6000 diagrams. The large number and the complexity of the diagrams require developping improved reduction algorithms, in order to keep the expressions manageable and to produce an efficient and numerically stable computer code.

Because of the complicated multi-particle final state, the loop integrals appearing, in general cannot be evaluated with standard methods. Using the Passarino–Veltman reduction to calculate the tensor integrals leads to serious numerical problems when the Gram determinants that appear in the denominators become small. This usually happens near the boundary of phase space but can also occur within phase space because of the indefinite Minkowski metric. Thus, in order to obtain numerically stable results, one has to devise and implement alternative methods for the calculation of the tensor integrals, at least, in the critical regions.

The inclusion of the finite gauge-boson decay width constitutes a further important problem in the calculation of radiative corrections to W-pair-mediated four-fermion production. An appropriate description of resonances in perturbation theory requires a Dyson summation of self-energy insertions in the resonant propagators, in order to introduce the imaginary part provided by the finite decay width into the propagator denominators. It is well known that this procedure in general violates gauge invariance, i.e. destroys Slavnov–Taylor and Ward identities and disturbs the cancellation of gauge-parameter dependences, because different perturbative orders are mixed [33,34]. Several solutions have been described for lowest-order predictions. The early attempts have been summarized in Ref. [35], and some of the schemes have been compared in Ref. [36]. More recent approaches include the "pole-scheme" [37,38], the "fermion-loop scheme" [34,36,39,40], the use of effective Lagrangians [41,42][¶], and the "complex-mass scheme" (CMS) [29]. Apart from the pole expansions, none of these approaches has been elaborated beyond tree level so far. The pole scheme provides a gauge-invariant answer in terms of an expansion about the resonance, but is only applicable sufficiently far above the W-pair threshold. However, in the full calculation we need a unified description that is valid everywhere in phase space, without any matching between different treatments for different regions. Some problems related to the finite width appearing in a calculation of radiative corrections to $e^+e^- \to \mu^-\bar{\nu}_\mu u\bar{d}$ are illustrated in Ref. [43]. Here we solve these problems by using a generalization of the CMS,

[¶]The recently proposed approach [42] to describe unstable particles within an effective field theory is equivalent to a pole expansion.

which was introduced in Ref. [29] for lowest-order calculations, to the one-loop level.

1.6 The topics of the thesis

We present the results of a complete $\mathcal{O}(\alpha)$ calculation (improved by higher-order ISR) for the $4f$ final states $\nu_\tau\tau^+\mu^-\bar{\nu}_\mu$, $u\bar{d}\mu^-\bar{\nu}_\mu$, and $u\bar{d}s\bar{c}$, which are relevant for W-pair production.[‖] We provide numerical results for total cross sections without cuts and various differential cross sections of physical interest.

Technically the occurring one-loop tensor integrals comprise 5- and 6-point functions up to rank 3, and conceptually the W-boson resonances require a treatment in loop diagrams that preserves gauge invariance. We present details of our solutions to the above-mentioned problems. We discuss, in particular, our method for the algebraic reduction of the one-loop amplitude and describe the use of the CMS at the one-loop level.

In Section 2 we fix our conventions and sketch the general strategy of our calculation. Our method for the reduction of spinor chains to a few standard structures are described in Section 3. Section 4 is devoted to the description of the complex-mass scheme for loop calculations with complex masses. In Section 5, we present explicit numerical results on total cross sections without phase-space cuts for scattering energies from near the W-pair-production threshold up to 2 TeV, where we paid particular attention to a comparison with the DPA and IBA approaches used at LEP2, and we discuss corrections for various distributions of physical interest. We note that Sections 3, 4, and 5 can be read independently. Section 6 contains our conclusions.

The results of this thesis are based on a collaboration with S. Dittmaier and M. Roth from the Max-Plank-Institut for Physics in Munich, and are published in Refs. [44,45].[**] Within our group, two completely independent calculations have been performed, one calculation implemented by A. Denner and L. H. Wieders and the other implemented by our collaborators S. Dittmaier and M. Roth. All algebraic manipulations, including the generation of Feynman diagrams, the simplification of amplitudes and the reduction of spinor structures to standard forms, have been implemented by L. H. Wieders and S. Dittmaier independently, resulting in two self-contained programs. The evaluations of all scalar and tensor loop integrals are based on two independent

[‖] Electrons and/or positrons in the final state are not yet considered; they deserve further refinements, in particular the inclusion of finite-electron-mass effects in the domain of forward-scattered $e^\pm$. We also do not yet include final states that can also be produced via two resonant Z bosons, so called mixed CC/NC reactions. These can be taken into account in lowest order in RacoonWW.

[**] In this thesis, these publications are not always referred to in particular.

in-house libraries, one done by A. Denner and the other done by S. Dittmaier and M. Roth.

Chapter 2

Strategy of the calculation

The goal of this work is the calculation of the complete electroweak $\mathcal{O}(\alpha)$ corrections to charged-current $e^+e^- \to 4\,f$ processes. The actual calculation builds upon the RacoonWW approach [25,27], where real-photonic corrections are based on full matrix elements and virtual corrections are treated in DPA. Real and virtual corrections are combined either using two-cutoff phase-space slicing or employing the dipole subtraction method as formulated in Ref. [46] for photon radiation. We also include leading-logarithmic initial-state radiation (ISR) beyond $\mathcal{O}(\alpha)$ in the structure-function approach (see Ref. [18] and references therein). The presented calculation differs from RacoonWW in the treatment of the (IR and collinear finite part of the) virtual corrections. Therefore, we only describe the calculation of the complete $\mathcal{O}(\alpha)$ virtual corrections in the following. We neglect the masses of the fermions whenever possible, i.e. everywhere but in the mass-singular logarithms, and set the quark-mixing matrix to the unit matrix.*

2.1 Notation and conventions

We consider the process

$$\begin{aligned} e^+(p_+,\sigma_+) + e^-(p_-,\sigma_-) \;\to\; & f_1(k_1,\sigma_1) + \bar{f}_2(k_2,\sigma_2) \\ & + f_3(k_3,\sigma_3) + \bar{f}_4(k_4,\sigma_4). \end{aligned} \tag{2.1.1}$$

The arguments label the momenta $p_\pm$, k_i $(i = 1,2,3,4)$ and helicities $\sigma_\pm$, $\sigma_i = \pm 1/2$ of the corresponding particles. We often use only the signs to

*Neglecting the masses of the external fermions at the scale of the considered processes, introduces an error of the order of magnitude of m_f^2/M_W^2 in the Born and of $\frac{\alpha}{\pi} m_f^2/M_W^2 \log(m_f/M_W)^2$ at one-loop, which is beyond the aimed precision of this calculation at the per-mille level. In this case and the sum over the quark-mixing final states, the CKM matrix factorizes to the amplitude because of unitarity.

denote the helicities. The particle momenta obey the mass-shell conditions $p_\pm^2 = m_\mathrm{e}^2$ and $k_i^2 = m_i^2$. The masses of the external fermions are neglected whenever possible, i.e. everywhere but in the mass-singular logarithms. For later use, the following set of kinematical invariants is defined:

$$\begin{aligned} s &= (p_1 + p_2)^2, & s_{ij} &= (k_i + k_j)^2, \\ t_{\pm i} &= (p_\pm - k_i)^2, & i,j &= 1,2,3,4. \end{aligned} \tag{2.1.2}$$

In this paper we consider only final states where f_1 and f_3 are different fermions excluding electrons and electron neutrinos; f_2 and f_4 are their isospin partners, respectively. This corresponds to the CC11 family in the classification of Ref. [19]. It represents the gauge-invariant subclass of general $\mathrm{e}^+\mathrm{e}^- \to 4f$ processes that includes all diagrams with pairs of potentially resonant W bosons. In this class, the lowest-order and one-loop amplitudes vanish unless $\sigma = \sigma_- = -\sigma_+$, $\sigma_1 = -\sigma_2$, and $\sigma_3 = -\sigma_4$. Moreover, the helicities of the outgoing fermions are fixed, $\sigma_{1,3} = -\sigma_{2,4} = -1/2$, owing to the left-handed coupling of the W bosons. In general this does not hold for other $\mathrm{e}^+\mathrm{e}^- \to 4f$ final states and diagrams. We set the quark-mixing matrix to the unit matrix, but in the limit of small masses for the external fermions a non-trivial quark-mixing matrix can be easily taken into account by rescaling the cross sections for definite flavours accordingly.

The lowest-order cross section reads

$$\sigma_0 = \frac{1}{2s} \int \mathrm{d}\Phi_4 \sum_{\sigma=\pm\frac{1}{2}} \frac{1}{4}(1+2P_-\sigma)(1-2P_+\sigma)\,|\mathcal{M}_0^{\sigma--}|^2. \tag{2.1.3}$$

Here $\mathcal{M}_0^{\sigma\sigma_1\sigma_3}$ denotes the lowest-order matrix element, $P_\pm$ the polarization degrees of the $\mathrm{e}^\pm$ beams, and $\mathrm{d}\Phi_4$ the 4-particle phase-space volume element

$$\mathrm{d}\Phi_4 = \left(\prod_{i=1}^{4} \frac{\mathrm{d}^3\mathbf{k}_i}{(2\pi)^3 2k_i^0}\right) (2\pi)^4 \delta\left(p_+ + p_- - \sum_{j=1}^{4} k_j\right). \tag{2.1.4}$$

2.2 Survey of one-loop diagrams

The virtual corrections receive contributions from self-energy, vertex, box, pentagon, and hexagon diagrams. In this section, we survey the diagrams contributing to the massless charged-current processes $\mathrm{e}^+\mathrm{e}^- \to f_1\bar{f}_2 f_3 \bar{f}_4$, where f_1 and f_3 are different fermions, excluding electrons and electron neutrinos, and f_2 and f_4 their respective isospin partners.

The contributions from self-energy and vertex corrections are obtained by inserting self-energies and vertex corrections in all propagators and vertices of the tree-level diagrams shown in Figure 2.1. When inserting a self-energy in

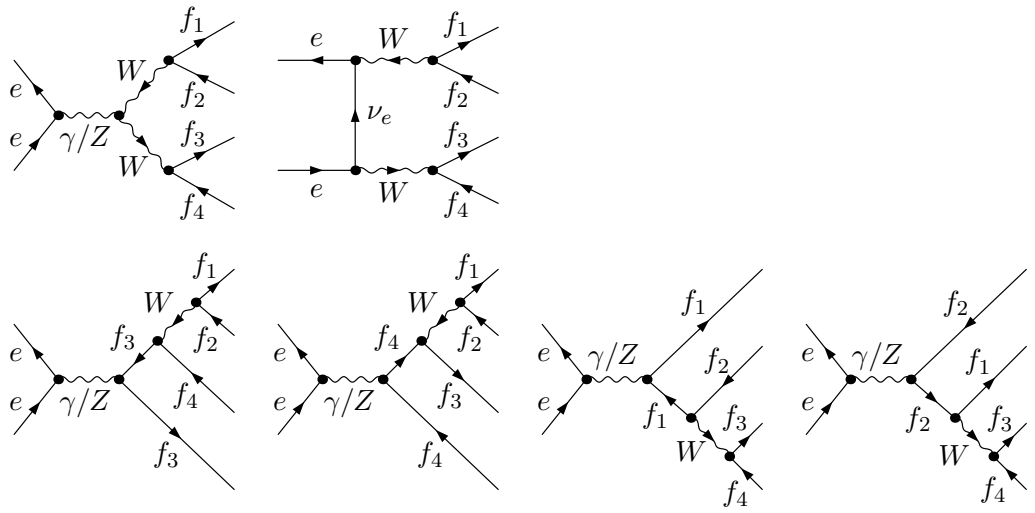

Figure 2.1: Lowest-order diagrams for $e^+e^- \to f_1\bar{f}_2 f_3\bar{f}_4$

a γ/Z line one obtains $\gamma\gamma$ and ZZ self-energies as well as γZ and $Z\gamma$ mixing-energies. Since we neglect the masses of the external fermions, all diagrams that involve Higgs-boson couplings to these fermions obviously vanish. Nevertheless there remain diagrams containing contributions to the $H\gamma$, HZ, and ϕW mixing energies and to the Hee and ϕff vertices with on-shell fermions, where ϕ denotes the would-be Goldstone boson corresponding to the W boson. One can easily verify that these contributions also vanish in the limit of vanishing masses for the external fermions.

The diagrams for the appearing $ee\gamma$, eeZ, $e\nu_e W$, γWW, and ZWW vertex functions are listed in Ref. [12], where the process $e^+e^- \to W^+W^-$ was treated at one loop. The diagrams for the other $\gamma f\bar{f}$, $Zf\bar{f}$, $Wf\bar{f}'$ vertex functions are simply obtained from the latter by obvious substitutions and adding some diagrams with internal Z bosons replaced by photons, which are absent for the $e\nu_e W$ vertex because of the vanishing charge of the neutrino. The diagrams for the gauge-boson and fermion self-energies can be found in Ref. [47]. For all these vertex functions, the corresponding counterterm diagrams must be included.

The generic contributions of the different vertex functions with more than three external legs are shown in Figure 2.2. These are all ultraviolet (UV) finite. There are 40 hexagon diagrams, 112 pentagon diagrams, and 227 (220) box diagrams in the conventional 't Hooft–Feynman gauge (background-field gauge [48]). A set of hexagon diagrams is shown in Figure 2.3 and one set

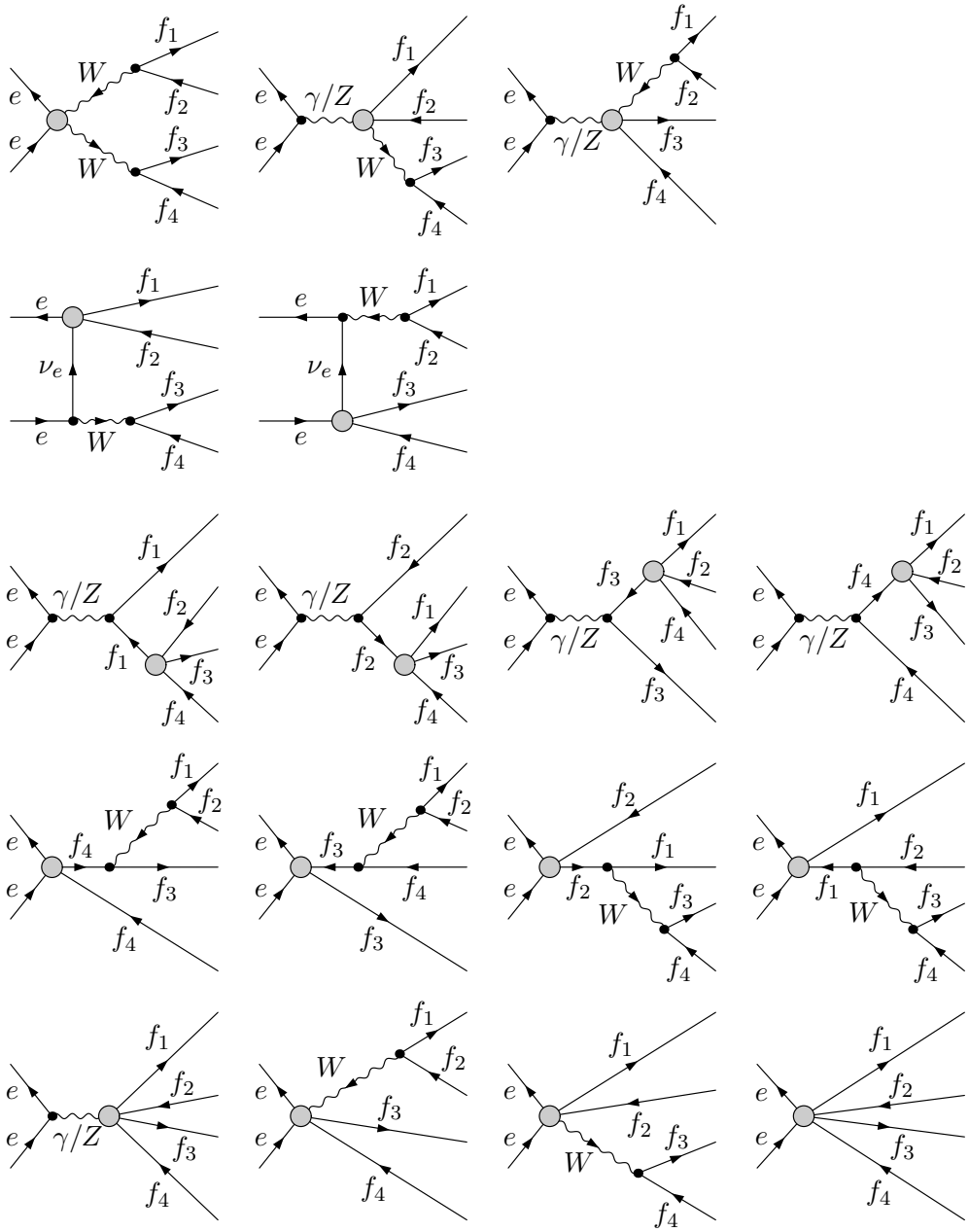

Figure 2.2: Contributions of vertex functions with at least four external legs to $e^+e^- \to f_1\bar{f}_2 f_3\bar{f}_4$

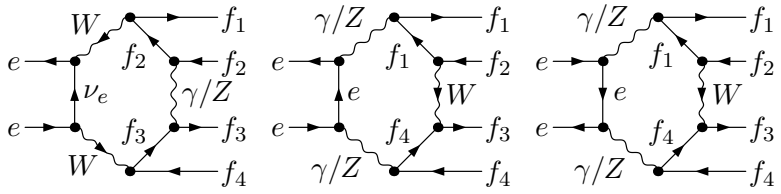

Figure 2.3: Ten hexagon diagrams for $e^+e^- \to f_1\bar{f}_2f_3\bar{f}_4$. The remaining 30 hexagon diagrams are obtained by reversing the fermion flow in one or both of the fermion lines of the outgoing fermions and by exchanging $f_1 \leftrightarrow f_2$ and/or $f_3 \leftrightarrow f_4$.

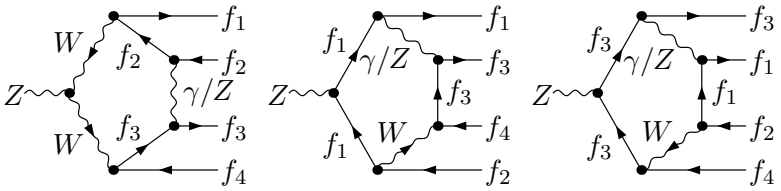

Figure 2.4: Six pentagon diagrams contributing to the $Zf_1f_2f_3f_4$ vertex function. The remaining 18 diagrams are obtained by reversing the fermion flow in one or both of the fermion lines of the outgoing fermions and by exchanging $f_1 \leftrightarrow f_2$ and/or $f_3 \leftrightarrow f_4$.

of pentagon diagrams for the $Zf_1f_2f_3f_4$ vertex function in Figure 2.4. In both cases there are three further sets of diagrams that are obtained by reversing the fermion flow in one or both of the fermion lines of the outgoing fermions and by exchanging $f_1 \leftrightarrow f_2$ and/or $f_3 \leftrightarrow f_4$. Those for the $\gamma f_1f_2f_3f_4$ vertex function are simply obtained by replacing the external Z boson by a photon in the diagrams for the $Zf_1f_2f_3f_4$ vertex function. A set of diagrams for the eef_1f_2W vertex function is listed in Figure 2.5 and a further set is obtained from those by reversing the fermion flow in the fermion chain of the outgoing fermions and by exchanging $f_1 \leftrightarrow f_2$. The diagrams for the eef_3f_4W vertex function can be obtained from the latter by obvious substitutions. The box diagrams of the ZWf_1f_2 vertex function are depicted in Figure 2.6 and those for the ZWf_3f_4 vertex can again be obtained from those. The diagrams for the γWf_1f_2 and γWf_3f_4 boxes are obtained by replacing the external Z boson by a photon and omitting the diagrams with internal H lines. The diagrams for

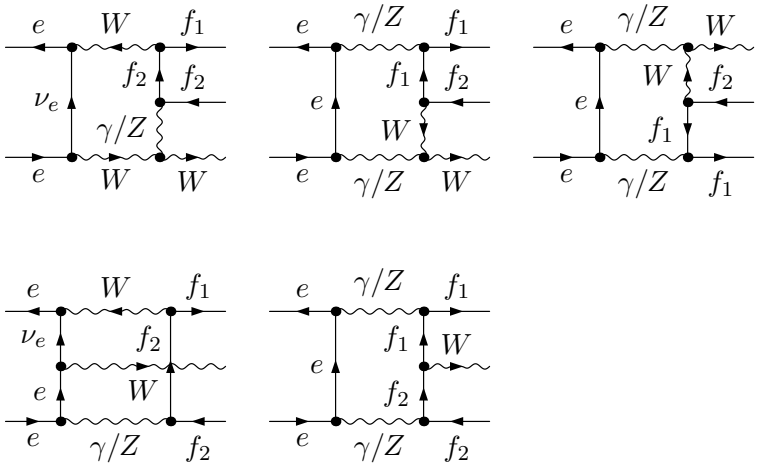

Figure 2.5: A set of 16 diagrams contributing to the $ee f_1 f_2 W$ vertex function. The remaining 16 diagrams contributing to this vertex function are obtained from those by reversing the fermion flow in the fermion line of the outgoing fermions and by exchanging $f_1 \leftrightarrow f_2$.

the $eeWW$, $f_1 f_2 f_3 f_4$, and $ee f_1 f_1$ boxes are compiled in Figures 2.7, 2.8, and 2.9. The $e\nu_e f_1 f_2$ and $e\nu_e f_3 f_4$ box functions are special cases of the $f_1 f_2 f_3 f_4$ box function.

2.3 Calculational framework

The amplitudes of our calculation are generated with FeynArts version 3, as described in Ref. [50]. The algebraic manipulations are performed, using in-house programs implemented in Mathematica which build upon FormCalc [51]. Since FormCalc is by no means sufficient to obtain results for the processes under consideration, many improvements have been necessary. This includes the construction and simplification of the spinor structures, the algebraic simplification of the Feynman diagrams, the incorporation of six-point functions, and the implementation of a complex renormalization scheme.

By structuring the output of FormCalc and introducing suitable abbreviations we could reduce the size of the algebraic expression drastically for the tree and one-loop amplitudes. By systematically avoiding multiple calculation of the same building blocks such as tensor integrals or in algebraic expressions, we speeded up our programs considerably. In addition, we extended FormCalc to include 6-point functions up to tensor rank 3 and implemented extra

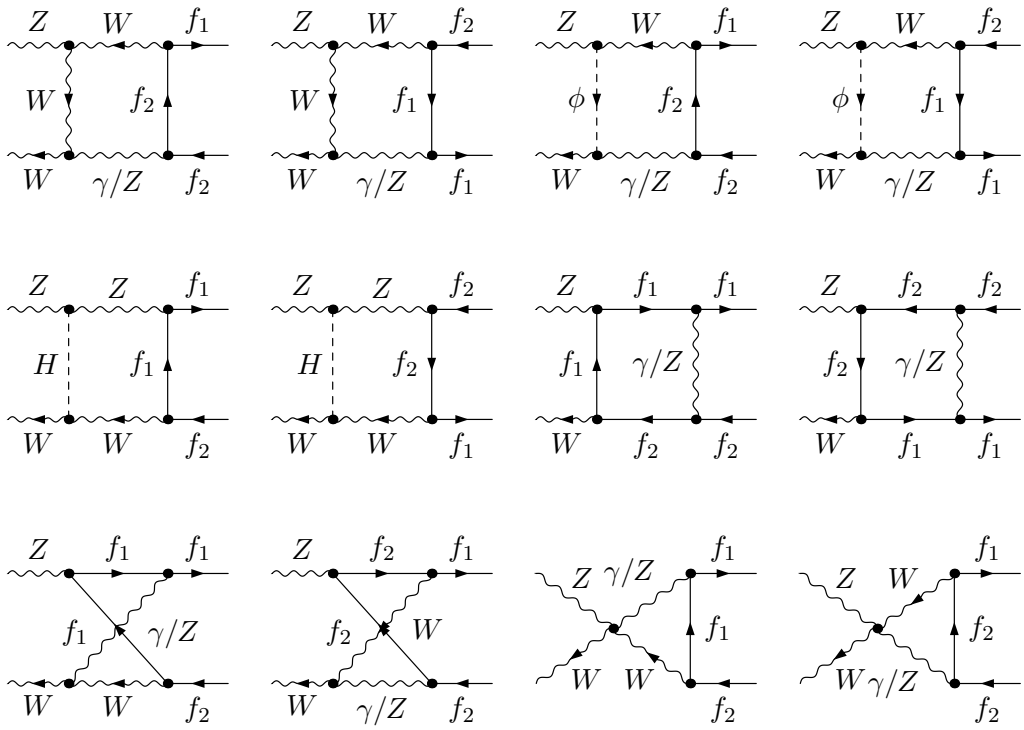

Figure 2.6: Diagrams contributing to the ZWf_1f_2 vertex function

generic fermions into the model file of FeynArts. This allows us to calculate the algebraic amplitudes for different processes generically.

All contributions to the matrix elements involve three spinor chains, corresponding to the three different fermion–antifermion pairs, which are contracted with each other and with four-momenta in many different ways. There are $\mathcal{O}(10^3)$ different spinor structures to calculate for $e^+e^- \to f_1\bar{f}_2f_3\bar{f}_4$ so that an algebraic reduction to a standard form which involves only very few standard chains is desirable. We have worked out an algorithm that reduces all occurring spinor chains to two standard structures for the considered processes, the standard matrix elements (SMEs), without introducing coefficients that lead to numerical problems. This algorithm is described in Section 3.

It is convenient to separate the matrix elements into invariant coefficient functions F_n, containing the loop integrals, and SMEs $\hat{\mathcal{M}}_n$, containing all

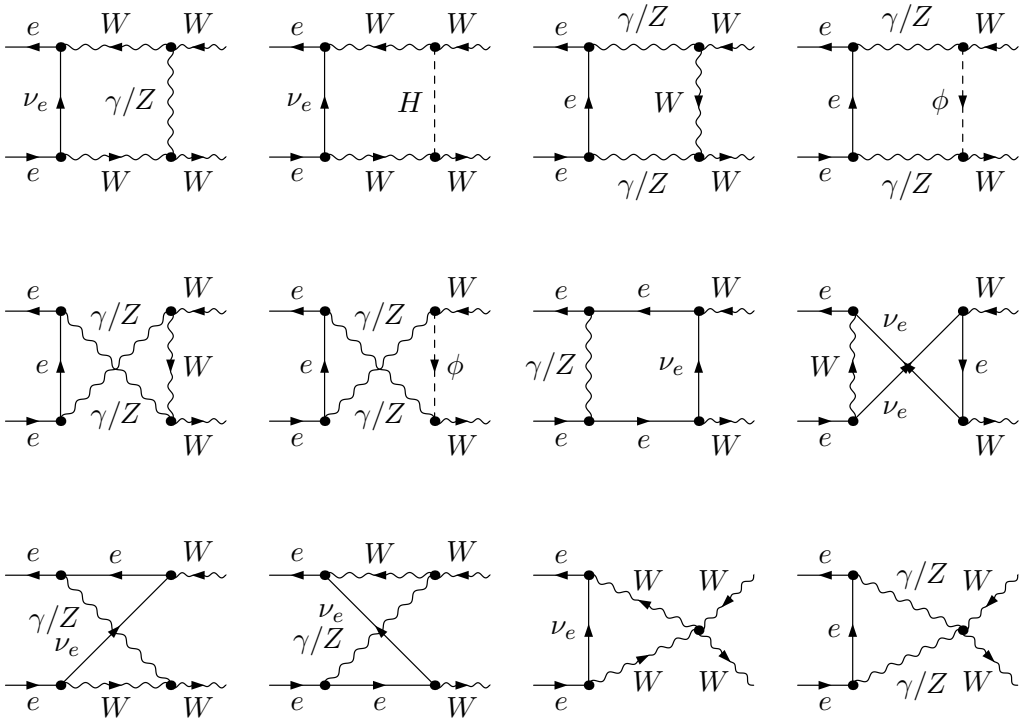

Figure 2.7: Diagrams contributing to the $eeWW$ vertex function

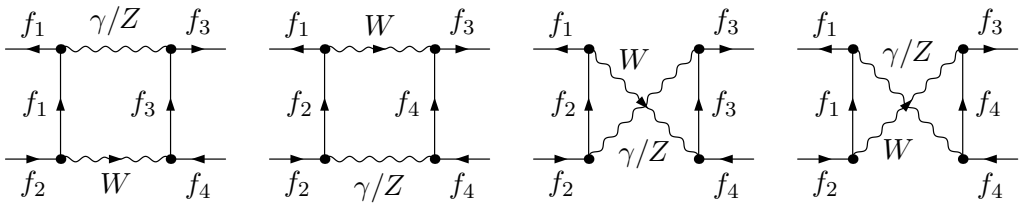

Figure 2.8: Diagrams contributing to the $f_1 f_2 f_3 f_4$ vertex function

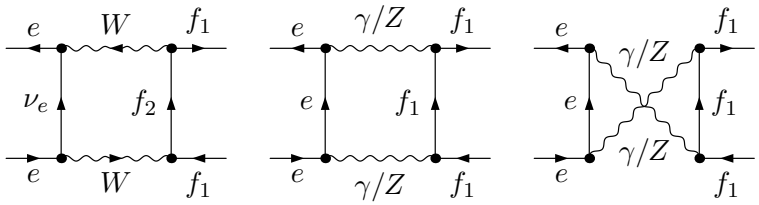

Figure 2.9: Diagrams contributing to the eef_1f_1 vertex function

spinorial objects and the dependence on the helicities of the external particles [52]. After the reduction of the spinor structures, the amplitudes take the form

$$\mathcal{M}^{\sigma\sigma_1\sigma_3} = \sum_n F_n^{\sigma\sigma_1\sigma_3}(\{s, s_{ij}, t_{\pm i}\})\hat{\mathcal{M}}_n^{\sigma\sigma_1\sigma_3}(p_+, p_-, k_1, k_2, k_3, k_4). \tag{2.3.1}$$

The invariant functions F_n are linear combinations of one-loop integrals with coefficients that depend on scalar kinematical variables, particle masses, and coupling factors.

The calculation of the virtual corrections has been repeated by our collaborators S. Dittmaier and M. Roth also using the background-field method [48], where the individual contributions from self-energy, vertex, box, and pentagon corrections differ from their counterparts in the conventional formalism, apart from those that involve only fermion–gauge-boson couplings in the loops. The total one-loop corrections of the conventional and of the background-field approach were found to be in numerical agreement.

The contribution of the virtual corrections to the cross section is given by

$$\delta\sigma_{\text{virt}} = \frac{1}{2s}\int \mathrm{d}\Phi_4 \sum_{\sigma=\pm\frac{1}{2}} \frac{1}{4}(1+2P_-\sigma)(1-2P_+\sigma)\, 2\,\mathrm{Re}\left\{\mathcal{M}_1^{\sigma--}\left(\mathcal{M}_0^{\sigma--}\right)^*\right\}, \tag{2.3.2}$$

where $\mathcal{M}_1^{\sigma\sigma_1\sigma_3}$ denotes the one-loop contributions to the helicity amplitudes.

2.4 Calculation of loop integrals

For the calculation of the loop integrals we use an improved version of the standard approach. All coefficient integrals are algebraically reduced to a set of master integrals. The reduction formulas are implemented into Fortran codes, and the reduction is performed numerically. Finally, the master integrals are either calculated from explicit formulas or from numerical integration as explained below.

Let us first describe our standard approach that we use as long as it yields numerically stable results. The 6-point integrals are directly expressed in terms of six 5-point functions, as described in Refs. [52,53]. The 5-point integrals are written in terms of five 4-point functions following the method of Ref. [54]. The 3-point and 4-point tensor integrals are algebraically reduced to the (standard) scalar 1-point, 2-point, 3-point, and 4-point functions, which are the master integrals, with the Passarino–Veltman algorithm [55]. Finally, the remaining scalar integrals are evaluated based on generalizations of the methods and results of Refs. [56–58]. Ultraviolet divergences are regulated dimensionally and IR divergences with an infinitesimal photon mass[†] m_γ.

The standard approach leads to serious numerical problems when the Gram determinants, which appear in the denominator of the Passarino–Veltman reduction, become small. This happens usually near the boundary of phase space but also occurs within phase space because of the indefinite Minkowski metric. Since we use Passarino–Veltman reduction only for 3-point and 4-point functions, the dangerous Gram determinants are those involving two or three momenta. Our reduction of 5- and 6-point functions, on the other hand, does not involve inverse Gram determinants composed of external momenta, which naturally occur in the Passarino–Veltman reduction [55] of tensor to scalar integrals. Instead, it involves so-called (modified) Cayley determinants, the zeroes of which are related to the Landau singularities of the (sub-)diagrams. We did not encounter numerical problems with these determinants. For the 2-point tensor coefficients numerically stable explicit results exist for arbitrary momenta [55].

For the regions where the Gram determinants become small, we have worked out two alternative calculational methods. The basic strategy of the first method, implemented by A. Denner, makes use of expansions of the tensor coefficients about the limit of vanishing Gram determinants. Using this, again all tensor coefficients can be expressed in terms of the standard scalar 1-point, 2-point, 3-point, and 4-point functions. In the second, alternative method, implemented by S. Dittmaier, a specific tensor coefficient is evaluated, the integrand of which is logarithmic in Feynman parametrization, by numerical integration. Then the remaining coefficients as well as the standard scalar integral (numerator equal to one) are algebraically derived from this coefficient. This reduction again involves only inverse Cayley determinants, but no inverse Gram determinants. In this approach, the set of master integrals is not given by the standard scalar integrals anymore. For some specific 3-point integrals,

[†]At one loop the photon-mass regularization is equivalent to dimensional regularization ($D = 4 - 2\varepsilon$) with reference mass μ via the correspondence $\ln(m_\gamma^2) \leftrightarrow 1/\varepsilon + \ln(4\pi\mu^2) - \gamma_{\mathrm{E}}$ as long as collinear singularities are regularized with fermion masses.

where the Cayley determinant vanishes exactly, analytical results have been worked out that allow for a stable numerical evaluation.

2.5 Checks on the calculation

In order to prove the reliability of our results, we have performed a number of checks.

- *UV finiteness* is checked by verifying the independence of the (arbitrary) reference scale μ of dimensional regularization.

- *IR finiteness* is checked by varying the logarithm $\ln \lambda$ of the (formally infinitesimal) photon mass λ, which leaves the sum of the virtual and the soft-photonic corrections (slicing approach) or of the virtual and endpoint contributions (i.e. the singular parts that are subtracted from the virtual corrections in the subtraction approach) invariant.

- *Mass singularities* related to collinear photon emission or exchange are checked by verifying the independence of the sum of the virtual corrections and the subtraction endpoint contributions from the small masses of the external fermions.

- *Gauge invariance* is checked by comparing the result obtained within the 't Hooft–Feynman gauge with an independent result obtained within the background-field formalism [48] by our collaborators. Apart from diagrams that involve only fermion–gauge-boson couplings in the loops, the contributions of individual Feynman graphs are in general different in the two approaches.

- *The real corrections* are taken over from RacoonWW [25,29], where they were checked by two independent calculations in detail. Moreover, agreement was found between the results obtained with phase-space slicing or dipole subtraction.

- *The scalar loop integrals* for complex masses have been calculated in two completely independent ways and implemented in two independent in-house libraries. We checked that these results agree with each other and in the limit of zero width also with FF [59].

- *Two completely independent* calculations have been performed within our group, one calculation implemented by A. Denner and L. H. Wieders and the other implemented by our collaborators S. Dittmaier and M. Roth, revealing good agreement.

- All algebraic manipulations, including the generation of Feynman diagrams and the reduction of amplitudes to standard forms, have been implemented by L. H. Wieders and S. Dittmaier independently, resulting in two self-contained programs.[‡] In Section 3.2 we describe the strategy for a full reduction of the spinor structures, developed by L. H. Wieders, in detail.
- The evaluations of all scalar and tensor loop integrals are based on two independent in-house libraries, one done by A. Denner and the other done by S. Dittmaier and M. Roth, which employ the two different rescue systems mentioned above.

We consider this as the most important and convincing check.

We emphasize that all these checks, including the gauge-invariance check, have been carried out for non-zero gauge-boson widths.

[‡]The amplitudes are generated with FeynArts, using the two independent versions 1 (used by our collaborator S. Dittmaier) and 3, as described in Refs. [49] and [50], respectively. The algebraic manipulations are performed using two independent in-house programs implemented in Mathematica, where our builds upon FormCalc [51].

Chapter 3

Algebraic reduction of spinor chains

One-loop amplitudes for processes with six external fermions involve $\mathcal{O}(10^3)$ different spinor structures, which are products of three spinor chains. These structures are, however, not independent, but can be related by using the Dirac algebra, the Dirac equation, momentum conservation, and relations that follow from the four-dimensionality of space–time. Of course, the latter relations can only be used after cancelling UV divergences, which are regularized dimensionally in our work.

Below we describe two strategies that can be exploited to express any product of three spinor chains for a reaction involving six external massless fermions (and no external bosons) in terms of very few standard structures. Note that none of the following steps leads to Gram determinants in denominator factors, which potentially spoil the numerical stability*. For generic reasons we take all six fermion momenta p_i as incoming ($\sum_{i=1}^{6} p_i = 0$) and use the following shorthand notation for a spinor chain,

$$\Big[A\Big]_{ab}^{\pm} = \bar{v}_a(p_a)\, A\, \omega_{\pm}\, u_b(p_b)\,, \tag{3.0.1}$$

where $\bar{v}_a(p_a)$ and $u_b(p_b)$ are the usual spinors for the (anti-)fermions and

$$\omega_{\pm} = \frac{1}{2}(1 \pm \gamma_5) \tag{3.0.2}$$

the chirality projectors. Since we deal with massless fermions, the matrices A, which act in Dirac space, always consist of a product of an odd number of

*Inverse Gram determinants, e.g., appear in the reduction proposed in Ref. [60].

Dirac matrices γ^μ. The quantities that we want to simplify have the general structure

$$\bar{v}_1(p_1)A\omega_\rho u_2(p_2)\ \bar{v}_3(p_3)B\omega_\sigma u_4(p_4)\ \bar{v}_5(p_5)C\omega_\tau u_6(p_6) \equiv \Big[A\Big]^\rho_{12}\Big[B\Big]^\sigma_{34}\Big[C\Big]^\tau_{56}. \tag{3.0.3}$$

We start out by deriving and summarizing some basic relations that are used in the reduction.

3.1 Basic relations

3.1.1 Identities for Dirac matrices

The four-dimensionality of space–time leads to the Chisholm identity

$$\gamma^\alpha\gamma^\beta\gamma^\gamma = g^{\alpha\beta}\gamma^\gamma - g^{\alpha\gamma}\gamma^\beta + g^{\beta\gamma}\gamma^\alpha + \mathrm{i}\epsilon^{\alpha\beta\gamma\delta}\gamma_\delta\gamma_5, \tag{3.1.1}$$

which can be used to express products $\gamma^\alpha\gamma^\beta\gamma^\gamma$ of Dirac matrices in terms of single Dirac matrices dressed by γ_5 factors and totally antisymmetric tensors $\epsilon^{\alpha\beta\gamma\delta}$ (we adopt the convention $\epsilon^{0123} = +1$).

If at least two Dirac chains are involved, this identity can be applied to shift factors of Dirac matrices from one chain to another without introducing ϵ-tensors, provided the two chains are Lorentz contracted with each other:

$$\begin{aligned}
\gamma^\mu\gamma^\alpha\gamma^\beta\otimes\gamma_\mu &\overset{(3.1.1)}{=} \Big(g^{\mu\alpha}\gamma^\beta - g^{\mu\beta}\gamma^\alpha + g^{\alpha\beta}\gamma^\mu + \mathrm{i}\epsilon^{\mu\alpha\beta\nu}\gamma_\nu\gamma_5\Big)\otimes\gamma_\mu \\
&= \gamma^\beta\otimes\gamma^\alpha - \gamma^\alpha\otimes\gamma^\beta + g^{\alpha\beta}\gamma^\mu\otimes\gamma_\mu \\
&\quad -\gamma_\nu\gamma_5\otimes\Big(\mathrm{i}\epsilon^{\nu\alpha\beta\mu}\gamma_\mu\gamma_5\Big)\gamma_5 \\
&\overset{(3.1.1)}{=} \gamma^\beta\otimes\gamma^\alpha - \gamma^\alpha\otimes\gamma^\beta + g^{\alpha\beta}\gamma^\mu\otimes\gamma_\mu \\
&\quad + \gamma^\alpha\gamma_5\otimes\gamma^\beta\gamma_5 - \gamma^\beta\gamma_5\otimes\gamma^\alpha\gamma_5 \\
&\quad + g^{\alpha\beta}\gamma^\mu\gamma_5\otimes\gamma_\mu\gamma_5 - \gamma_\mu\gamma_5\otimes\gamma^\mu\gamma^\alpha\gamma^\beta\gamma_5.
\end{aligned} \tag{3.1.2}$$

Here and in the following the symbol $\otimes$ denotes the direct product in Dirac space, i.e. Dirac matrices are not sandwiched between Dirac spinors in this case. Relation (3.1.2) can be expressed in a very compact way after introducing the chirality projectors (3.0.2) and rearranging the order of some Dirac matrices,

$$\begin{aligned}
\gamma^\mu\gamma^\alpha\gamma^\beta\omega_\pm\otimes\gamma_\mu\omega_\pm &= \gamma^\mu\omega_\pm\otimes\gamma_\mu\gamma^\beta\gamma^\alpha\omega_\pm, \\
\gamma^\alpha\gamma^\beta\gamma^\mu\omega_\pm\otimes\gamma_\mu\omega_\pm &= \gamma^\mu\omega_\pm\otimes\gamma^\beta\gamma^\alpha\gamma_\mu\omega_\pm, \\
\gamma^\mu\gamma^\alpha\gamma^\beta\omega_\pm\otimes\gamma_\mu\omega_\mp &= \gamma^\mu\omega_\pm\otimes\gamma^\alpha\gamma^\beta\gamma_\mu\omega_\mp, \\
\gamma^\alpha\gamma^\beta\gamma^\mu\omega_\pm\otimes\gamma_\mu\omega_\mp &= \gamma^\mu\omega_\pm\otimes\gamma_\mu\gamma^\alpha\gamma^\beta\omega_\mp.
\end{aligned} \tag{3.1.3}$$

The second and the fourth relations are equivalent forms of the other two.

Equations (3.1.3) lead to analogous relations for direct products of Dirac chains with more than one contraction.† For two contractions we get

$$\begin{aligned}\gamma^\mu\gamma^\alpha\gamma^\nu\omega_\pm \otimes \gamma_\mu\gamma^\beta\gamma_\nu\omega_\pm &= 4g^{\alpha\beta}\gamma^\mu\omega_\pm \otimes \gamma_\mu\omega_\pm,\\ \gamma^\mu\gamma^\alpha\gamma^\nu\omega_\pm \otimes \gamma_\mu\gamma^\beta\gamma_\nu\omega_\mp &= 4\gamma^\beta\omega_\pm \otimes \gamma^\alpha\omega_\mp.\end{aligned} \tag{3.1.4}$$

The first of these relations is obtained by multiplying the second chain of the first relation of (3.1.3) by $\gamma^\gamma\gamma_\beta$ from the right and renaming the indices $\beta \to \nu$ and $\gamma \to \beta$ after some obvious algebra. The second relation is found analogously.

Relations for direct products of Dirac chains with three contractions directly result from (3.1.4) upon contraction with $g_{\alpha\beta}$,

$$\begin{aligned}\gamma^\mu\gamma^\nu\gamma^\rho\omega_\pm \otimes \gamma_\mu\gamma_\nu\gamma_\rho\omega_\pm &= 16\gamma^\mu\omega_\pm \otimes \gamma_\mu\omega_\pm,\\ \gamma^\mu\gamma^\nu\gamma^\rho\omega_\pm \otimes \gamma_\mu\gamma_\nu\gamma_\rho\omega_\mp &= 4\gamma^\mu\omega_\pm \otimes \gamma_\mu\omega_\mp.\end{aligned} \tag{3.1.5}$$

Relations for more than three contractions could be derived from the above results recursively, but are not needed in our case.

3.1.2 Identities for products of spinor chains

Further interesting relations follow if we sandwich the Dirac matrices in the above relations between spinors and perform some simplifications. For instance, if we contract the second relation in (3.1.4) with $p_{1,\alpha}p_{3,\beta}$, then from the r.h.s. multiply the first chain of Dirac matrices by A and the second by B, where here A and B stand for the unit matrix $\mathbf{1}$ or any product of an even number of Dirac matrices, and finally attach the external spinors, we obtain

$$\Big[\gamma^\mu \not{p}_1 \gamma^\nu A\Big]^\pm_{12}\Big[\gamma_\mu \not{p}_3 \gamma_\nu B\Big]^\mp_{34} = 4\Big[\not{p}_3 A\Big]^\pm_{12}\Big[\not{p}_1 B\Big]^\mp_{34}. \tag{3.1.6}$$

On the l.h.s. we can eliminate $\not{p}_1$ and $\not{p}_3$ by the respective Dirac equations and obtain $4(p_1p_3)\Big[\gamma^\nu A\Big]^\pm_{12}\Big[\gamma_\nu B\Big]^\mp_{34}$. Three similar relations can be derived from (3.1.4) with other suitable contractions. The resulting four relations read

$$\begin{aligned}\Big[A\not{p}_3\Big]^\pm_{12}\Big[\not{p}_2 B\Big]^\pm_{34} &= (p_2p_3)\Big[A\gamma^\mu\Big]^\pm_{12}\Big[\gamma_\mu B\Big]^\pm_{34},\\ \Big[\not{p}_4 A\Big]^\pm_{12}\Big[B\not{p}_1\Big]^\pm_{34} &= (p_1p_4)\Big[\gamma^\mu A\Big]^\pm_{12}\Big[B\gamma_\mu\Big]^\pm_{34},\\ \Big[\not{p}_3 A\Big]^\pm_{12}\Big[\not{p}_1 B\Big]^\mp_{34} &= (p_1p_3)\Big[\gamma^\mu A\Big]^\pm_{12}\Big[\gamma_\mu B\Big]^\mp_{34},\\ \Big[A\not{p}_4\Big]^\pm_{12}\Big[B\not{p}_2\Big]^\mp_{34} &= (p_2p_4)\Big[A\gamma^\mu\Big]^\pm_{12}\Big[B\gamma_\mu\Big]^\mp_{34}.\end{aligned} \tag{3.1.7}$$

†Such relations can also be found in Ref. [61].

3.1.3 Decomposition of the metric tensor

In four dimensions the metric tensor $g^{\mu\nu}$ can be decomposed in terms of four independent orthonormal four-vectors n_j^μ,

$$g^{\mu\nu} = \sum_{i,j=0}^{3} g^{ij}\, n_i^\mu\, n_j^\nu\,, \tag{3.1.8}$$

with orthonormal components $n_i^\mu\, n_{j,\mu} = g_{ij}$, where $g_{ij} = g^{ij} = \mathrm{diag}(1,-1,-1,-1)$, as described in the appendices of Refs. [62,63]. The four four-vectors n_i^μ can be constructed from three linearly-independent momenta p_i, p_j, p_k. In the case of massless momenta, $p_i^2 = p_j^2 = p_k^2 = 0$, they can be defined as

$$\begin{aligned}
n_0^\mu(p_i,p_j,p_k) &= \frac{1}{\sqrt{2\,(p_ip_j)}}\,\left(p_i^\mu + p_j^\mu\right)\,,\\
n_1^\mu(p_i,p_j,p_k) &= \frac{1}{\sqrt{2\,(p_ip_j)}}\,\left(p_i^\mu - p_j^\mu\right)\,,\\
n_2^\mu(p_i,p_j,p_k) &= -\frac{1}{\sqrt{2\,(p_ip_j)\,(p_ip_k)\,(p_jp_k)}}\left[(p_jp_k)\,p_i^\mu + (p_ip_k)\,p_j^\mu - (p_ip_j)\,p_k^\mu\right],\\
n_3^\mu(p_i,p_j,p_k) &= -\frac{1}{\sqrt{2\,(p_ip_j)\,(p_ip_k)\,(p_jp_k)}}\,\epsilon^{\mu\alpha\beta\gamma}\,p_{i,\alpha}\,p_{j,\beta}\,p_{k,\gamma}\,.
\end{aligned} \tag{3.1.9}$$

The decomposition of the metric tensor (3.1.8) can be used to disconnect contractions of spinor chains or other objects. Note that the construction of the four vectors n_i from the three independent vectors p_i, p_j, p_k, in particular the definition of n_3, avoids an inverse Gram determinant in (3.1.8); if we decomposed the metric into four totally independent momenta, the result would get the Gram determinant of those four momenta in the denominator.

3.1.3.1 Identities involving ϵ-tensors

The fact that there is no totally antisymmetric tensor of rank 5 in four space–time dimensions leads to the Schouten identity

$$\epsilon_{[\alpha\beta\gamma\delta}\,g_{\mu]\nu} = 0\,, \tag{3.1.10}$$

where $[\ldots]$ means antisymmetrization in $\alpha, \beta, \gamma, \delta$, and μ.

The product of totally antisymmetric tensors can be expressed as a determinant of metric tensors,

$$\epsilon^{\alpha\beta\gamma\delta}\epsilon^{\mu\nu\rho\sigma} = -\begin{vmatrix} g^{\alpha\mu} & g^{\alpha\nu} & g^{\alpha\rho} & g^{\alpha\sigma} \\ g^{\beta\mu} & g^{\beta\nu} & g^{\beta\rho} & g^{\beta\sigma} \\ g^{\gamma\mu} & g^{\gamma\nu} & g^{\gamma\rho} & g^{\gamma\sigma} \\ g^{\delta\mu} & g^{\delta\nu} & g^{\delta\rho} & g^{\delta\sigma} \end{vmatrix} . \tag{3.1.11}$$

3.2 Strategy for reducing spinor structures

In this section we describe our algorithm for the reduction of spinor chains. The algorithm described here reduces all spinor chains to a minimal set.[‡] Although this algorithm is applicable more generally, we refer in the description to the massless charged-current $6f$ processes $\mathrm{e}^+\mathrm{e}^- \bar{f}_1 f_2 \bar{f}_3 f_4 \to 0$, where f_1 and f_3 are different fermions excluding electrons and electron neutrinos and f_2 and f_4 their isospin partners.

Step 1 *Reduction of contractions between spinor chains*

As first step in the reduction, spinor chains contracted with other spinor chains or ϵ-tensors are disconnected.[§] This is achieved by introducing a decomposition of the metric tensor (3.1.8) between contracted Dirac matrices or contractions between a totally antisymmetric tensor and a Dirac matrix:

$$\begin{aligned} \gamma_\mu \otimes \gamma^\mu &= g^{\mu\nu}\, \gamma_\mu \otimes \gamma_\nu \overset{(3.1.8)}{=} \sum_{i,j=0}^{3} g^{ij}\, \not{n}_i \otimes \not{n}_j \,, \\ \epsilon^{\mu\nu\rho\sigma}\, \gamma_\mu &= \epsilon^{\mu\nu\rho\sigma}\, g_{\mu\alpha}\, \gamma^\alpha \overset{(3.1.8)}{=} \epsilon^{\mu\nu\rho\sigma} \sum_{i,j=0}^{3} g^{ij}\, n_{i,\mu}\, \not{n}_j \,. \end{aligned} \tag{3.2.1}$$

The choice of momenta for a suitable decomposition of the metric tensor depends on the positions of the contracted matrices in the spinor chains. Preferably the momenta p_i, p_j, p_k entering (3.1.9) and thus (3.1.8) are selected in such a way that the Dirac equations $\bar{v}(p_i)\not{p}_i = 0 = \not{p}_i u(p_i)$ or the mass-shell condition $\not{p}_i^2 = p_i^2 = 0$ can be used most directly, i.e. without unnecessary anticommutations of Dirac matrices by means of the Dirac algebra, since additional terms come with it. Therefore, we count the number of anticommutations of

[‡]The independent approach of our collaborator S. Dittmaier, avoids scalar products in the denominator, but leads to more SMEs.

[§]The explicit ϵ-tensors result from calculating the traces of Dirac matrices in diagrams with closed fermion loops.

the slashed momenta $\not{p}_i$, introduced by the decomposition of the metric tensor, with Dirac matrices of the chain that would be necessary in order to apply the Dirac equation or the mass-shell condition. We choose the three momenta with the fewest necessary anticommutations.¶

The following substeps are recursively applied until no contractions of spinor chains are left:

- Disconnect a single Lorentz contraction between two spinor chains or between a totally antisymmetric tensor and a spinor chain by (3.2.1).
- Use the Dirac algebra together with the Dirac equation or the mass-shell condition $\not{p}_i^2 = 0$ in order to shorten spinor chains.
- Replace contractions between totally antisymmetric tensors and n_3:

$$\epsilon^{\mu\alpha\beta\gamma}\, n_{3,\mu}(p_i, p_j, p_k) \overset{(3.1.11)}{=} \frac{1}{\sqrt{2\,(p_i p_j)\,(p_i p_k)\,(p_j p_k)}}\, p_i^{[\alpha}\, p_j^{\beta}\, p_k^{\gamma]}\,, \tag{3.2.2}$$

  where $[\ldots]$ means antisymmetrization in α, β, and γ.

- Eliminate $\not{n}_3$ in spinor chains by using

$$\not{n}_3(p_i, p_j, p_k) \overset{(3.1.1)}{=} -\frac{\mathrm{i}\,[\not{p}_i \not{p}_j \not{p}_k - (p_i p_j)\,\not{p}_k + (p_i p_k)\,\not{p}_j - (p_j p_k)\,\not{p}_i]\,\gamma_5}{\sqrt{2\,(p_i p_j)\,(p_i p_k)\,(p_j p_k)}}\,. \tag{3.2.3}$$

After this step, the (disconnected) spinor chains we are left with are of the form $[\not{p}_j]^{\pm}_{ab}$ with $j \neq a, b$ and $[\not{p}_i\, \not{p}_j\, \not{p}_k]^{\pm}_{ab}$ with pairwise different i, j, k, a, b for processes involving six external fermions. Since there are many different types of multiple contractions of spinor chains, we can only illustrate this reduction step, and particularly the first substep, in three representative examples:

$$\begin{aligned}\left[\gamma^\mu\right]^{\sigma}_{ab} \left[\gamma_\mu\right]^{\tau}_{cd} &\overset{(3.2.1)}{=} \sum_{i,j=0}^{3} g^{ij} \left[\not{n}_i(p_a, p_b, p_c)\right]^{\sigma}_{ab} \left[\not{n}_j(p_a, p_b, p_c)\right]^{\tau}_{cd} \\ &\overset{(3.2.3)}{=} \frac{1}{2} \left[\not{p}_c\right]^{\sigma}_{ab} \left(\frac{1}{(p_a p_c)} \left[\not{p}_a\right]^{\tau}_{cd} + \frac{1}{(p_b p_c)} \left[\not{p}_b\right]^{\tau}_{cd} \right)\end{aligned}$$

¶More precisely: If the metric tensor between two spinor chains is eliminated, we count the necessary anticommutations for each momentum in both spinor chains, say N_1 and N_2 with $N_1 \leq N_2$, and set N_2 to infinity if the momentum does not appear in one of the chains. Then we choose the momenta with smallest $N_1 - 1/N_2$. If, on the other hand, the metric tensor between a spinor chain and an ϵ-tensor is replaced, we proceed analogously, but set the number of necessary anticommutations to zero for those momenta that are already contracted with the ϵ-tensor and to infinity otherwise.

$$
\begin{aligned}
&- \frac{1}{2} \left[\not{p}_c \gamma_5\right]^{\sigma}_{ab} \Big(\frac{1}{(p_a p_c)} \left[\not{p}_a \gamma_5\right]^{\tau}_{cd} - \frac{1}{(p_b p_c)} \left[\not{p}_b \gamma_5\right]^{\tau}_{cd} \Big) \\
&= \left[\not{p}_c\right]^{\sigma}_{ab} \left(\frac{1}{(p_a p_c)} \left[\not{p}_a\right]^{\tau}_{cd} \delta_{\sigma,-\tau} + \frac{1}{(p_b p_c)} \left[\not{p}_b\right]^{\tau}_{cd} \delta_{\sigma,\tau} \right), \qquad (3.2.4)
\end{aligned}
$$

$$
\begin{aligned}
&\left[\gamma^\mu\right]^{+}_{12} \left[\not{p}_2 \, \gamma_\mu \, \gamma_\nu\right]^{-}_{34} \left[\gamma^\nu\right]^{-}_{56} \\
&\overset{(3.2.1)}{=} \sum_{i,j=0}^{3} g^{ij} \left[\not{n}_i(p_2,p_1,p_3)\right]^{+}_{12} \left[\not{p}_2 \not{n}_j(p_2,p_1,p_3) \, \gamma_\nu\right]^{-}_{34} \left[\gamma^\nu\right]^{-}_{56} \\
&\overset{(3.2.3)}{=} -\frac{1}{(p_1 p_3)} \left[\not{p}_3\right]^{+}_{12} \left[\not{p}_1 \not{p}_2 \, \gamma_\nu\right]^{-}_{34} \left[\gamma^\nu\right]^{-}_{56} \\
&\overset{(3.2.1)}{=} -\frac{1}{(p_1 p_3)} \left[\not{p}_3\right]^{+}_{12} \sum_{i,j=0}^{3} g^{ij} \left[\not{p}_1 \not{p}_2 \not{n}_i(p_2,p_4,p_5)\right]^{-}_{34} \left[\not{n}_j(p_2,p_4,p_5)\right]^{-}_{56} \\
&\overset{(3.2.3)}{=} -\frac{1}{(p_1 p_3)\,(p_4 p_5)} \left[\not{p}_3\right]^{+}_{12} \left[\not{p}_1 \not{p}_2 \not{p}_5\right]^{-}_{34} \left[\not{p}_4\right]^{-}_{56}, \qquad (3.2.5)
\end{aligned}
$$

$$
\begin{aligned}
&\mathrm{i}\, \epsilon^{\mu\alpha\gamma\delta} \, p_{1,\alpha} \, p_{3,\gamma} \, p_{4,\delta} \left[\gamma_\mu\right]^{-}_{12} \\
&\overset{(3.2.1)}{=} \mathrm{i}\, \epsilon^{\mu\alpha\gamma\delta} \, p_{1,\alpha} \, p_{3,\gamma} \, p_{4,\delta} \sum_{i,j=0}^{3} g^{ij} \, n_{i,\mu}(p_1,p_2,p_3) \left[\not{n}_j(p_1,p_2,p_3)\right]^{-}_{12} \\
&\underset{(3.2.3)}{\overset{(3.2.2)}{=}} \frac{1}{2\,(p_2 p_3)} \left[\not{p}_3\right]^{-}_{12} \Big((p_1 p_2)\,(p_3 p_4) - (p_1 p_3)(p_2 p_4) \\
&\qquad + (p_1 p_4)(p_2 p_3) - \mathrm{i}\, \epsilon^{\alpha\beta\gamma\delta} \, p_{1,\alpha} \, p_{2,\beta} \, p_{3,\gamma} \, p_{4,\delta} \Big) \\
&= \frac{1}{2\,(p_2 p_3)} \left[\not{p}_3\right]^{-}_{12} A^{+-++}_{1\,2\,3\,4}, \qquad (3.2.6)
\end{aligned}
$$

where we introduced the abbreviation

$$
A^{a\,b\,c\,d}_{i\,j\,k\,l} = a\,(p_i p_j)\,(p_k p_l) + b\,(p_i p_k)\,(p_j p_l) + c\,(p_i p_l)\,(p_j p_k) - d\,\mathrm{i}\,\epsilon_{i\,j\,k\,l} \qquad (3.2.7)
$$

with $\epsilon_{i\,j\,k\,l} = \epsilon_{\alpha\beta\gamma\delta}\, p_i^\alpha p_j^\beta p_k^\gamma p_l^\delta$ and upper index combinations $(-\,+\,+\pm)$, $(+\,-\,+\pm)$, and $(+\,+\,-\pm)$ for $(a\,b\,c\,d)$.

Step 2 *Reduction of a spinor chain to standard form*

Since all spinor structures are disconnected after the first step, we can focus on single spinor chains in this step, i.e. spinor chains of the form $[B]^{\sigma}_{ab}$ where all Dirac matrices in B are contracted with momenta. These spinor chains can be reduced to the standard form $[\not{p}]^{\pm}_{ab}$ with a freely chosen momentum $p = p_n$, $p_n \neq p_a, p_b$, by recursively applying the following substeps:

- For $p_m \neq p_a, p_b, p$, replace $\not{p}_m$ by

$$\not{p}_m \overset{(3.1.8)}{=} p_{m,\mu} \sum_{i,j=0}^{3} g^{ij}\, n_i^\mu \not{n}_j \tag{3.2.8}$$

- Eliminate $\not{n}_3$ via (3.2.3).

- Use the Dirac algebra together with the Dirac equation or the mass-shell condition $p_i^2 = 0$ in order to shorten the spinor chain.

Since for our case only two different types of spinor chains are left after the first step, we can demonstrate the reduction procedure of the two cases in full detail. The first case is reduced as:

$$\begin{aligned}
\left[\not{p}_m\right]_{ab}^{\pm} &\overset{(3.2.8)}{=} p_{m,\mu} \sum_{i,j=0}^{3} g^{ij}\, n_i^\mu(p_a,p_b,p_n) \left[\not{n}_j(p_a,p_b,p_n)\right]_{ab}^{\pm} \\
&\overset{(3.2.3)}{=} \frac{(p_a p_n)\,(p_b p_m) - (p_a p_b)\,(p_n p_m) + (p_a p_m)\,(p_n p_b) \pm \mathrm{i}\,\epsilon_{a\,n\,b\,m}}{2\,(p_a p_n)\,(p_b p_n)} \left[\not{p}_n\right]_{ab}^{\pm} \\
&\overset{(3.2.7)}{=} \frac{1}{2\,(p_a p_n)\,(p_b p_n)}\, A^{+-+\mp}_{a\,n\,b\,m} \left[\not{p}_n\right]_{ab}^{\pm}.
\end{aligned} \tag{3.2.9}$$

The second case can be reduced to the first case as follows:

$$\begin{aligned}
\left[\not{p}_m \not{p}_l \not{p}_k\right]_{ab}^{\pm} &\overset{(3.2.8)}{=} p_{l,\mu} \sum_{i,j=0}^{3} g^{ij}\, n_i^\mu(p_m,p_k,p_b) \left[\not{p}_m \not{n}_j(p_m,p_k,p_b)\, \not{p}_k\right]_{ab}^{\pm} \\
&\overset{(3.2.3)}{=} \frac{(p_b p_m)\,(p_l p_k) - (p_b p_l)\,(p_m p_k) + (p_b p_k)\,(p_m p_l)}{2\,(p_b p_m)(p_b p_k)} \left[\not{p}_m \not{p}_b \not{p}_k\right]_{ab}^{\pm} \\
&\quad - \mathrm{i}\,\frac{\epsilon_{b\,m\,l\,k}}{2\,(p_b p_m)(p_b p_k)} \left[\not{p}_m \gamma_5 \not{p}_b \not{p}_k\right]_{ab}^{\pm} \\
&= \frac{(p_b p_m)\,(p_l p_k) - (p_b p_l)\,(p_m p_k) + (p_b p_k)\,(p_m p_l) \mp \mathrm{i}\,\epsilon_{b\,m\,l\,k}}{(p_b p_m)} \left[\not{p}_m\right]_{ab}^{\pm} \\
&\overset{(3.2.7)}{=} \frac{1}{(p_b p_m)}\, A^{+-+\pm}_{b\,m\,l\,k} \left[\not{p}_m\right]_{ab}^{\pm}.
\end{aligned} \tag{3.2.10}$$

Thus, we end up with spinor chains in standard form and prefactors S containing only scalar products of external momenta $(p_i p_j)$, $\epsilon_{i\,j\,k\,l}$, and the abbreviations (3.2.7). Note that (3.2.10) could be applied recursively to longer spinor chains.

Thus, for processes with six external fermions, all Dirac structures occurring in one-loop amplitudes, i.e. all structures of the form (3.0.3), can be brought to the form

$$S \left[\not{p}_3\right]_{12}^{\rho} \left[\not{p}_1\right]_{34}^{\sigma} \left[\not{p}_1\right]_{56}^{\tau}, \tag{3.2.11}$$

where we have chosen the momenta p_3, p_1, and p_1 in the spinor chains by convention. Accordingly, the SMEs can be chosen as

$$\hat{\mathcal{M}}^{\rho\sigma\tau} = \left[\not{p}_3\right]_{12}^{\rho} \left[\not{p}_1\right]_{34}^{\sigma} \left[\not{p}_1\right]_{56}^{\tau}, \tag{3.2.12}$$

and there is only one SME for each helicity combination of the external fermions. For purely W-mediated charged-current processes, there are only two non-vanishing helicity combinations and thus only two different SMEs.

Step 3 *Simplification of scalar factors*

After the reduction steps above, each spinor structure has the form (3.2.12) with prefactors S containing products of scalars products $(p_i p_j)$ in the denominator, and possibly polynomials of scalar products, of ϵ_{ijkl}, and of $A_{ijkl}^{abc\pm}$ in the numerator. These prefactors can be simplified further by means of relations we describe now.

The quantity $A_{ijkl}^{abc\pm}$ defined in (3.2.7) transforms under exchange of two momenta, corresponding to two of the indices $(ijkl)$, as

$$A_{ijkl}^{abc\pm} = A_{jikl}^{acb\mp} = A_{ijlk}^{acb\mp} = A_{kjil}^{cba\mp} = A_{iljk}^{cba\mp} = A_{ljki}^{bac\mp} = A_{ikjl}^{bac\mp}, \tag{3.2.13}$$

and is therefore invariant under exchange of two distinct pairs of momenta,

$$A_{ijkl}^{abc\pm} = A_{jilk}^{abc\pm} = A_{klij}^{abc\pm} = A_{lkji}^{abc\pm}. \tag{3.2.14}$$

Owing to these relations, any $A_{i'j'k'l'}^{abc\pm}$, where $(i'j'k'l')$ is an arbitrary permutation of $(i\,j\,k\,l)$, can be transformed into one of the six elements

$$A_{ijkl}^{-++\pm},\ A_{ijkl}^{+-+\pm},\ \text{or}\ A_{ijkl}^{++-\pm}. \tag{3.2.15}$$

In the following, we use only these independent quantities (3.2.15), i.e. for each set of indices $(i\,j\,k\,l)$ of $A_{ijkl}^{abc\pm}$ we define a standard order.

The identity for products of totally antisymmetric tensors (3.1.11) leads to relations among the $A_{ijkl}^{abc\pm}$. Relations for products of $A_{ijkl}^{abc\pm}$ with the same momenta are

$$\begin{aligned}
A_{ijkl}^{-++\pm}\, A_{ijkl}^{-++\mp} &= 4\,(p_ip_k)(p_jp_l)\,(p_ip_l)(p_jp_k)\,,\\
A_{ijkl}^{+-+\pm}\, A_{ijkl}^{+-+\mp} &= 4\,(p_ip_j)(p_kp_l)\,(p_ip_l)(p_jp_k)\,,\\
A_{ijkl}^{++-\pm}\, A_{ijkl}^{++-\mp} &= 4\,(p_ip_j)(p_kp_l)\,(p_ip_k)(p_jp_l)\,,
\end{aligned} \tag{3.2.16}$$

and

$$\begin{aligned}
A_{ijkl}^{+-+\pm}\, A_{ijkl}^{++-\pm} &= -2\,(p_ip_j)(p_kp_l)\, A_{ijkl}^{-++\mp}\\
A_{ijkl}^{-++\pm}\, A_{ijkl}^{++-\pm} &= -2\,(p_ip_k)(p_jp_l)\, A_{ijkl}^{+-+\mp}\,,\\
A_{ijkl}^{-++\pm}\, A_{ijkl}^{+-+\pm} &= -2\,(p_ip_l)(p_jp_k)\, A_{ijkl}^{++-\mp}\,.
\end{aligned} \tag{3.2.17}$$

Note that in these and the following formulas double Latin indices are not summed. In (3.2.16) and (3.2.17) the second and third lines are obtained from the first by the substitutions $(j \leftrightarrow k)$ and $(i \leftrightarrow k)$, respectively, and subsequent transformation to the six elements (3.2.15).

Relations for products of $A^{a\,b\,c\,\pm}_{i\,j\,k\,l}$ which differ in one momentum read

$$\begin{aligned} A^{-++\pm}_{i\,j\,k\,l} &= \tfrac{1}{2\,(p_i p_m)(p_j p_m)}\, A^{-++\pm}_{i\,j\,k\,m}\, A^{-++\mp}_{i\,j\,l\,m} \\ &= \tfrac{1}{2\,(p_k p_m)(p_l p_m)}\, A^{++-\pm}_{i\,k\,l\,m}\, A^{++-\mp}_{j\,k\,l\,m}\,, \end{aligned} \tag{3.2.18}$$

and

$$\begin{aligned} A^{+-+\pm}_{i\,j\,k\,l} A^{++-\pm}_{i\,j\,k\,m} &= -\frac{(p_i p_j)}{(p_i p_m)} A^{-++\mp}_{i\,j\,k\,m} A^{-++\pm}_{i\,k\,l\,m} \\ &= +\frac{(p_i p_j)}{(p_l p_m)} A^{++-\mp}_{i\,k\,l\,m} A^{+-+\mp}_{j\,k\,l\,m} \\ &= -\frac{(p_i p_j)}{(p_j p_l)} A^{-++\mp}_{i\,j\,k\,l} A^{-++\pm}_{j\,k\,l\,m}\,. \end{aligned} \tag{3.2.19}$$

Two further relations can be obtained from each of the equations in (3.2.18) and (3.2.19) via the substitutions $(j \leftrightarrow k)$ and $(i \leftrightarrow k)$. Three further sets of relations can finally be constructed by substituting $(l \leftrightarrow m)$ in all these relations derived from (3.2.19).

Step 3 consists of two parts:

- First, we try to eliminate *sums* containing $A^{a\,b\,c\,\pm}_{i\,j\,k\,l}$, $(p_i p_j)\,(p_k p_l)$, $\epsilon_{i\,j\,k\,l}$, and products thereof. To this end, we use the Schouten identity (3.1.10), the relations (3.2.16)–(3.2.19), and linear relations like $A^{+-+\pm}_{i\,j\,k\,l} = 2\,(p_i p_j)\,(p_k p_l) - A^{++-\mp}_{i\,j\,k\,l}$ or $(p_i p_j)\,(p_k p_l) \pm \mathrm{i}\,\epsilon_{i\,j\,k\,l} = A^{++-\mp}_{i\,j\,k\,l} - (p_i p_k)\,(p_j p_l) + (p_i p_l)\,(p_j p_k)$ that follow from the definition of the $A^{a\,b\,c\,\pm}_{i\,j\,k\,l}$ (3.2.7). All these relations are applied recursively to parts of S in (3.2.12) as long as they lead to simplifications.

  When starting from structures of the form (3.0.3), we succeeded in this way to eliminate all sums, and the resulting S involve only products of $A^{a\,b\,c\,\pm}_{i\,j\,k\,l}$ and scalar products in the numerator, and products of scalar products in the denominator.

- Second, the *products* of $A^{a\,b\,c\,\pm}_{i\,j\,k\,l}$ are simplified further and brought into a standard form by using the relations (3.2.16)–(3.2.19).

Typical results are

$$\left[\gamma^\mu\gamma^\nu\gamma^\rho\right]^\sigma_{12}\left[\gamma_\mu\gamma_\nu\gamma_\rho\right]^\tau_{34} = \frac{4}{(p_1 p_3)}\left(\frac{2\,A^{-++\sigma}_{1\,2\,3\,4}}{(p_1 p_4)\,(p_2 p_3)}\,\delta_{\sigma,\tau} + \delta_{\sigma,-\tau}\right)$$

$$
\begin{aligned}
&\times \Big[\not{p}_3\Big]_{12}^{\sigma}\Big[\not{p}_1\Big]_{34}^{\tau}\,,\\
\Big[\not{p}_3\not{p}_5\gamma^\mu\Big]_{12}^{-}\Big[\gamma_\mu\Big]_{56}^{-} &= 0\,,\\
\Big[\not{p}_3\gamma^\mu\gamma^\nu\Big]_{12}^{+}\Big[\gamma_\mu\gamma^\rho\gamma^\kappa\Big]_{34}^{-}\Big[\gamma_\nu\gamma_\rho\gamma_\kappa\Big]_{56}^{-} &= 0\,,\\
\Big[\not{p}_3\gamma^\mu\gamma^\nu\Big]_{12}^{\sigma}\Big[\gamma_\nu\gamma^\rho\gamma^\kappa\Big]_{34}^{-}\Big[\gamma_\mu\gamma_\rho\gamma_\kappa\Big]_{56}^{-} &= \frac{-4\,A^{-+++}_{13\,45}\,A^{+-++}_{13\,46}}{(p_1p_3)\,(p_1p_4)\,(p_1p_5)\,(p_1p_6)\,(p_3p_4)}\\
&\quad\times\Big[\not{p}_3\Big]_{12}^{\sigma}\Big[\not{p}_1\Big]_{34}^{-}\Big[\not{p}_1\Big]_{56}^{-}\Big(\delta_{\sigma,-}+2\,\delta_{\sigma,+}\Big)\,,\\
\Big[\not{p}_3\gamma^\mu\gamma^\nu\gamma^\rho\gamma^\kappa\Big]_{12}^{-}\Big[\gamma_\nu\gamma_\rho\gamma_\kappa\Big]_{34}^{-}\Big[\gamma_\mu\Big]_{56}^{-} &= \frac{8\,A^{-++-}_{12\,34}\,A^{-++-}_{13\,56}}{(p_1p_3)\,(p_1p_4)\,(p_1p_5)\,(p_1p_6)\,(p_2p_3)}\\
&\quad\times\Big[\not{p}_3\Big]_{12}^{-}\Big[\not{p}_1\Big]_{34}^{-}\Big[\not{p}_1\Big]_{56}^{-}\,,\\
-\mathrm{i}\epsilon^{\mu\nu\rho\sigma}\,p_{1,\sigma}\Big[\gamma_\mu\Big]_{12}^{+}\Big[\gamma_\nu\Big]_{34}^{-}\Big[\gamma_\rho\Big]_{56}^{-} &= \frac{A^{+-+-}_{12\,35}}{2\,(p_1p_3)\,(p_1p_5)\,(p_2p_3)}\\
&\quad\times\Big[\not{p}_3\Big]_{12}^{+}\Big[\not{p}_1\Big]_{34}^{-}\Big[\not{p}_1\Big]_{56}^{-}\,.
\end{aligned}
\tag{3.2.20}
$$

The entire reduction algorithm, described in the three steps above, reduces the spinor chains of the considered processes to the SMEs (3.2.12) and about 35 different $A^{a\,b\,c\,\pm}_{i\,j\,k\,l}$. When inserting the results into the amplitudes, further simplifications between contributions of different spinor structures can be performed owing to the simple structure of the SMEs. This speeds up the calculations considerably.

The spinor structures could alternatively be evaluated directly in the Weyl–van der Waerden spinor formalism, as described in some detail in the appendix. Although most of the relations given in this section can be easily derived using the spinor formalism, many simplifications that are based on four-momenta are harder to perform in that approach.

Chapter 4

The complex mass scheme at one loop

The description of resonances in perturbation theory requires at least a partial Dyson summation of self-energy insertions. This leads to a mixing of perturbative orders and, if done carelessly, can easily jeopardise gauge invariance [33,34]. Therefore, the proper introduction of finite-width effects is a non-trivial problem. While several solutions have been described for lowest-order predictions [29,34–42], no viable, universally valid scheme exists so far for a consistent evaluation of radiative corrections in the presence of resonances. A pole expansion [35,37,38,42] provides a gauge-invariant answer and is applicable to radiative corrections, but restricts the validity of the result to the resonance region only and is not reliable in threshold regions. In our calculation we want to cover both the threshold region, where the pole approximation is not applicable, and the continuum above threshold, where threshold expansions are not valid. Moreover, the calculation should be valid both for resonant and non-resonant regions in phase space. In other words, we are after a unified description that is applicable in the complete phase space and does not require any matching between different treatments for different regions.

Such a description is provided by the "complex-mass scheme" (CMS), which was introduced in Ref. [29] for lowest-order calculations. In this approach the W- and Z-boson masses are consistently considered as complex quantities, defined as the locations of the poles in the complex k^2 plane of the corresponding propagators with momentum k. Gauge invariance is preserved if the complex masses are introduced everywhere in the Feynman rules, in particular in the definition of the weak mixing angle,

$$\cos^2\theta_{\mathrm{W}} \equiv c_{\mathrm{w}}^2 = 1 - s_{\mathrm{w}}^2 = \frac{\mu_{\mathrm{W}}^2}{\mu_{\mathrm{Z}}^2}, \tag{4.0.1}$$

which is derived from the ratio of the complex mass squares of the gauge bosons,*

$$\mu_{\mathrm{W}}^2 = M_{\mathrm{W}}^2 - \mathrm{i}M_{\mathrm{W}}\Gamma_{\mathrm{W}}, \qquad \mu_{\mathrm{Z}}^2 = M_{\mathrm{Z}}^2 - \mathrm{i}M_{\mathrm{Z}}\Gamma_{\mathrm{Z}}. \tag{4.0.2}$$

The (algebraic) relations, such as Ward identities, that follow from gauge invariance remain valid, because the gauge-boson masses are modified only by an analytic continuation. As a consequence unitarity cancellations are respected, and the amplitudes have a decent high-energy behaviour.

While necessary in the resonant propagators, the consistent introduction of complex gauge-boson masses introduces spurious terms in other places, as e.g. in the weak mixing angle (4.0.1). When using the CMS at tree level, which amounts to replacing the real gauge-boson masses by the complex masses (4.0.2) and the weak mixing angle by (4.0.1) in tree-level amplitudes, the spurious terms are of order $\mathcal{O}(\Gamma_{\mathrm{W}}/M_{\mathrm{W}}) = \mathcal{O}(\alpha)$ relative to the lowest-order term (both in resonant and non-resonant regions).

Here we use a generalization of the CMS to higher orders, which was proposed in Ref. [44,45]. The complex masses are introduced directly at the level of the Lagrangian by splitting the bare masses into complex renormalized masses and complex counterterms. This scheme has the following properties:

- From the Lagrangian we obtain Feynman rules with complex masses and counterterms with which we can perform perturbative calculations as usual. Since we do not change the theory at all, but only rearrange its perturbative expansion, no double counting of terms occurs.

- For each unstable particle mass, we add and subtract the same imaginary part in the Lagrangian. One of these terms provides the imaginary part for the mass parameter and becomes part of the free propagator, while the other becomes part of a counterterm vertex. The first term is, thus, resummed but the second is not. Independently of the imaginary part that is added and subtracted, this procedure does not spoil the algebraic relations that govern gauge invariance, and unitarity cancellations are exactly respected. In practice, this means that we can insert values for the gauge-boson widths that are not directly related to the one-loop order to which the corrections for the process are calculated. We could even

*While it is generally accepted that the mass and width of unstable particles are related to the pole of the propagator in the complex plane, this does not define the mass and the width separately. This arbitrariness is discussed in detail in Ref. [64], where also a definition of the mass and width is proposed such that the width is given by the inverse lifetime. We have chosen the popular definition (4.0.2), but the complex renormalization scheme is applicable to other definitions as well.

go beyond one loop in the calculation of the widths or take an empirical value.

- Performing an $\mathcal{O}(\alpha)$ calculation in the CMS yields $\mathcal{O}(\alpha)$ accuracy everywhere in phase space provided the width that enters in the resonant propagators via the complex mass is calculated including at least $\mathcal{O}(\alpha)$ corrections. This is evident away from the resonances, where one could expand in terms of the width, thus recovering the usual perturbative expansion. In the resonance region, where the resonant contributions dominate, both the prefactors of the resonant propagators and the resonant propagators themselves are taken into account in $\mathcal{O}(\alpha)$ and our results differ by $\mathcal{O}(\alpha^2)$ terms from a leading pole approximation where this is applicable. Thus, any spurious terms are of order $\mathcal{O}(\alpha^2)$.

Introducing complex masses and couplings seems to violate unitarity. Obviously, the Cutkosky cutting equations [65] are no longer valid, and unitarity cannot simply be proven order by order anymore. However, since we do not modify the bare Lagrangian, the unitarity-violating terms are of higher order, i.e. of $\mathcal{O}(\alpha^2)$ in an $\mathcal{O}(\alpha)$ calculation. Moreover, this unitarity violation cannot be enhanced, because all Ward identities are exactly preserved. In this respect one should also mention that unstable particles should be excluded as external states and only the S-matrix connecting stable particle states needs to be unitary, as has already been pointed out by Veltman in the sixties [66]. Of course, before the described CMS can be viewed as a rigorous procedure to define a renormalized quantum field theory it has to be clarified whether one can directly prove unitarity order by order in this formalism. In particular, it is an interesting question whether one can construct modified cutting equations in the CMS.

4.1 Complex renormalization – 't Hooft–Feynman gauge

The consistent introduction of complex masses in loop calculations necessitates the formulation of an appropriate renormalization prescription. To this end, the on-shell renormalization scheme formulated in Refs. [48,52,67] is generalized at the one-loop level in a straight-forward way [44,45].

Following the conventions of Ref. [52], the renormalized transverse (T) gauge-boson self-energies read

$$\begin{aligned}
\hat{\Sigma}^{W}_{\mathrm{T}}(k^2) &= \Sigma^{W}_{\mathrm{T}}(k^2) - \delta\mu^2_{\mathrm{W}} + (k^2 - \mu^2_{\mathrm{W}})\delta\mathcal{Z}_W, \\
\hat{\Sigma}^{ZZ}_{\mathrm{T}}(k^2) &= \Sigma^{ZZ}_{\mathrm{T}}(k^2) - \delta\mu^2_{\mathrm{Z}} + (k^2 - \mu^2_{\mathrm{Z}})\delta\mathcal{Z}_{ZZ}, \\
\hat{\Sigma}^{AA}_{\mathrm{T}}(k^2) &= \Sigma^{AA}_{\mathrm{T}}(k^2) + k^2\delta\mathcal{Z}_{AA},
\end{aligned}$$

$$\hat{\Sigma}_{\mathrm{T}}^{AZ}(k^2) = \Sigma_{\mathrm{T}}^{AZ}(k^2) + k^2\frac{1}{2}\delta\mathcal{Z}_{AZ} + (k^2 - \mu_{\mathrm{Z}}^2)\frac{1}{2}\delta\mathcal{Z}_{ZA}, \tag{4.1.1}$$

where A denotes the photon field, and the hat indicates renormalized self-energies. Compared to Ref. [52], the renormalized on-shell masses and mass counterterms are replaced by the renormalized complex masses μ_{W} and μ_{Z} everywhere, i.e. also within the self-energies. The field renormalization constants are denoted in the CMS by calligraphic letters. The complex renormalized masses and mass counterterms result from a splitting of the real bare masses squared,[†]

$$M_{\mathrm{W},0}^2 = \mu_{\mathrm{W}}^2 + \delta\mu_{\mathrm{W}}^2, \qquad M_{\mathrm{Z},0}^2 = \mu_{\mathrm{Z}}^2 + \delta\mu_{\mathrm{Z}}^2, \tag{4.1.2}$$

where here and in the following bare quantities are indicated by a subscript 0. Similarly, splitting the bare fields in complex field renormalization constants and renormalized fields

$$\begin{aligned} W_0^{\pm} &= (1 + \tfrac{1}{2}\delta\mathcal{Z}_W)W^{\pm}, \\ \begin{pmatrix} Z_0 \\ A_0 \end{pmatrix} &= \begin{pmatrix} 1 + \frac{1}{2}\delta\mathcal{Z}_{ZZ} & \frac{1}{2}\delta\mathcal{Z}_{ZA} \\ \frac{1}{2}\delta\mathcal{Z}_{AZ} & 1 + \frac{1}{2}\delta\mathcal{Z}_{AA} \end{pmatrix} \begin{pmatrix} Z \\ A \end{pmatrix}, \end{aligned} \tag{4.1.3}$$

implies that the bare and renormalized fields have different phases. Thus, for instance, the renormalized Z-boson field becomes complex, while the corresponding bare field is real. As a consequence, the renormalized Lagrangian, i.e. the Lagrangian in terms of renormalized fields without counterterms, is not hermitian, but the total Lagrangian (which is equal to the bare Lagrangian) of course is.

In order to fix the counterterms, the renormalization conditions of the complete on-shell scheme [52,67] are generalized as

$$\begin{aligned} \hat{\Sigma}_{\mathrm{T}}^{W}(\mu_{\mathrm{W}}^2) &= 0, & \hat{\Sigma}_{\mathrm{T}}^{ZZ}(\mu_{\mathrm{Z}}^2) &= 0, & & \\ \hat{\Sigma}_{\mathrm{T}}^{AZ}(0) &= 0, & \hat{\Sigma}_{\mathrm{T}}^{AZ}(\mu_{\mathrm{Z}}^2) &= 0, & & \\ \hat{\Sigma}_{\mathrm{T}}^{\prime W}(\mu_{\mathrm{W}}^2) &= 0, & \hat{\Sigma}_{\mathrm{T}}^{\prime ZZ}(\mu_{\mathrm{Z}}^2) &= 0, & \hat{\Sigma}_{\mathrm{T}}^{\prime AA}(0) &= 0, \end{aligned} \tag{4.1.4}$$

where the prime denotes differentiation with respect to the argument. The conditions (4.1.4), in particular the first two, fix the mass counterterms in such a way that the renormalized mass is equal to the location of the propagator pole in the complex plane. This is a gauge-invariant quantity, as pointed out and shown in Refs. [37,69]. The last five renormalization conditions in (4.1.4) fix the field renormalization constants. Note that the field renormalization constants of the gauge-boson fields exactly drop out in all S-matrix

[†]Similar ideas were proposed in Ref. [68].

elements that do not involve external gauge bosons, but allow to render all vertex functions finite. This generally holds for all field renormalization constants of unstable particles as long as one does not consider S-matrix elements for external unstable particles. Unlike in Refs. [52,67], real parts are not taken in the renormalization conditions (4.1.4), and thus not only the mass renormalization constants but also the field renormalization constants become in general complex. This ansatz is supported by the fact that the imaginary part of one-loop scattering amplitudes involving unstable external particles becomes gauge dependent if the imaginary parts of the counterterms are not included [70]. For the definition of the renormalized mass and width this scheme is exactly the one described in Appendix D of Ref. [36]. As a matter of fact, the renormalization constant $\delta\mathcal{Z}_W$ applies to both the W^+ and W^- field, i.e. the imaginary part of $\delta\mathcal{Z}_W$ is fixed by the renormalization condition and does not change sign when going from the W^+ to the W^- field.

The renormalization conditions (4.1.4) have the solutions

$$\begin{aligned}
\delta\mu_{\mathrm{W}}^2 &= \Sigma_{\mathrm{T}}^{W}(\mu_{\mathrm{W}}^2), \qquad & \delta\mu_{\mathrm{Z}}^2 &= \Sigma_{\mathrm{T}}^{ZZ}(\mu_{\mathrm{Z}}^2),\\
\delta\mathcal{Z}_{ZA} &= \frac{2}{\mu_{\mathrm{Z}}^2}\Sigma_{\mathrm{T}}^{AZ}(0), \qquad & \delta\mathcal{Z}_{AZ} &= -\frac{2}{\mu_{\mathrm{Z}}^2}\Sigma_{\mathrm{T}}^{AZ}(\mu_{\mathrm{Z}}^2),\\
\delta\mathcal{Z}_{W} &= -\Sigma_{\mathrm{T}}^{\prime W}(\mu_{\mathrm{W}}^2), \qquad & \delta\mathcal{Z}_{ZZ} &= -\Sigma_{\mathrm{T}}^{\prime ZZ}(\mu_{\mathrm{Z}}^2),\\
\delta\mathcal{Z}_{AA} &= -\Sigma_{\mathrm{T}}^{\prime AA}(0), & &
\end{aligned} \tag{4.1.5}$$

which require to calculate the self-energies for complex squared momenta. This would demand an analytic continuation of the 2-point functions entering the self-energies in the momentum variable to the unphysical Riemann sheet. In order to avoid this complication, an appropriate expansion about real arguments is performed,

$$\begin{aligned}
\Sigma_{\mathrm{T}}^{W}(\mu_{\mathrm{W}}^2) &= \Sigma_{\mathrm{T}}^{W}(M_{\mathrm{W}}^2) + (\mu_{\mathrm{W}}^2 - M_{\mathrm{W}}^2)\Sigma_{\mathrm{T}}^{\prime W}(M_{\mathrm{W}}^2) + \mathcal{O}(\alpha^3),\\
\Sigma_{\mathrm{T}}^{ZZ}(\mu_{\mathrm{Z}}^2) &= \Sigma_{\mathrm{T}}^{ZZ}(M_{\mathrm{Z}}^2) + (\mu_{\mathrm{Z}}^2 - M_{\mathrm{Z}}^2)\Sigma_{\mathrm{T}}^{\prime ZZ}(M_{\mathrm{Z}}^2) + \mathcal{O}(\alpha^3),\\
\frac{1}{\mu_{\mathrm{Z}}^2}\Sigma_{\mathrm{T}}^{AZ}(\mu_{\mathrm{Z}}^2) &= \frac{1}{\mu_{\mathrm{Z}}^2}\Sigma_{\mathrm{T}}^{AZ}(0) + \frac{1}{M_{\mathrm{Z}}^2}\Sigma_{\mathrm{T}}^{AZ}(M_{\mathrm{Z}}^2)\\
&\quad -\frac{1}{M_{\mathrm{Z}}^2}\Sigma_{\mathrm{T}}^{AZ}(0) + \mathcal{O}(\alpha^2),
\end{aligned} \tag{4.1.6}$$

as done similarly in Appendix D of Ref. [36]. The $\mathcal{O}(\alpha^2)$ and $\mathcal{O}(\alpha^3)$ contributions result from products of terms $\Sigma^W = \mathcal{O}(\alpha)$, $\Sigma^{ZZ} = \mathcal{O}(\alpha)$, $\Sigma^{AZ} = \mathcal{O}(\alpha)$, $(\mu_{\mathrm{W}}^2 - M_{\mathrm{W}}^2) = \mathcal{O}(\alpha)$, and $(\mu_{\mathrm{Z}}^2 - M_{\mathrm{Z}}^2) = \mathcal{O}(\alpha)$ and are UV-finite by construction at the one-loop level.

By neglecting these $\mathcal{O}(\alpha^2)$ and $\mathcal{O}(\alpha^3)$ terms, one can replace (4.1.5) by

$$\begin{aligned}
\delta\mu_{\mathrm{W}}^2 &= \Sigma_{\mathrm{T}}^{W}(M_{\mathrm{W}}^2) + (\mu_{\mathrm{W}}^2 - M_{\mathrm{W}}^2)\Sigma_{\mathrm{T}}^{\prime W}(M_{\mathrm{W}}^2),\\
\delta\mu_{\mathrm{Z}}^2 &= \Sigma_{\mathrm{T}}^{ZZ}(M_{\mathrm{Z}}^2) + (\mu_{\mathrm{Z}}^2 - M_{\mathrm{Z}}^2)\Sigma_{\mathrm{T}}^{\prime ZZ}(M_{\mathrm{Z}}^2),
\end{aligned} \tag{4.1.7}$$

and

$$\begin{aligned}
\delta\mathcal{Z}_{ZA} &= \frac{2}{\mu_{\mathrm{Z}}^2}\Sigma_{\mathrm{T}}^{AZ}(0), \\
\delta\mathcal{Z}_{AZ} &= -\frac{2}{M_{\mathrm{Z}}^2}\Sigma_{\mathrm{T}}^{AZ}(M_{\mathrm{Z}}^2) + \left(\frac{\mu_{\mathrm{Z}}^2}{M_{\mathrm{Z}}^2} - 1\right)\delta\mathcal{Z}_{ZA}, \\
\delta\mathcal{Z}_W &= -\Sigma_{\mathrm{T}}'^{W}(M_{\mathrm{W}}^2), \qquad \delta\mathcal{Z}_{ZZ} = -\Sigma_{\mathrm{T}}'^{ZZ}(M_{\mathrm{Z}}^2).
\end{aligned} \tag{4.1.8}$$

We use these counterterms in our calculation. While the missing $\mathcal{O}(\alpha^2)$ terms in $\delta\mathcal{Z}_{AZ}$ do not influence our results, since the gauge-boson field renormalization constants drop out as there is no external gauge boson in the process under consideration, the missing (finite) $\mathcal{O}(\alpha^3)$ terms in the mass counterterms are beyond the accuracy of our calculation. The counterterms (4.1.7) involve only functions that appear also in the usual on-shell renormalization scheme [52,67], but consistently take into account the imaginary parts.

When inserting the counterterms (4.1.7) and (4.1.8) into (4.1.1), one can rewrite the renormalized self-energies in the CMS as

$$\begin{aligned}
\hat{\Sigma}_{\mathrm{T}}^{W}(k^2) &= \Sigma_{\mathrm{T}}^{W}(k^2) - \delta M_{\mathrm{W}}^2 + (k^2 - M_{\mathrm{W}}^2)\delta Z_W, \\
\hat{\Sigma}_{\mathrm{T}}^{ZZ}(k^2) &= \Sigma_{\mathrm{T}}^{ZZ}(k^2) - \delta M_{\mathrm{Z}}^2 + (k^2 - M_{\mathrm{Z}}^2)\delta Z_{ZZ}, \\
\hat{\Sigma}_{\mathrm{T}}^{AA}(k^2) &= \Sigma_{\mathrm{T}}^{AA}(k^2) + k^2\delta Z_{AA}, \\
\hat{\Sigma}_{\mathrm{T}}^{AZ}(k^2) &= \Sigma_{\mathrm{T}}^{AZ}(k^2) + k^2\frac{1}{2}\delta Z_{AZ} + (k^2 - M_{\mathrm{Z}}^2)\frac{1}{2}\delta Z_{ZA}
\end{aligned} \tag{4.1.9}$$

with

$$\begin{aligned}
\delta M_{\mathrm{W}}^2 &= \Sigma_{\mathrm{T}}^{W}(M_{\mathrm{W}}^2), \qquad \delta M_{\mathrm{Z}}^2 = \Sigma_{\mathrm{T}}^{ZZ}(M_{\mathrm{Z}}^2), \\
\delta Z_{ZA} &= \frac{2}{M_{\mathrm{Z}}^2}\Sigma_{\mathrm{T}}^{AZ}(0), \qquad \delta Z_{AZ} = -\frac{2}{M_{\mathrm{Z}}^2}\Sigma_{\mathrm{T}}^{AZ}(M_{\mathrm{Z}}^2), \\
\delta Z_W &= -\Sigma_{\mathrm{T}}'^{W}(M_{\mathrm{W}}^2), \qquad \delta Z_{ZZ} = -\Sigma_{\mathrm{T}}'^{ZZ}(M_{\mathrm{Z}}^2), \\
\delta Z_{AA} &= -\Sigma_{\mathrm{T}}'^{AA}(0).
\end{aligned} \tag{4.1.10}$$

Equations (4.1.9) with (4.1.10) have exactly the form of the renormalized self-energies in the usual on-shell scheme, but without taking the real part of the counterterms. While in the on-shell scheme the self-energies are calculated in terms of the real renormalized masses M_{Z}^2 and M_{W}^2, in (4.1.9) and (4.1.10) the self-energies are to be calculated in terms of the complex masses μ_{Z}^2 and μ_{W}^2, although with real squared momenta. Note that this difference between usual on-shell and complex renormalization also changes the form of the IR divergence appearing in the W-field renormalization constant δZ_W. In the former scheme, it appears as logarithm $\ln m_\gamma$ of an infinitesimally small photon

mass (or as the related $1/(4-D)$ pole in dimensional regularization); in the latter, the W width regularizes the singularity via $\ln \Gamma_{\mathrm{W}}$.

Owing to its definition (4.0.1), the renormalization of the complex weak mixing angle is determined by

$$\frac{\delta s_{\mathrm{w}}}{s_{\mathrm{w}}} = -\frac{c_{\mathrm{w}}^2}{s_{\mathrm{w}}^2}\frac{\delta c_{\mathrm{w}}}{c_{\mathrm{w}}} = -\frac{c_{\mathrm{w}}^2}{2s_{\mathrm{w}}^2}\left(\frac{\delta\mu_{\mathrm{W}}^2}{\mu_{\mathrm{W}}^2} - \frac{\delta\mu_{\mathrm{Z}}^2}{\mu_{\mathrm{Z}}^2}\right). \tag{4.1.11}$$

The electric charge is fixed in the on-shell scheme by requiring that there are no higher-order corrections to the $ee\gamma$ vertex in the Thomson limit. In the CMS this condition reads

$$\frac{\delta e}{e} = \frac{1}{2}\Sigma'^{AA}(0) - \frac{s_{\mathrm{w}}}{c_{\mathrm{w}}}\frac{\Sigma_{\mathrm{T}}^{AZ}(0)}{\mu_{\mathrm{Z}}^2}. \tag{4.1.12}$$

Because of the presence of the complex masses in the loop integrals, the charge renormalization constant and thus the renormalized charge become complex. Since the imaginary part of the bare charge vanishes, the imaginary part of the charge renormalization constant is directly fixed by the imaginary part of self-energies. In a one-loop calculation, the imaginary part of the renormalized charge drops out in the corrections to the absolute square of the matrix element, because the charge factorizes from the lowest-order matrix element. Starting from the two-loop level, the imaginary part has to be taken into account.

For a correct description of the resonances at the $\mathcal{O}(\alpha)$ level, we need the width including $\mathcal{O}(\alpha)$ corrections. The width is defined via (4.1.7). Using $\delta\mu_{\mathrm{W}}^2 = M_{\mathrm{W},0}^2 - \mu_{\mathrm{W}}^2$ and taking the imaginary part of (4.1.7) yields

$$M_{\mathrm{W}}\Gamma_{\mathrm{W}} = \mathrm{Im}\{\Sigma_{\mathrm{T}}^{W}(M_{\mathrm{W}}^2)\} - M_{\mathrm{W}}\Gamma_{\mathrm{W}}\,\mathrm{Re}\{\Sigma_{\mathrm{T}}'^{W}(M_{\mathrm{W}}^2)\} + \mathcal{O}(\alpha^3), \tag{4.1.13}$$

which can be iteratively solved for Γ_{W}. In $\mathcal{O}(\alpha^2)$, i.e. including first-order corrections to the width, the result is equivalent to the one obtained in the usual on-shell scheme. To this order the imaginary part of the self-energy is required in two-loop accuracy, but it can be more easily obtained by calculating the one-loop corrections to the decay processes $\mathrm{W} \to \bar{f}f'$ [36]. In our numerical calculation, we calculate the width from the decay processes including $\mathcal{O}(\alpha)$ corrections [16].

In our calculation we consider external fermions only in the massless limit, in which these fermions are stable. Therefore, the corresponding on-shell self-energies do not involve any absorptive parts. Nevertheless they become complex via the complex renormalized weak mixing angle and the complex gauge-boson masses, and thus the field renormalization constants $\delta\mathcal{Z}_{f,\sigma}$ of the fermion fields f^σ, defined by

$$f_0^\sigma = (1 + \tfrac{1}{2}\delta\mathcal{Z}_{f,\sigma})f^\sigma, \qquad \sigma = \mathrm{R}, \mathrm{L}, \tag{4.1.14}$$

become complex. As in the case of $\delta\mathcal{Z}_W$, also these complex field renormalization constants apply both for fermions and antifermions, i.e. fields and antifields are not connected by complex conjugation anymore. Explicitly the $\delta\mathcal{Z}_{f,\sigma}$ are given by

$$\delta\mathcal{Z}_{f,\sigma} = -\Sigma^{f,\sigma}(m_f^2) - m_f^2\left[\Sigma'^{f,\mathrm{R}}(m_f^2) + \Sigma'^{f,\mathrm{L}}(m_f^2) + 2\Sigma'^{f,\mathrm{S}}(m_f^2)\right], \quad (4.1.15)$$

where $\sigma = \mathrm{R}, \mathrm{L}$ refers to the right- and left-handed components of the fermion self-energy $\Sigma^f(p)$ following the conventions of Ref. [52]. Note that again no real part was taken in this relation in contrast to the usual on-shell renormalization. In contrast to $\delta\mathcal{Z}_W$, there are soft IR divergences in the field renormalization constants $\delta\mathcal{Z}_f$ that are not regularized by finite widths but by the usual IR regulators such as m_γ.

In the massless limit, the fermion-mass renormalization constant δm_f tends to zero, and the quark-mixing matrix, if assumed to be different from the unit matrix, need not be renormalized. Since the top-quark and the Higgs boson do not appear in the lowest-order matrix elements for the processes under consideration, the corresponding mass and field counterterms are not needed in our calculation. Also the gauge-fixing term need not be renormalized.

In summary, in the CMS the usual renormalization conditions of the on-shell scheme can be used, but without taking any real parts. All parameters, in particular also the renormalization points, become complex. The calculation of self-energies with complex momentum arguments can be avoided by expanding these about real values. Performing these expansions appropriately and neglecting (UV-finite) higher-order terms, the renormalized self-energies are obtained just as in the usual on-shell scheme with renormalization constants determined for real momenta. However, all the mass arguments are complex and no real parts must be taken.

4.2 Complex renormalization – Background-field gauge

Using the background-field method, the gauge-boson field renormalization constants can be determined in terms of the parameter renormalization in such a way that Ward identities possess the same form before and after renormalization [48]. Real parameters have to be substituted by the corresponding complex parameters everywhere when the complex renormalization is employed. The complex parameter renormalization is fixed as above in (4.1.7), (4.1.11) and (4.1.12). Note that $\Sigma_{\mathrm{T}}^{AZ}(0)$ vanishes in the background-field gauge as a consequence of the background-field gauge invariance of the effective action, which in particular simplifies the charge renormalization constant (4.1.12).

Since the gauge-boson field renormalization constants drop out in the S-matrix elements without external gauge-boson fields, we can alternatively also use the definitions in (4.1.8) in the calculation.

4.3 Complex renormalization – Loop integrals

The consistent use of complex gauge-boson masses requires to use these also in the loop integrals. Thus, we need one-loop integrals with complex internal masses. The IR-singular integrals can be found in Ref. [57]. Concerning the non-IR singular cases, we have analytically continued the results of Ref. [56] for the 2-point and 3-point functions[‡], and the relevant results of Ref. [58] for the 4-point functions. We have checked all these results by independent direct calculation of the Feynman-parameter integrals.[§]

[‡]Note that the result of Ref. [56] for the scalar two-point function is not valid in general for complex masses. In this case an extra η function has to be added. The same comment applies to the results for the 2-point tensor integrals in Ref. [55].

[§]The described work on the loop integrals has been carried out by A. Denner and S. Dittmaier.

Chapter 5

Numerical results

5.1 Input parameters and setup

The numerical results are based on the same set of input parameters as in Ref. [44]:

$$
\begin{array}{llll}
G_\mu &= 1.16637 \times 10^{-5}\,\mathrm{GeV}^{-2}, & \alpha(0) = 1/137.03599911, & \alpha_\mathrm{s} = 0.1187, \\
M_\mathrm{W} &= 80.425\,\mathrm{GeV}, & M_\mathrm{Z} = 91.1876\,\mathrm{GeV}, & \Gamma_\mathrm{Z} = 2.4952\,\mathrm{GeV}, \\
M_\mathrm{H} &= 115\,\mathrm{GeV}, & & \\
m_\mathrm{e} &= 0.51099892\,\mathrm{MeV}, & m_\mu = 105.658369\,\mathrm{MeV}, & m_\tau = 1.77699\,\mathrm{GeV}, \\
m_\mathrm{u} &= 66\,\mathrm{MeV}, & m_\mathrm{c} = 1.2\,\mathrm{GeV}, & m_\mathrm{t} = 178\,\mathrm{GeV}, \\
m_\mathrm{d} &= 66\,\mathrm{MeV}, & m_\mathrm{s} = 150\,\mathrm{MeV}, & m_\mathrm{b} = 4.3\,\mathrm{GeV},
\end{array}
\tag{5.1.1}
$$

which essentially follows Ref. [71]. For the top-quark mass m_t we have taken the more recent value of Ref. [72]. The masses of the light quarks are adjusted to reproduce the hadronic contribution to the photonic vacuum polarization of Ref. [73]. Since we parametrize the lowest-order cross section with the Fermi constant G_μ (G_μ scheme), i.e. we derive the electromagnetic coupling α according to $\alpha_{G_\mu} = \sqrt{2} G_\mu M_\mathrm{W}^2 (1 - M_\mathrm{W}^2/M_\mathrm{Z}^2)/\pi$, the results are practically independent of the masses of the light quarks. Moreover, this procedure absorbs the corrections proportional to $m_\mathrm{t}^2/M_\mathrm{W}^2$ in the fermion–W-boson couplings and the running of $\alpha(Q^2)$ from $Q^2 = 0$ to the electroweak scale. In the relative radiative corrections, we use, however, $\alpha(0)$ as coupling parameter, which is the correct effective coupling for real photon emission.

QCD corrections are treated in the "naive" approach of multiplying cross sections and partial decay rates by factors $(1+\alpha_\mathrm{s}/\pi)$ per hadronically decaying

W boson. The W-boson width Γ_W is calculated from the above input including electroweak $\mathcal{O}(\alpha)$ and QCD corrections, yielding

$$\Gamma_W = 2.09269848\ldots \text{ GeV}. \tag{5.1.2}$$

This procedure ensures that the effective branching ratios for the leptonic, semileptonic, and hadronic W decays, which result from the integration over the decay fermions, add up to 1. In order to keep this normalization also for the IBA, Γ_W is calculated in the corresponding approximation, i.e. in the G_μ scheme without electroweak corrections, yielding

$$\Gamma_W\Big|_{\text{IBA}} = 2.10009936\ldots \text{ GeV}. \tag{5.1.3}$$

A detailed description of the IBA, as used in RacoonWW, can be found in Ref. [26]. The value for the Z decay width Γ_Z, which is needed because of the Z resonance in the ISR convolution below the W-pair threshold, is taken from experiment [71]. All other particles, including the top quark and the Higgs boson, are taken as stable.

5.2 Total and differential cross sections

5.2.1 Without phase-space cuts

In the following we discuss total cross sections without any phase-space cuts. The presented results have been published in Ref. [44] and are obtained with 10^7 events, using the subtraction method. Tables 5.1–5.3 show some representative results on total cross sections for the final states $\nu_\tau\tau^+\mu^-\bar{\nu}_\mu$, $u\bar{d}\mu^-\bar{\nu}_\mu$, and $u\bar{d}s\bar{c}$ in various approximations for different CM energies $\sqrt{s}$. The numbers in parentheses represent the uncertainties from Monte Carlo integration in the last digits of the predictions. Columns two and three in each table contain the two versions of the lowest-order cross section for the full $e^+e^- \to 4f$ processes corresponding to the different treatments of finite-width effects as provided by the "fixed-width scheme" (FW) and the complex-mass scheme (CMS). In the FW scheme the finite constant width, and thus the complex mass, is only inserted into the resonant propagators. The relative difference $\sigma_{\text{Born}}(\text{CMS})/\sigma_{\text{Born}}(\text{FW}) - 1$ of the schemes in lowest order is given by the numbers in square brackets in the third columns. Note that the difference is only 0.06% for the considered energies, so that it is not essential to which Born cross section we normalize relative corrections. We have not given an error on this difference, because the two Born predictions are strongly correlated. The fourth columns show the IBA [26] implemented in RacoonWW, which is based on universal corrections only and includes

$e^+e^- \to \nu_\tau \tau^+ \mu^- \bar{\nu}_\mu$

$\sqrt{s}$/GeV	Born(FW)	Born(CMS)	IBA	DPA	ee4f
161	50.04(2)	50.01(2)	37.18(2)	37.08(2)	37.95(2)
		[−0.06%]	[−25.67(6)%]	[−25.90(3)%]	[−24.12(4)%]
170	160.53(6)	160.44(6)	129.12(6)	129.17(6)	129.23(6)
		[−0.06%]	[−19.52(5)%]	[−19.53(3)%]	[−19.45(3)%]
189	216.57(8)	216.45(8)	191.89(8)	191.66(9)	190.89(9)
		[−0.06%]	[−11.35(5)%]	[−11.50(2)%]	[−11.81(3)%]
200	220.41(9)	220.29(9)	201.13(9)	200.04(10)	199.21(10)
		[−0.06%]	[−8.70(6)%]	[−9.24(2)%]	[−9.57(3)%]
500	86.95(5)	86.90(5)	92.79(5)	89.81(6)	89.13(6)
		[−0.06%]	[+6.78(9)%]	[+3.29(3)%]	[+2.57(4)%]
1000	33.35(2)	33.33(2)	38.04(4)	35.76(3)	35.37(3)
		[−0.06%]	[+14.12(14)%]	[+7.21(5)%]	[+6.12(6)%]

Table 5.1: Total cross sections in fb for $e^+e^- \to \nu_\tau \tau^+ \mu^- \bar{\nu}_\mu$ in Born approximation (in the fixed-width and complex-mass schemes), IBA, DPA, and using the full $\mathcal{O}(\alpha)$ correction (ee4f); all but the Born cross sections include higher-order ISR corrections.

solely the contributions of the CC03 diagrams; the numbers in square brackets are defined as $\delta_{\rm IBA} = \sigma_{\rm IBA}/\sigma_{\rm Born}({\rm CMS}) - 1$. The fifth columns show the DPA of RacoonWW*, which comprises also non-universal corrections [25]; the numbers in square brackets are defined as $\delta_{\rm DPA} = \sigma_{\rm DPA}/\sigma_{\rm Born}({\rm FW}) - 1$. We normalize $\sigma_{\rm DPA}$ to $\sigma_{\rm Born}$(FW), because the lowest-order part of the DPA is per default evaluated in the FW scheme in RacoonWW. Finally, the last columns (ee4f) contain the full one-loop corrections to $e^+e^- \to 4f$; the numbers in square brackets are defined as $\delta_{\rm ee4f} = \sigma_{\rm ee4f}/\sigma_{\rm Born}({\rm CMS}) - 1$. Here we normalize to $\sigma_{\rm Born}$(CMS), because the full $e^+e^- \to 4f$ calculation is consistently performed in the CMS. Note that all but the "Born" numbers include improvements by ISR effects beyond $\mathcal{O}(\alpha)$, as described in Ref. [25]. Additionally the results on the semileptonic and hadronic cross sections (all but the Born cross results) include naive QCD corrections, as explained in Section 5.1. For better illustration Figure 5.1 depicts the predictions for the energy ranges

*We recall that the DPA of RacoonWW goes beyond a pure pole approximation in two respects. The real-photonic corrections are based on the full $e^+e^- \to 4f + \gamma$ matrix elements, and the Coulomb singularity is included for off-shell W bosons. Further details can be found in Ref. [25].

$e^+e^- \to u\bar{d}\mu^-\bar{\nu}_\mu$

$\sqrt{s}$/GeV	Born(FW)	Born(CMS)	IBA	DPA	ee4f
161	150.15(7)	150.07(7)	115.75(7)	115.48(7)	118.12(8)
		[−0.06%]	[−22.87(6)%]	[−23.09(3)%]	[−21.29(4)%]
170	481.6(2)	481.3(2)	402.0(2)	401.8(2)	402.1(2)
		[−0.06%]	[−16.48(5)%]	[−16.58(3)%]	[−16.47(3)%]
189	649.7(3)	649.4(3)	597.4(3)	596.1(3)	593.8(3)
		[−0.06%]	[−8.00(5)%]	[−8.26(3)%]	[−8.55(3)%]
200	661.3(3)	660.9(3)	626.2(3)	622.2(3)	619.7(3)
		[−0.06%]	[−5.26(6)%]	[−5.91(3)%]	[−6.24(3)%]
500	260.9(1)	260.8(1)	288.9(2)	279.6(2)	277.4(2)
		[−0.06%]	[+10.78(9)%]	[+7.14(4)%]	[+6.37(4)%]
1000	100.10(6)	100.04(6)	118.44(13)	111.45(9)	110.17(10)
		[−0.06%]	[+18.39(15)%]	[+11.34(5)%]	[+10.13(7)%]

Table 5.2: Total cross sections in fb for $e^+e^- \to u\bar{d}\mu^-\bar{\nu}_\mu$ in Born approximation (in the fixed-width and complex-mass schemes), IBA, DPA, and using the full $\mathcal{O}(\alpha)$ correction (ee4f); all but the Born cross sections include higher-order ISR and QCD corrections.

$e^+e^- \to u\bar{d}s\bar{c}$

$\sqrt{s}$/GeV	Born(FW)	Born(CMS)	IBA	DPA	ee4f
161	450.5(2)	450.3(2)	360.4(2)	359.7(2)	367.6(3)
		[−0.06%]	[−19.97(6)%]	[−20.16(4)%]	[−18.37(4)%]
170	1444.9(5)	1444.1(5)	1251.6(5)	1250.1(6)	1250.7(6)
		[−0.06%]	[−13.33(5)%]	[−13.49(3)%]	[−13.39(3)%]
189	1949.3(8)	1948.2(8)	1860.0(8)	1853.8(9)	1846.9(9)
		[−0.06%]	[−4.53(6)%]	[−4.90(3)%]	[−5.20(3)%]
200	1983.9(8)	1982.9(8)	1949.5(9)	1935.3(9)	1927.7(9)
		[−0.06%]	[−1.68(6)%]	[−2.45(3)%]	[−2.78(3)%]
500	782.9(4)	782.5(4)	899.4(5)	869.4(6)	862.9(6)
		[−0.06%]	[+14.94(9)%]	[+11.05(4)%]	[+10.27(4)%]
1000	300.3(2)	300.1(2)	368.7(4)	346.1(3)	342.1(3)
		[−0.06%]	[+22.86(16)%]	[+15.26(5)%]	[+13.98(7)%]

Table 5.3: As in Table 5.2, but for the process $e^+e^- \to u\bar{d}s\bar{c}$.

of LEP2 and of the high-energy phase of a future ILC, focusing on the leptonic final state $\nu_\tau\tau^+\mu^-\bar{\nu}_\mu$. The respective figures for the relative corrections δ to the semileptonic and hadronic final states look almost identical, up to an offset resulting from the QCD corrections.

A comparison between the DPA and the predictions based on the full $\mathcal{O}(\alpha)$ corrections reveals differences in the relative corrections δ of $\lesssim 0.5\%$ (0.7%) for CM energies ranging from $\sqrt{s} \sim 170\,\text{GeV}$ to 300 GeV (500 GeV). This is in agreement with the expected reliability of the DPA, as discussed in Refs. [20,24,25]. At higher energies, the deviations increase and reach 1−2% at $\sqrt{s} = 1{-}2\,\text{TeV}$. In the threshold region ($\sqrt{s} \lesssim 170\,\text{GeV}$), as expected, the DPA also becomes worse w.r.t. the full one-loop calculation, because the naive error estimate of $(\alpha/\pi) \times (\Gamma_\text{W}/M_\text{W})$ times some numerical safety factor of $\mathcal{O}(1{-}10)$ for the corrections missing in the DPA has to be replaced by $(\alpha/\pi) \times \Gamma_\text{W}/(\sqrt{s} - 2M_\text{W})$ in the threshold region and thus becomes large. In view of that, the DPA is even surprisingly good near threshold. For CM energies below 170 GeV the LEP2 cross section analysis was based on approximations like the shown IBA, which follows the full one-loop corrections even below the threshold at $\sqrt{s} = 2M_\text{W}$ within an accuracy of about 2%, as expected in Ref. [26]. The shape of the relative corrections in the threshold region is determined by ISR. The minimum in the relative corrections is correlated to the maximum in the slope of the total cross section.

A detailed comparison [20] between the DPA versions of Ref. [22], of YFSWW [23,24], and of RacoonWW [25,29,26] showed differences of the same order (or smaller) as the differences between the DPA of RacoonWW and the result based on the full one-loop calculation of $\text{e}^+\text{e}^- \to 4f$ discussed above. Therefore, these DPA predictions are consistent with the results based on the full one-loop calculation. The DPA version presented in Ref. [28], however, deviates from the full one-loop calculation by about 0.9% for typical LEP2 energies.

In addition to the above results which include ISR beyond $\mathcal{O}(\alpha)$ and QCD corrections, we present also explicit numbers that include only the genuine $\mathcal{O}(\alpha)$ corrections to facilitate a comparison to calculations made by other groups in the future. Table 5.4 shows the relative $\mathcal{O}(\alpha)$ corrections, i.e. without higher-order ISR improvements and without QCD corrections, both for the DPA of RacoonWW and for the full $\text{e}^+\text{e}^- \to 4f$ calculation for the three final states $\nu_\tau\tau^+\mu^-\bar{\nu}_\mu$, $\text{u}\bar{\text{d}}\mu^-\bar{\nu}_\mu$, and $\text{u}\bar{\text{d}}\text{s}\bar{\text{c}}$.

5.2.2 With phase-space cuts

In the following we discuss total and differential cross sections with phase-space cuts. The results of this section have been published in Ref. [45] and

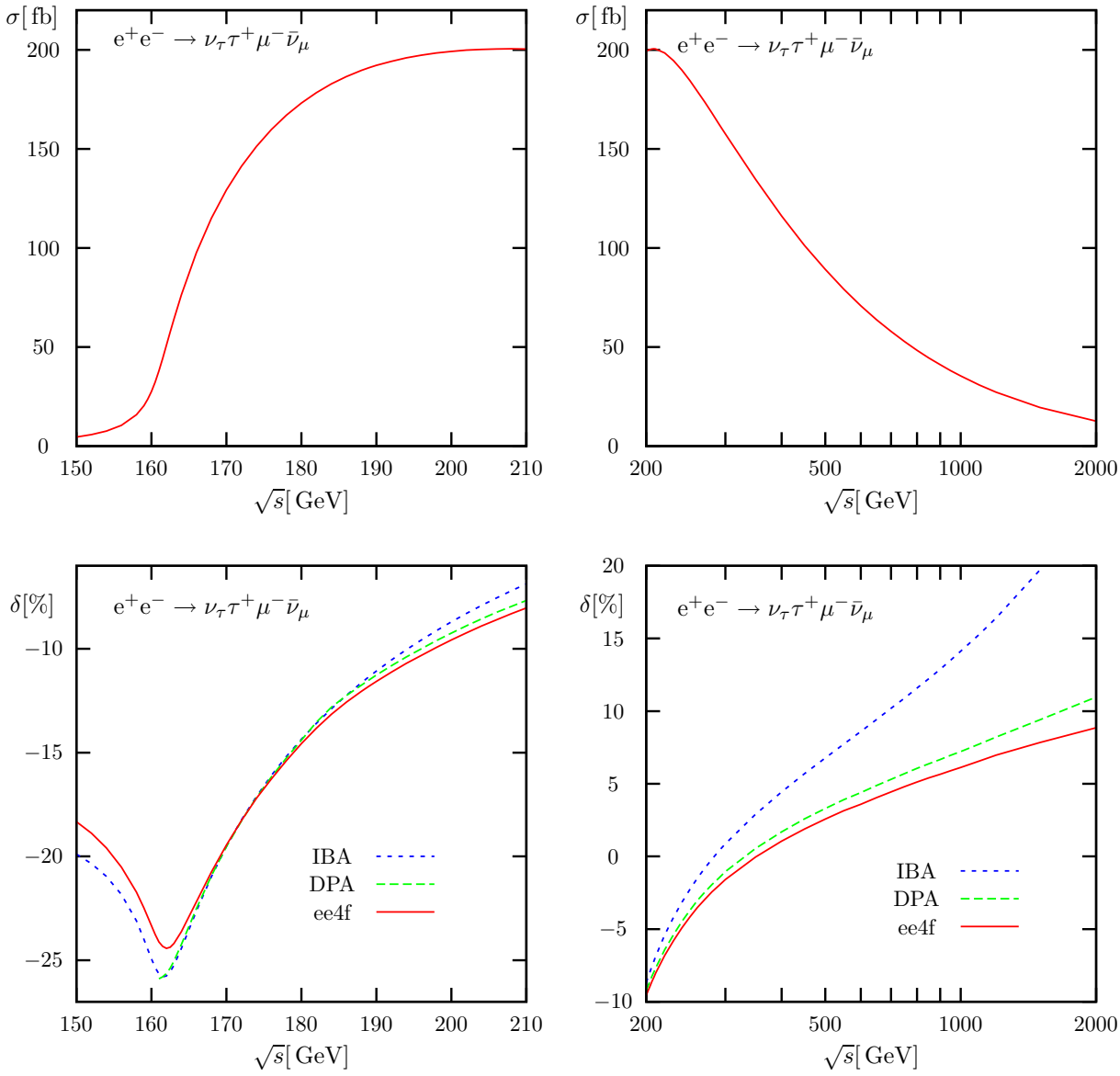

Figure 5.1: Absolute cross section σ (upper plots) and relative corrections δ (lower plots), as defined in the text, to the total cross section without cuts for $e^+e^- \to \nu_\tau \tau^+ \mu^- \bar{\nu}_\mu$ obtained from the IBA, DPA, and the full $\mathcal{O}(\alpha)$ calculation (ee4f). All predictions are improved by higher-order ISR.

$e^+e^- \to$	$\nu_\tau\tau^+\mu^-\bar{\nu}_\mu$		$u\bar{d}\mu^-\bar{\nu}_\mu$		$u\bar{d}s\bar{c}$	
$\sqrt{s}$/GeV	δ_{DPA}[%]	δ_{ee4f}[%]	δ_{DPA}[%]	δ_{ee4f}[%]	δ_{DPA}[%]	δ_{ee4f}[%]
161	−31.30(3)	−29.53(3)	−31.30(3)	−29.56(3)	−31.27(3)	−29.62(3)
170	−21.67(2)	−21.59(2)	−21.75(2)	−21.65(2)	−21.81(2)	−21.72(2)
189	−11.74(2)	−12.05(2)	−11.84(2)	−12.13(2)	−11.94(2)	−12.22(2)
200	−9.15(2)	−9.48(2)	−9.25(2)	−9.57(2)	−9.33(2)	−9.64(2)
500	+3.55(3)	+2.84(4)	+3.50(3)	+2.76(4)	+3.37(3)	+2.63(4)
1000	+7.08(5)	+5.98(6)	+7.16(5)	+5.98(7)	+6.89(5)	+5.69(7)

Table 5.4: Genuine relative $\mathcal{O}(\alpha)$ corrections, i.e. without higher-order ISR improvements and QCD corrections.

are obtained with 10^8 events, using the subtraction method. The setup differs from the one of the total cross sections of Section 5.2.1 only in the event selection. In contrast to the results of the last section, where no phase-space cuts were applied at all, we now impose selection cuts in conjunction with a photon recombination procedure. In detail, we adopt the same procedure as in Ref. [27]:

1. All bremsstrahlung photons within a cone of 5 degrees around the beams are treated as invisible, i.e. their momenta are disregarded when calculating angles, energies, and invariant masses.

2. Next, the invariant masses $M_{f\gamma}$ of the photon with each of the charged final-state fermions are calculated. If the smallest $M_{f\gamma}$ is smaller than $M_{\mathrm{rec}} = 25\,\mathrm{GeV}$ or if the energy of the photon is smaller than 1 GeV, the photon is combined with the charged final-state fermion that leads to the smallest $M_{f\gamma}$, i.e. the momenta of the photon and the fermion are added and associated with the momentum of the fermion, and the photon is discarded[†].

3. Finally, all events are discarded in which one of the charged final-state fermions is within a cone of 10 degrees around the beams (after a possible recombination with a photon). No other cuts are applied.

All but the lowest-order predictions include naive QCD corrections and improvements by ISR beyond $\mathcal{O}(\alpha)$, as described in Ref. [27].

[†]Except for the 1 GeV cut, the described cut and recombination procedure coincides with the one used in the first two papers of Ref. [25].

$\sqrt{s}$/GeV	Born(FW)	Born(CMS)	DPA	ee4f
$e^+e^- \to \nu_\tau\tau^+\mu^-\bar{\nu}_\mu$				
200	211.52(3)	211.40(3)	191.98(3)	191.18(3)
		[−0.06%]	[−9.24(1)%]	[−9.57(1)%]
500	62.17(1)	62.14(1)	65.48(2)	64.96(2)
		[−0.05%]	[+5.32(1)%]	[+4.54(1)%]
$e^+e^- \to u\bar{d}\mu^-\bar{\nu}_\mu$				
200	628.72(9)	628.37(9)	591.55(9)	589.11(10)
		[−0.06%]	[−5.91(1)%]	[−6.25(1)%]
500	180.83(4)	180.73(4)	197.87(5)	196.20(5)
		[−0.06%]	[+9.42(1)%]	[+8.56(2)%]
$e^+e^- \to u\bar{d}s\bar{c}$				
200	1868.9(3)	1867.8(3)	1822.6(3)	1815.3(3)
		[−0.06%]	[−2.48(1)%]	[−2.81(1)%]
500	526.1(1)	525.8(1)	597.1(2)	591.9(2)
		[−0.06%]	[+13.50(2)%]	[+12.58(2)%]

Table 5.5: Integrated cross sections in fb for $e^+e^- \to \nu_\tau\tau^+\mu^-\bar{\nu}_\mu$, $u\bar{d}\mu^-\bar{\nu}_\mu$, and $u\bar{d}s\bar{c}$ in Born approximation (in the fixed-width and complex-mass schemes), in DPA, and using the full $\mathcal{O}(\alpha)$ correction (ee4f); all but the Born cross sections include higher-order ISR and (if relevant) naive QCD corrections.

In this section we consider results for various distributions at $\sqrt{s} = 200\,\text{GeV}$ and $\sqrt{s} = 500\,\text{GeV}$ in the setup described above. For reference, in Table 5.5 we provide the corresponding integrated cross sections for the final states $\nu_\tau\tau^+\mu^-\bar{\nu}_\mu$, $u\bar{d}\mu^-\bar{\nu}_\mu$, and $u\bar{d}s\bar{c}$ in various approximations for different CM energies $\sqrt{s}$. Since the comments on the columns Born(FW), Born(CMS), DPA and ee4f of the tables of Section 5.2.1 also hold for table Table 5.5, we don't repeat them here. For $\sqrt{s} = 500\,\text{GeV}$ the difference between the predictions based on the full $\mathcal{O}(\alpha)$ corrections and on the DPA slightly increases by $\sim 0.1\%$ with respect to the results of the total cross section without phase-space cuts of Section 5.2.1. This tendency can be attributed to the fact that at high energies the cross section is dominated by forward-scattered nearly on-shell W-bosons. Such events are discarded by the cuts thus reducing the contribution of on-shell W-boson pairs and worsening the quality of the DPA.

For the differential distributions, we focus on the semileptonic process $e^+e^- \to u\bar{d}\mu^-\bar{\nu}_\mu$ in the following. The respective results for the final states $\nu_\tau\tau^+\mu^-\bar{\nu}_\mu$ and $u\bar{d}s\bar{c}$ look similar, up to an offset resulting from the QCD corrections; in particular, the difference between the DPA and the full $\mathcal{O}(\alpha)$ calculation are almost identical. We always display the lowest-order prediction (Born) and the result of the full one-loop calculation (ee4f) in the upper row of each figure. The relative corrections (in per cent) in the DPA approach (DPA), $\delta_{\mathrm{DPA}} = \mathrm{d}\sigma_{\mathrm{DPA}}/\mathrm{d}\sigma_{\mathrm{Born}}(\mathrm{FW}) - 1$, and in the full one-loop calculation (ee4f), $\delta_{\mathrm{ee4f}} = \mathrm{d}\sigma_{\mathrm{DPA}}/\mathrm{d}\sigma_{\mathrm{Born}}(\mathrm{CMS}) - 1$, are shown in the lower rows of the figures. These additionally include an inset depicting the relative difference between the full one-loop and the DPA calculation with respect to the DPA calculation, $\Delta = \mathrm{d}\sigma_{\mathrm{ee4f}}/\mathrm{d}\sigma_{\mathrm{DPA}} - 1$. We define all angles in the laboratory system, which is the CM system of the initial state. The momenta of the W^+ and W^- bosons are defined as

$$k_+ = k_1 + k_2, \qquad k_- = k_3 + k_4, \tag{5.2.1}$$

respectively, after a possible photon recombination. From these momenta the invariant masses of the virtual W bosons and their angles are calculated.

The invariant-mass distributions for the W^+ and W^- bosons are shown in Figures 5.2 and 5.3. From the plots for the relative corrections, it can be seen that the full one-loop corrections are smaller than the DPA corrections for invariant masses bigger than M_{W} and vice versa for invariant masses smaller than M_{W}. If neglected, this effect will give rise to a small shift in the direct reconstruction of the W-boson mass. The distribution in the cosine of the W^+ production angle θ_{W^+} is shown in Figure 5.4. While at LEP energies there is hardly any distortion of the shape induced by corrections beyond DPA, at 500 GeV the difference of the corrections in DPA and the complete $\mathcal{O}(\alpha)$ corrections rises from -1% to about -2.5% with increasing scattering angle. Note that such a distortion of the shape of the angular distribution can be a signal for anomalous triple gauge-boson couplings. The angular dependence of Δ is even more pronounced in the distribution in the decay angle $\theta_{\mathrm{W}^-\mu^-}$ presented in Figure 5.5. Note, however, that as a general feature the cross section is smallest where the corrections beyond DPA are largest. The distribution in the energy E_{μ^-} of the muon can be found in Figure 5.6. Again, for $\sqrt{s} = 200\,\mathrm{GeV}$ the corrections beyond DPA hardly depend on the muon energy in the interval $20\,\mathrm{GeV} \lesssim E_\mu \lesssim 80\,\mathrm{GeV}$, where two resonant W bosons are kinematically possible. Outside this interval, the DPA runs out of control, and the difference to the full calculation becomes big; but there the cross section is very small.

Finally, we consider the distributions in azimuthal angles that were also discussed in Ref. [27] including corrections in DPA. In Figure 5.7 we show the

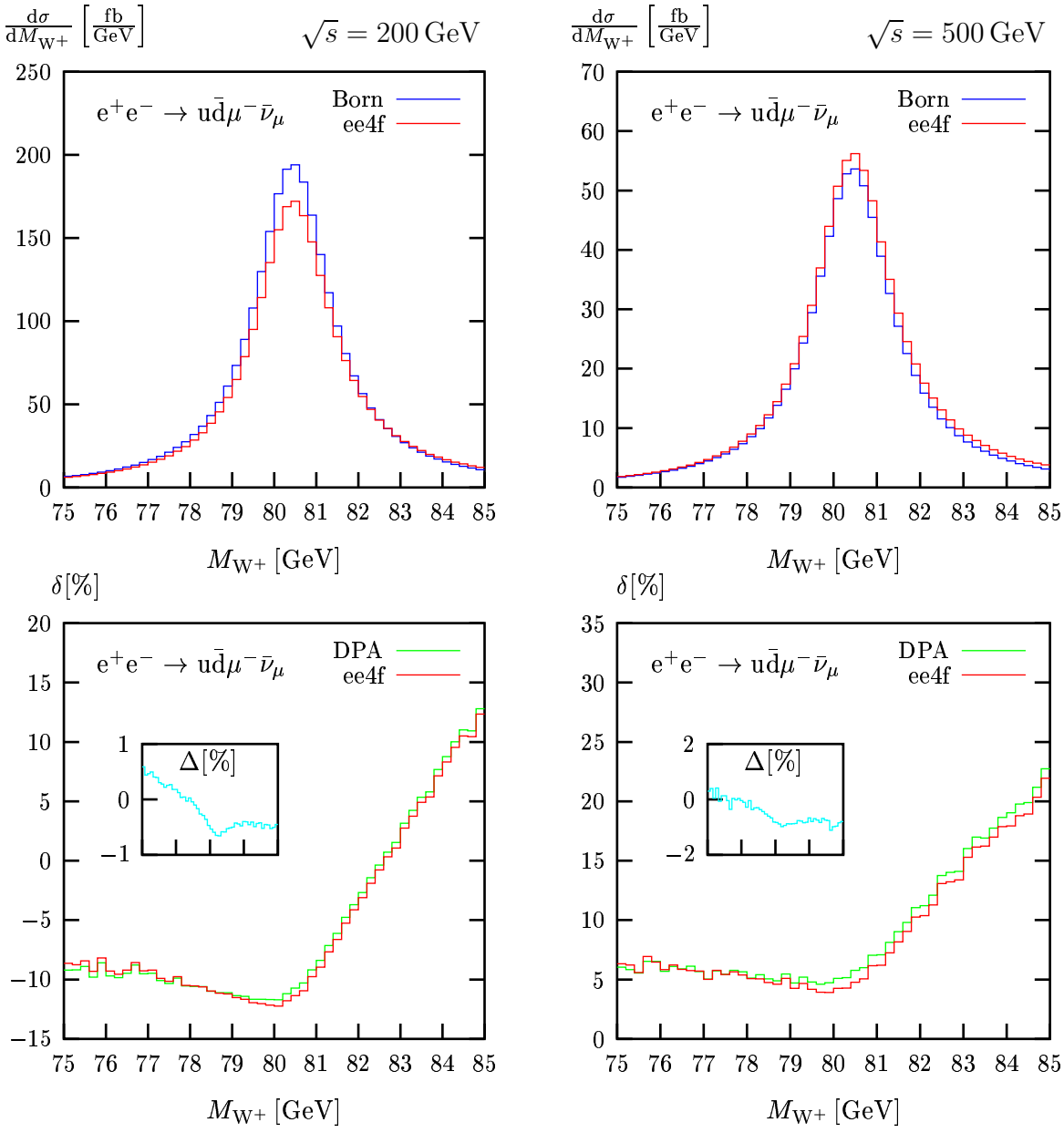

Figure 5.2: Distribution in the invariant mass of the W^+ boson (upper row) and the corresponding corrections (lower row) at $\sqrt{s} = 200\,\text{GeV}$ (l.h.s.) and $\sqrt{s} = 500\,\text{GeV}$ (r.h.s.) for $e^+e^- \to u\bar{d}\mu^-\bar{\nu}_\mu$. The inset plot shows the difference between the full $\mathcal{O}(\alpha)$ corrections and those in DPA.

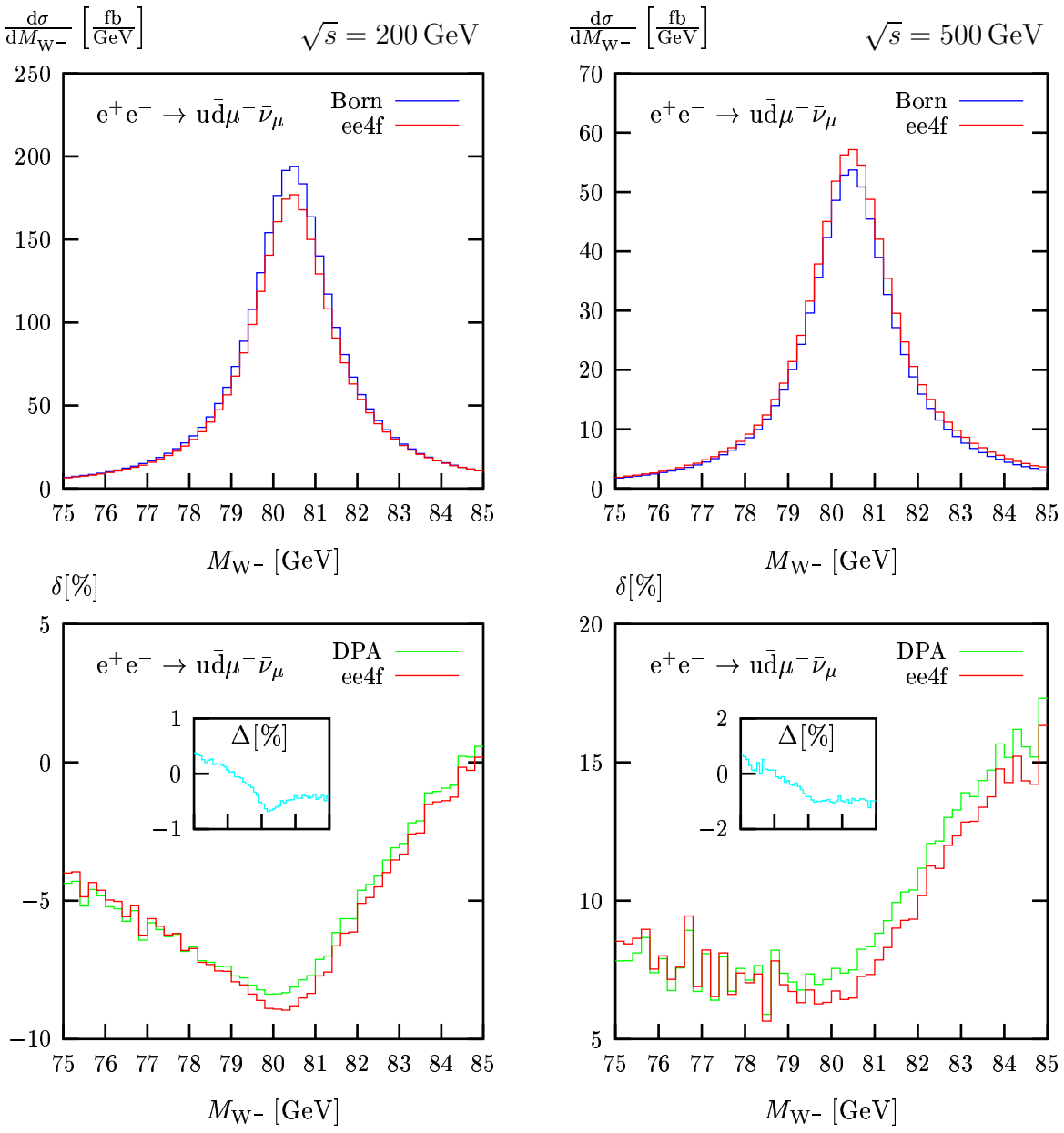

Figure 5.3: Distribution in the invariant mass of the W^- boson (upper row) and the corresponding corrections (lower row) at $\sqrt{s} = 200\,\text{GeV}$ (l.h.s.) and $\sqrt{s} = 500\,\text{GeV}$ (r.h.s.) for $e^+e^- \to u\bar{d}\mu^-\bar{\nu}_\mu$. The inset plot shows the difference between the full $\mathcal{O}(\alpha)$ corrections and those in DPA.

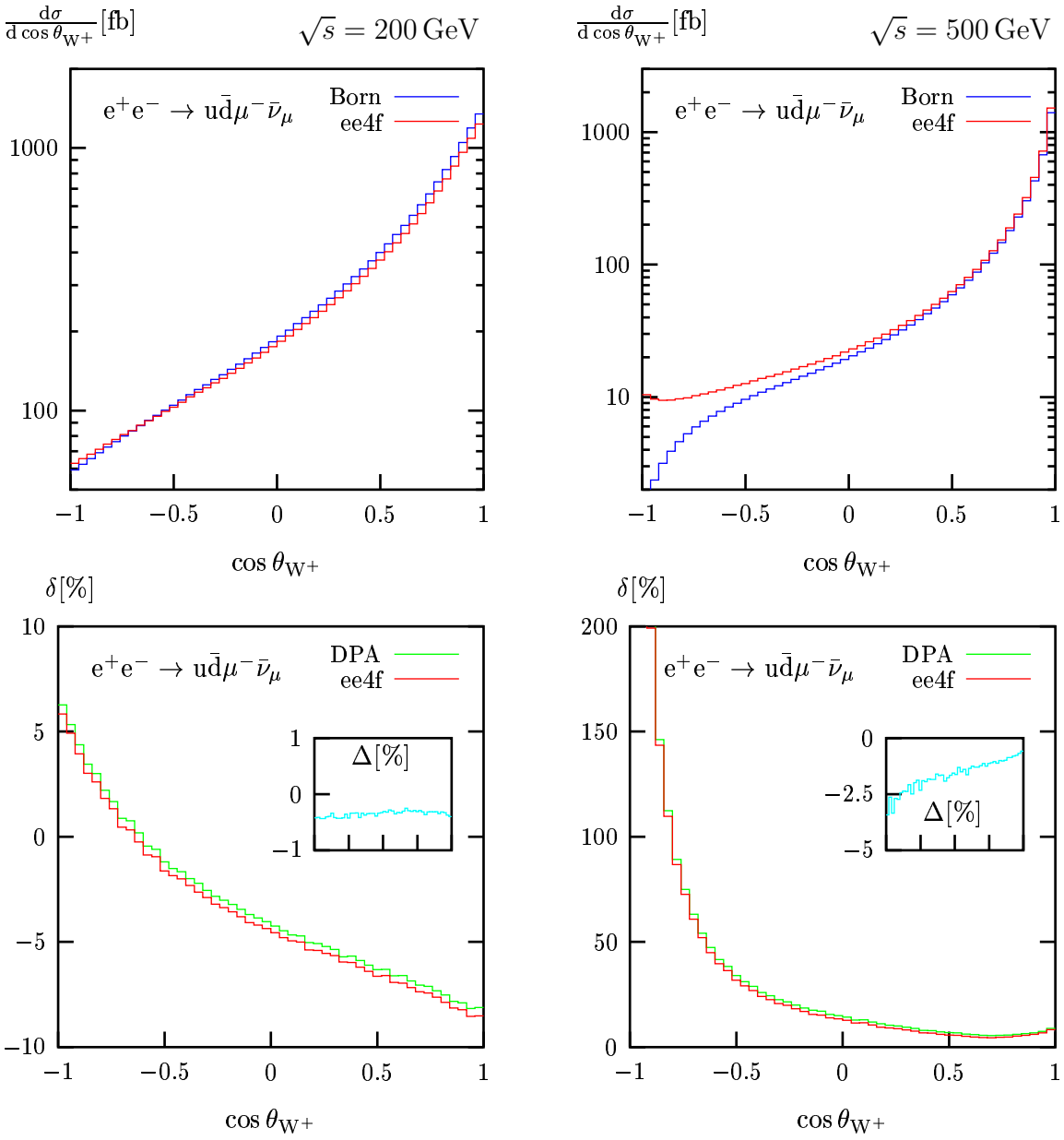

Figure 5.4: Distribution in the cosine of the W^+ production angle with respect to the e^+ beam (upper row) and the corresponding corrections (lower row) at $\sqrt{s} = 200\,\text{GeV}$ (l.h.s.) and $\sqrt{s} = 500\,\text{GeV}$ (r.h.s.) for $e^+e^- \to u\bar{d}\mu^-\bar{\nu}_\mu$. The inset plot shows the difference between the full $\mathcal{O}(\alpha)$ corrections and those in DPA.

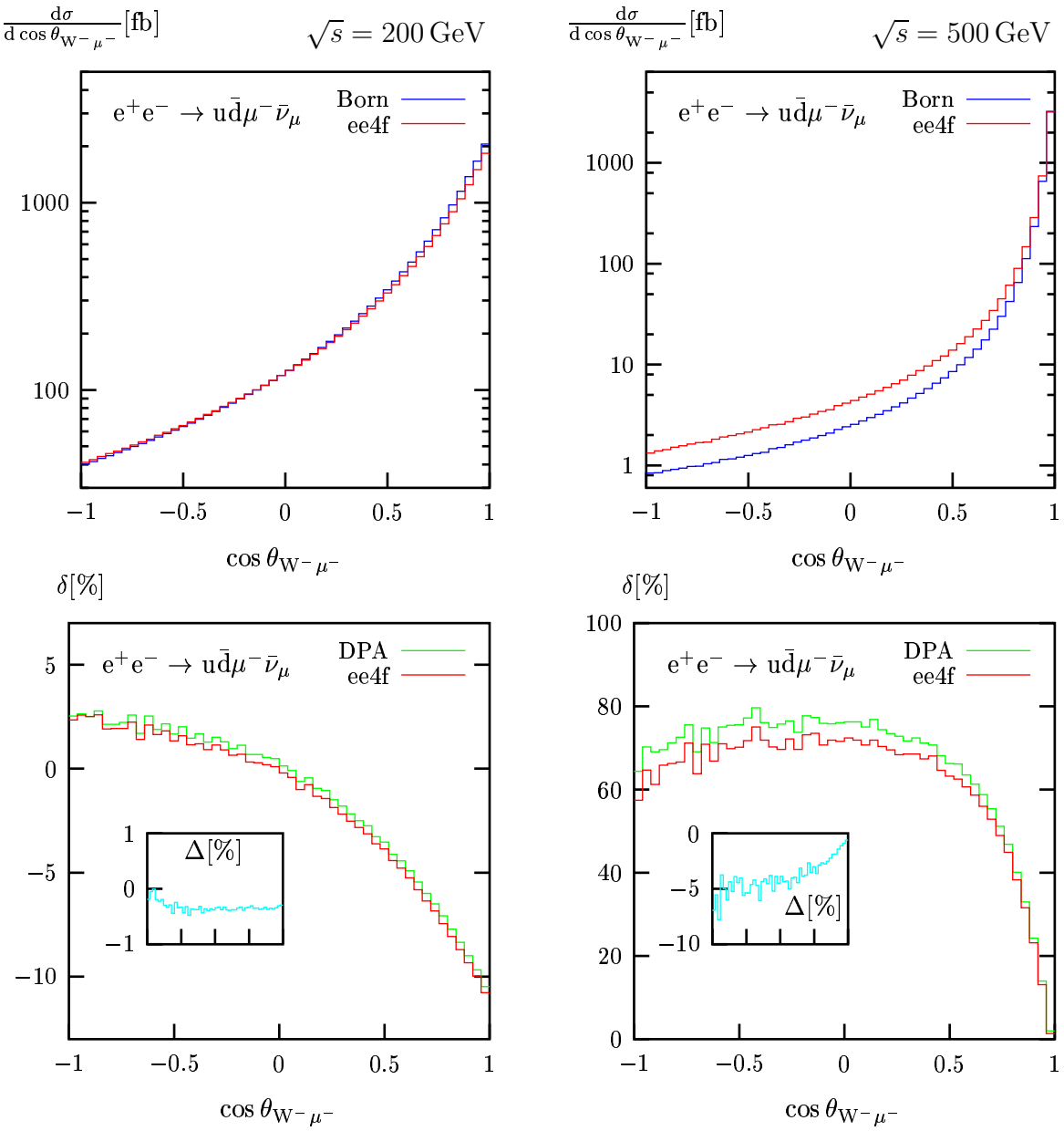

Figure 5.5: Distribution in the cosine of the μ^- decay angle with respect to the W^- direction (upper row) and the corresponding corrections (lower row) at $\sqrt{s} = 200\,\text{GeV}$ (l.h.s.) and $\sqrt{s} = 500\,\text{GeV}$ (r.h.s.) for $e^+e^- \to u\bar{d}\mu^-\bar{\nu}_\mu$. The inset plot shows the difference between the full $\mathcal{O}(\alpha)$ corrections and those in DPA.

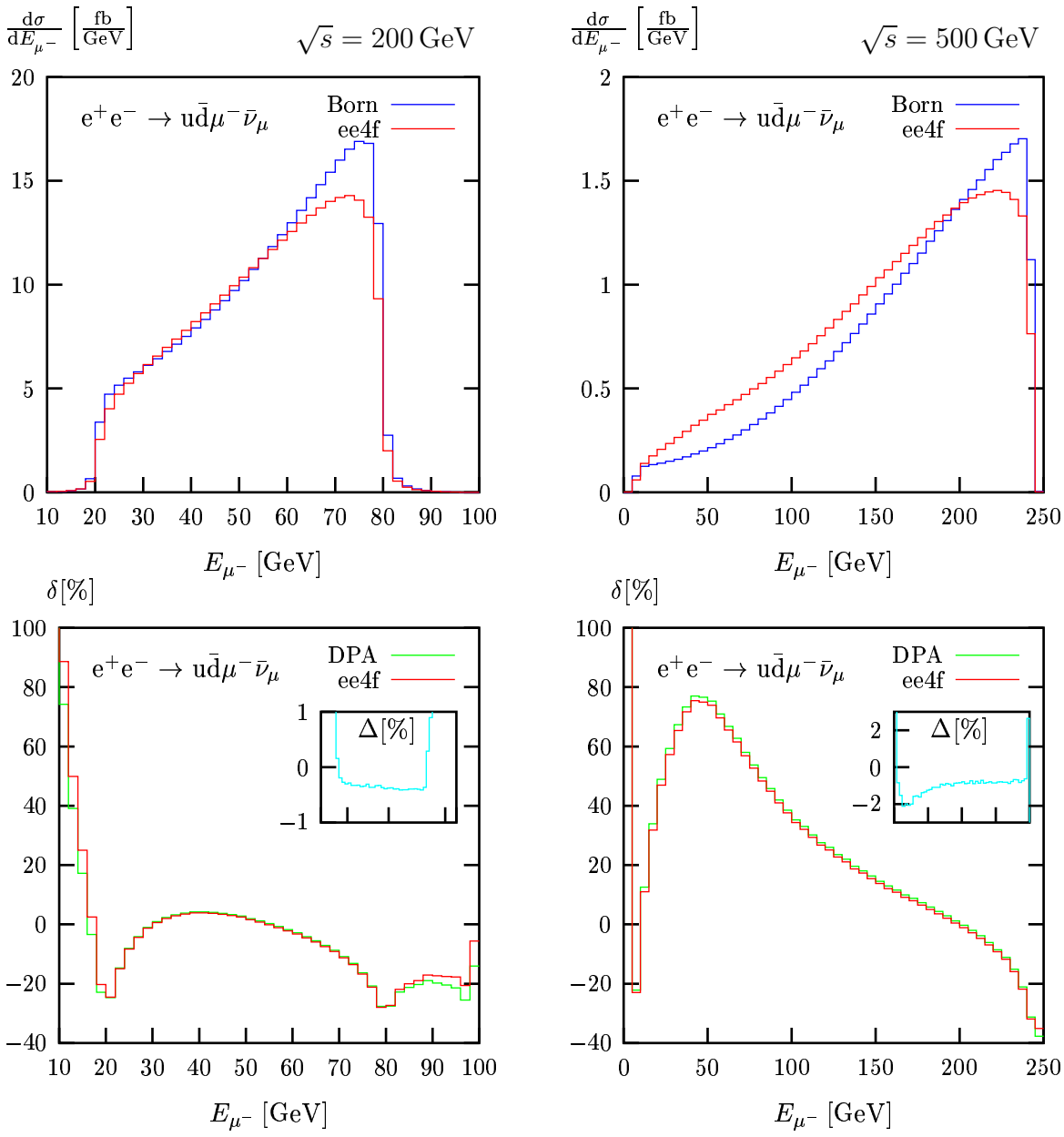

Figure 5.6: Distribution in the energy of the μ^- (upper row) and the corresponding corrections (lower row) at $\sqrt{s} = 200\,\text{GeV}$ (l.h.s.) and $\sqrt{s} = 500\,\text{GeV}$ (r.h.s.) for $e^+e^- \to u\bar{d}\mu^-\bar{\nu}_\mu$. The inset plot shows the difference between the full $\mathcal{O}(\alpha)$ corrections and those in DPA

distributions in the azimuthal decay angle ϕ_{W^+} of the W^+ boson, i.e. the angle between the decay plane of the W^+ and the plane of W-pair production,

$$\begin{aligned} \cos\phi_{\mathrm{W}^+} &= \frac{(\mathbf{k}_+ \times \mathbf{p}_+)(\mathbf{k}_+ \times \mathbf{k}_1)}{|\mathbf{k}_+ \times \mathbf{p}_+||\mathbf{k}_+ \times \mathbf{k}_1|}, \\ \mathrm{sgn}(\sin\phi_{\mathrm{W}^+}) &= \mathrm{sgn}\left\{\mathbf{k}_+ \cdot [(\mathbf{k}_+ \times \mathbf{p}_+) \times (\mathbf{k}_+ \times \mathbf{k}_1)]\right\}. \end{aligned} \tag{5.2.2}$$

Here, in particular at 200 GeV the difference between DPA and the full $\mathcal{O}(\alpha)$ corrections is approximately proportional to $\sin\phi_{\mathrm{W}^+}$ plus some constant offset. In the DPA, it can be deduced from Appendix A of Ref. [22], that the contributions of the imaginary parts of the one-loop coefficient functions always involve a factor $\sin\phi_{\mathrm{W}^+}$ or a factor $\sin\phi_{\mathrm{W}^-}$ together with symmetric functions in these angles. Contributions of real parts, on the other hand, are symmetric in these angles. In order to illustrate this feature, we have included an extra curve in the plots for the relative corrections to this distribution labelled "DPA (real)". In this curve, we have switched off all imaginary parts in the DPA calculation, apart from the finite width in the resonant propagators. As expected, these results are symmetric in the angle ϕ_{W^+} about 180°. The contribution proportional to $\sin\phi_{\mathrm{W}^+}$ in the difference of the full $\mathcal{O}(\alpha)$ calculation with respect to the DPA (real) is even larger than the corresponding difference with respect to the complete DPA. These properties of the DPA suggest, that also the sinusoidal dependence on ϕ_{W^+} in the latter difference results from imaginary parts. A possible source could be the missing imaginary parts of the counterterms in DPA.

The distributions in the angle ϕ between the two planes spanned by the momenta of the two fermion pairs in which the W bosons decay, i.e. (note that $\mathbf{k}_+ = -\mathbf{k}_-$ for non-photonic events)

$$\begin{aligned} \cos\phi &= \frac{(\mathbf{k}_+ \times \mathbf{k}_1)(-\mathbf{k}_- \times \mathbf{k}_3)}{|\mathbf{k}_+ \times \mathbf{k}_1||-\mathbf{k}_- \times \mathbf{k}_3|}, \\ \mathrm{sgn}(\sin\phi) &= \mathrm{sgn}\left\{\mathbf{k}_+ \cdot [(\mathbf{k}_+ \times \mathbf{k}_1) \times (-\mathbf{k}_- \times \mathbf{k}_3)]\right\}, \end{aligned} \tag{5.2.3}$$

are presented in Figure 5.8. The large corrections for angles ϕ near 0° or 180°, i.e. if the two decay planes coincide, result from the suppression of hard photonic corrections [27]. The corrections beyond DPA do hardly depend on ϕ.

5.3 Remaining theoretical uncertainties

We have reduced the TU for the charged-current processes $\mathrm{e}^+\mathrm{e}^- \to \nu_\tau\tau^+\mu^-\bar{\nu}_\mu$, $\mathrm{u\bar{d}}\mu^-\bar{\nu}_\mu$, $\mathrm{u\bar{d}s\bar{c}}$, in particular in the threshold region of W-pair production, considerably by calculating the full $\mathcal{O}(\alpha)$ corrections [44]. ISR beyond

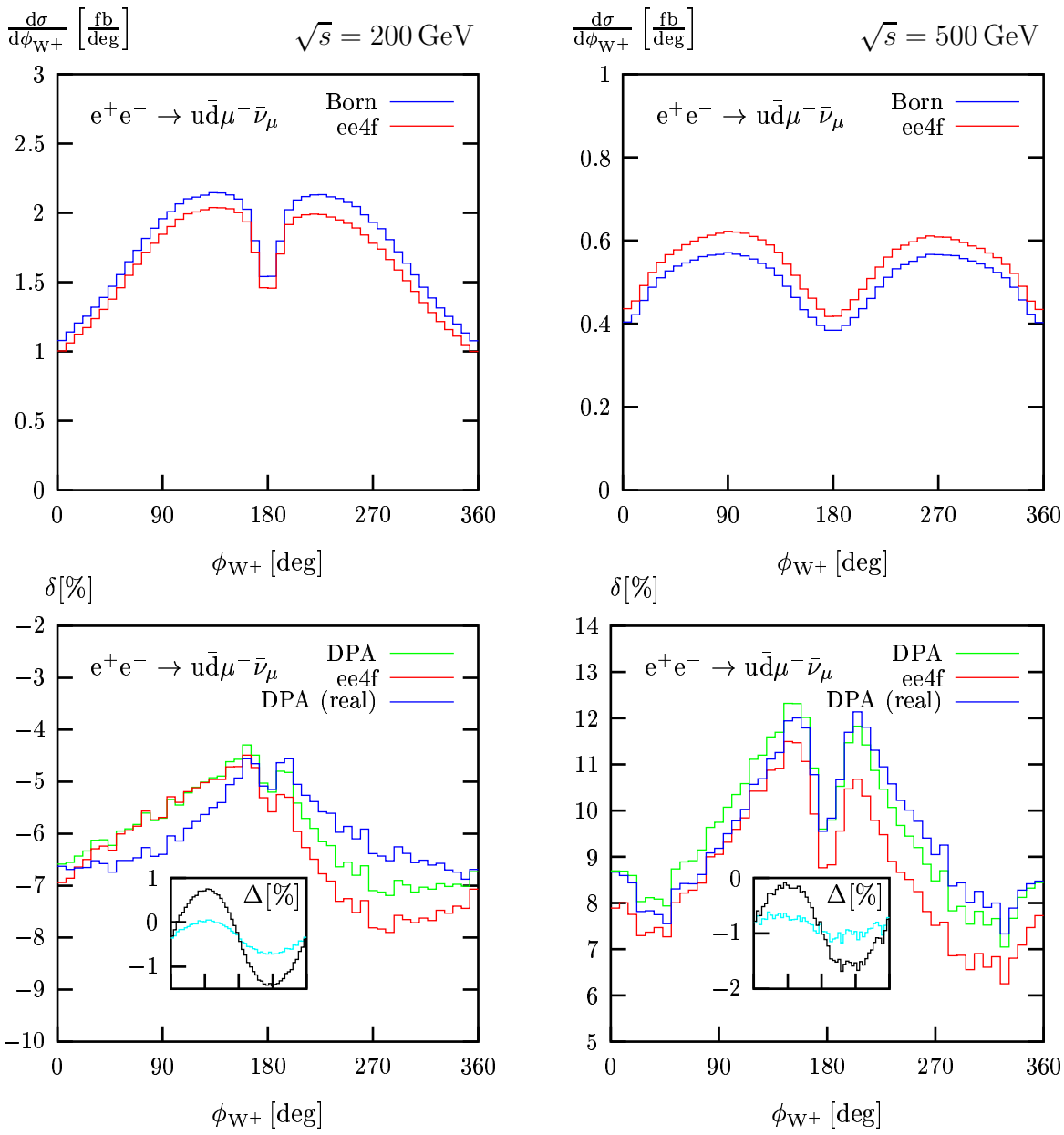

Figure 5.7: Distribution in the azimuthal decay angle of the W^+ (upper row) and the corresponding corrections (lower row) at $\sqrt{s} = 200\,\text{GeV}$ (l.h.s.) and $\sqrt{s} = 500\,\text{GeV}$ (r.h.s.) for $e^+e^- \to u\bar{d}\mu^-\bar{\nu}_\mu$. The inset plot shows the difference of the full $\mathcal{O}(\alpha)$ corrections to those in DPA and the larger difference to those in DPA (real), which is calculated without imaginary parts.

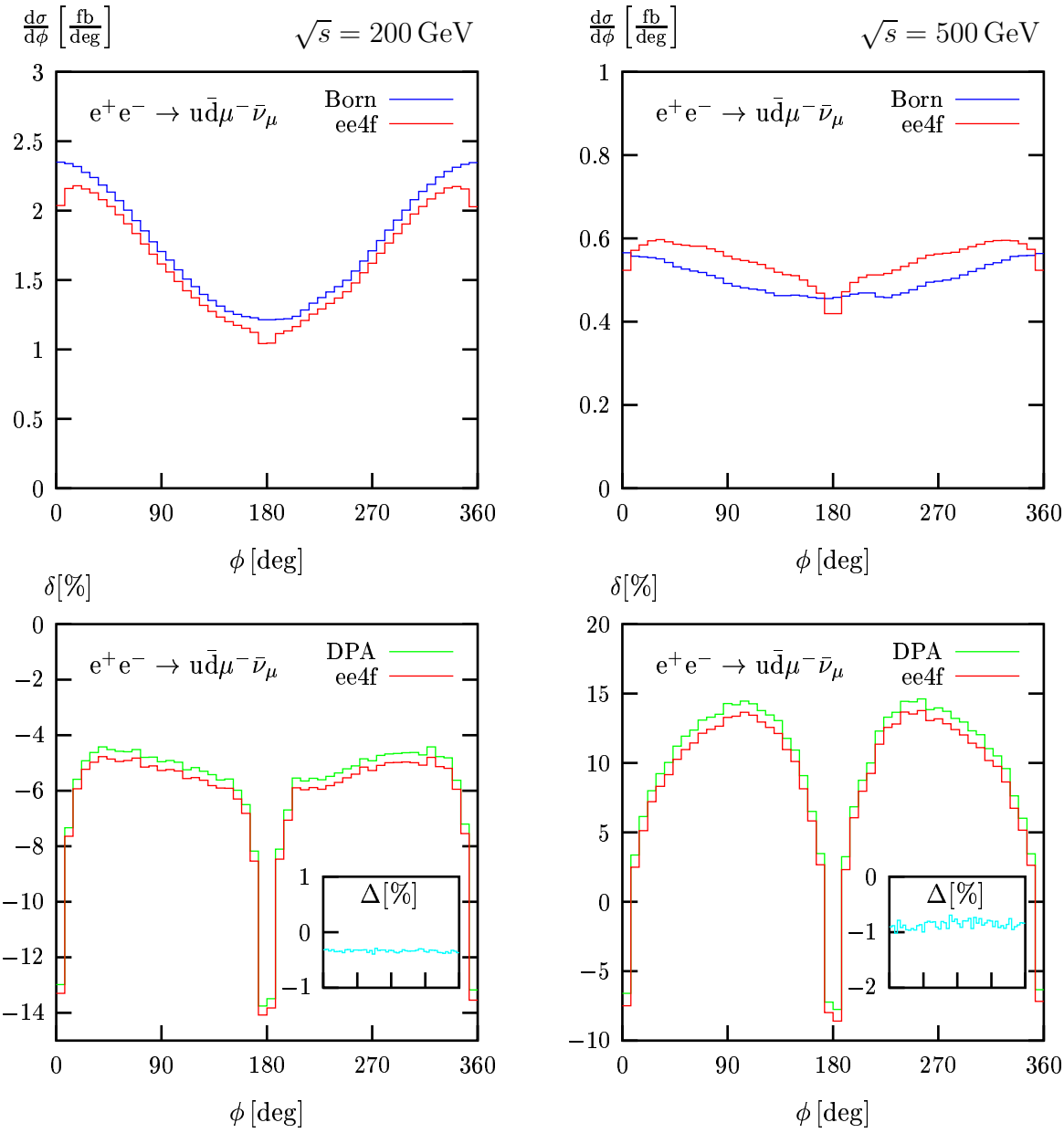

Figure 5.8: Distribution in the azimuthal angle ϕ (upper row) and the corresponding corrections (lower row) at $\sqrt{s} = 200\,\text{GeV}$ (l.h.s.) and $\sqrt{s} = 500\,\text{GeV}$ (r.h.s.) for $e^+e^- \to u\bar{d}\mu^-\bar{\nu}_\mu$. The inset plot shows the difference between the full $\mathcal{O}(\alpha)$ corrections and those in DPA.

$\mathcal{O}(\alpha)$ is included via structure functions in leading-logarithmic accuracy. For energies below $\sim 500\,\text{GeV}$, the remaining uncertainties resulting from missing electroweak corrections are then dominated by the next-to-leading logarithmic electromagnetic corrections of order $(\alpha/\pi)^2 \log(m_\text{e}^2/s)$ which can be estimated to contribute $\lesssim 0.1\%$. Near the W-pair-production threshold, higher-order effects of the Coulomb singularity are still missing. These are estimated to $\sim 0.2\%$ [75,76] for the total cross sections. Thus, we estimate the theoretical uncertainty due to unknown electroweak higher-order effects in the present calculation of the total cross sections to be a few 0.1% from the threshold region to about $\sim 500\,\text{GeV}$. At higher energies leading and subleading electroweak high-energy logarithms, such as Sudakov logarithms, beyond one loop have to be taken into account in addition to match this accuracy.

For a thorough estimate of the total theoretical uncertainty an inclusion of QCD effects is indispensable for the processes involving final-state quarks. In order to reach a precision of the order of a few 0.1% there, it is certainly necessary to improve the treatment of $\mathcal{O}(\alpha_\text{s})$ corrections (and beyond), including a proper matching with parton showers. Bose–Einstein and colour interconnection effects may also play an important role. For differential distributions the uncertainties from QCD effects are even more relevant.

Chapter 6

Conclusions

We have presented results on total and differential cross sections, as well as technical and conceptual details of our calculation for the charged-current four-fermion production processes $e^+e^- \to \nu_\tau\tau^+\mu^-\bar{\nu}_\mu$, $u\bar{d}\mu^-\bar{\nu}_\mu$, $u\bar{d}s\bar{c}$ which, for the first time, include the complete electroweak $\mathcal{O}(\alpha)$ corrections.

In particular, we have described a method how the $\mathcal{O}(10^3)$ occurring different spinor structures can be algebraically reduced to a few simple standard structures. The presented algorithm and the mechanisms for reducing and simplifying amplitudes, which shorten the analytical results considerably and thereby render the resulting computer code relatively short, is useful for other future calculations.

Moreover, a concept for consistently performing one-loop calculations with complex masses, to account for the finite widths of unstable particles, is presented. Technically the complex masses are introduced via an appropriate complex renormalization prescription at the level of the Lagrangian, so that the usual machinery of perturbation theory (Feynman rules etc.) can be used to organize the calculation. Since therefore the theory is not changed at all, there is no danger of double counting terms. The complex mass parameters, which also enter the weak mixing angle and coupling constants, can be viewed as an analytical continuation of the real masses. Consequently, all algebraic relations that follow from gauge invariance (Slavnov–Taylor identities, Ward identities, cancellation of gauge-parameter dependences) are valid in spite of the use of the complex masses which incorporate finite-width effects. The price to pay for this method is that all one-loop integrals have to be performed with complex mass parameters.

A comparison with the predictions for the total cross section without phase-space cuts based on the double-pole approximation (DPA) provided by the generator RacoonWW reveals corrections beyond DPA of $\lesssim 0.5\%$ (0.7%) for CM energies ranging from $\sqrt{s} \sim 170\,\text{GeV}$ to $300\,\text{GeV}$ ($500\,\text{GeV}$), consistent

with previous estimates on the intrinsic DPA uncertainty. The difference to the DPA increases to 1−2% for $\sqrt{s} \sim 1-2\,\text{TeV}$. At threshold, where predictions had to be based on an improved Born approximation (IBA) at LEP2, the full $\mathcal{O}(\alpha)$ calculation corrects the IBA by about 1.6%, which is also consistent with a previous error estimate. The full $\mathcal{O}(\alpha)$ calculation, improved by higher-order effects from initial-state radiation (ISR), reduces the remaining theoretical uncertainty (TU) due to unknown electroweak higher-order effects to a few 0.1% for scattering energies from the threshold region up to $\sim 500\,\text{GeV}$; above this energy leading high-energy logarithms, such as Sudakov logarithms, beyond one loop have to be taken into account to match this accuracy. At this level of accuracy, also improvements in the treatment of QCD corrections to semileptonic and hadronic $\text{e}^+\text{e}^- \to 4f$ processes will be necessary in the future.

Finally, we considered total cross sections with phase-space cuts and showed the effects of the complete $\mathcal{O}(\alpha)$ corrections to various differential cross sections of physical interest. In particular, we have considered differential cross sections sensitive to imaginary parts, as in the distribution of the azimuthal decay angle of the W^+. The results for the differential cross sections have also been compared to predictions based on the DPA, revealing that the latter approximation is not sufficient to fully exploit the potential of a future linear collider in an analysis of W-boson pairs at high energies. Specifically, at (and above) a CM energy of 500 GeV the corrections beyond DPA induce a non-negligible distortion in angular distributions that could be misinterpreted as signal for anomalous triple gauge-boson couplings if not taking into account the full electroweak $\mathcal{O}(\alpha)$ corrections.

We have presented methods that were successfully used for the first complete $\mathcal{O}(\alpha)$ calculation of electroweak corrections to a process with six external particles and involving unstable particles in intermediate states. Processes of this type will become more and more important in the future.

Our methods are not specifically adapted to the considered process and therefore are helpful in precision calculations for similar processes at future colliders.

Appendix A

The spinor reduction in the Weyl–van der Waerden formalism

In this appendix we inspect the reduction algorithm of Section 3.2 within the Weyl–van der Waerden (WvdW) spinor formalism, which is particularly simple for massless particles. We consistently employ the conventions of Ref. [74] for the spinor method and highlight only those features that are crucial for our manipulations.

In this formalism, Dirac spinors and momenta of massless fermions are described by Weyl spinors p_A, $p_{\dot{A}} = (p_A)^*$ which are related to the four-momentum p_μ according to

$$p_\mu \sigma^\mu_{\dot{A}B} = p_{\dot{A}} p_B, \tag{A.0.1}$$

where $\sigma^\mu_{\dot{A}B}$ denote the unit matrix ($\mu = 0$) and the Pauli matrices ($\mu = 1, 2, 3$). The matrices σ^μ also appear as the non-vanishing blocks in the Dirac matrices γ^μ. Thus, Dirac spinor chains translate into chains involving Weyl spinors and σ^μ matrices. Coupled chains can be separated by using the relation

$$\sigma^\mu_{\dot{A}B} \sigma_{\mu,\dot{C}D} = 2\epsilon_{\dot{A}\dot{C}} \epsilon_{BD}, \tag{A.0.2}$$

where ϵ_{AB} is the totally antisymmetric tensor in two dimensions and $\epsilon_{\dot{A}\dot{B}}$ is its complex conjugate. In this way, all Weyl spinors get contracted in so-called spinor products

$$\langle p_i p_j \rangle = \epsilon^{AB} p_{i,A} p_{j,B} \tag{A.0.3}$$

or their complex conjugates. Using (A.0.2), Lorentz products can also be translated into spinor products. We illustrate the above considerations by the simplest examples:

$$\begin{aligned}(p_i p_j) &= \frac{1}{2}\langle p_i p_j\rangle\langle p_i p_j\rangle^*,\\ \left[\not{p}_k\right]^-_{ij} &= \langle p_k p_i\rangle\langle p_k p_j\rangle^*,\\ \left[\not{p}_k\right]^+_{ij} &= \langle p_k p_i\rangle^*\langle p_k p_j\rangle.\end{aligned} \tag{A.0.4}$$

Dirac chains of the form (3.0.3) involving no additional $\epsilon^{\mu\nu\rho\sigma}$ can thus be directly reduced to a product of (at least four) spinor products. The totally antisymmetric tensor $\epsilon^{\mu\nu\rho\sigma}$ is translated into WvdW objects according to

$$\epsilon^{\mu\nu\rho\kappa} \;=\; \frac{\mathrm{i}}{4}\left(\sigma^{\mu}_{\dot{A}B}\sigma^{\nu,B\dot{C}}\sigma^{\kappa}_{\dot{C}D}\sigma^{\rho,D\dot{A}} - \sigma^{\mu}_{\dot{A}B}\sigma^{\rho,B\dot{C}}\sigma^{\kappa}_{\dot{C}D}\sigma^{\nu,D\dot{A}}\right), \tag{A.0.5}$$

so that contractions with $\epsilon^{\mu\nu\rho\sigma}$ can also be expressed in terms of WvdW spinor products. The two-dimensionality of the WvdW spinor space is rather restrictive and leads to the identity

$$\langle p_i p_j\rangle\langle p_k p_l\rangle + \langle p_i p_k\rangle\langle p_l p_j\rangle + \langle p_i p_l\rangle\langle p_j p_k\rangle = 0, \tag{A.0.6}$$

which frequently admits simplifications in complicated expressions. In the cases relevant for the considered processes, these identities allow to combine the sums that result from the application of (A.0.5), so that also all spinorial expressions involving contractions with $\epsilon^{\mu\nu\rho\sigma}$ can be reduced to a product of spinor products.

The identities (A.0.5) and (A.0.6) also allow to write the combinations A^{abcd}_{ijkl} of (3.2.7) as simple factors of spinor products:

$$\begin{aligned}A^{++-+}_{ijkl} &= \frac{1}{2}\langle p_i p_j\rangle\langle p_k p_l\rangle\langle p_i p_k\rangle^*\langle p_j p_l\rangle^*,\\ A^{+-++}_{ijkl} &= \frac{1}{2}\langle p_i p_l\rangle\langle p_k p_j\rangle\langle p_i p_j\rangle^*\langle p_k p_l\rangle^*,\\ A^{-+++}_{ijkl} &= \frac{1}{2}\langle p_i p_k\rangle\langle p_j p_l\rangle\langle p_i p_l\rangle^*\langle p_j p_k\rangle^*,\\ A^{abc-}_{ijkl} &= (A^{abc+}_{ijkl})^*.\end{aligned} \tag{A.0.7}$$

When expressing the A^{abcd}_{ijkl} in terms of spinor products, the relations (3.2.16)–(3.2.19) become trivial. The relations (A.0.7) and the fact that in the WvdW formalism all spinor chains can be expressed in terms of products of spinor products explains why in the formalism of Section 3.2 all spinor

chains could be reduced to a simple product of $A_{i\,j\,k\,l}^{a\,b\,c\,d}$ and scalar products. The results of (3.2.20) read in the WvdW formalism

$$\begin{aligned}
\left[\gamma^\mu\gamma^\nu\gamma^\rho\right]_{12}^{\sigma}\left[\gamma_\mu\gamma_\nu\gamma_\rho\right]_{34}^{\tau} &= 8(4\langle p_2p_4\rangle\langle p_1p_3\rangle^*\delta_{\tau_+}+\langle p_2p_3\rangle\langle p_1p_4\rangle^*\delta_{\tau_-})\delta_{\sigma+}\\
&\quad + 8(4\langle p_2p_4\rangle^*\langle p_1p_3\rangle\delta_{\tau_-}+\langle p_2p_3\rangle^*\langle p_1p_4\rangle\delta_{\tau_+})\delta_{\sigma-},\\
\left[\not{p}_3\gamma^\mu\gamma^\nu\right]_{12}^{\sigma}\left[\gamma_\nu\gamma^\rho\gamma^\kappa\right]_{34}^{-}\left[\gamma_\mu\gamma_\rho\gamma_\kappa\right]_{56}^{-} &= 32\langle p_3p_5\rangle\langle p_4p_6\rangle^*(\langle p_2p_3\rangle\langle p_1p_3\rangle^*\delta_{\sigma+}\\
&\quad + \langle p_1p_3\rangle\langle p_2p_3\rangle^*\delta_{\sigma_-})\,,\\
\left[\not{p}_3\gamma^\mu\gamma^\nu\gamma^\rho\gamma^\kappa\right]_{12}^{-}\left[\gamma_\nu\gamma_\rho\gamma_\kappa\right]_{34}^{-}\left[\gamma_\mu\right]_{56}^{-} &= 64\langle p_1p_3\rangle\langle p_3p_5\rangle\langle p_2p_4\rangle^*\langle p_3p_6\rangle^*\,,\\
-\mathrm{i}\epsilon^{\mu\nu\rho\sigma}\,p_{1,\sigma}\left[\gamma_\mu\right]_{12}^{+}\left[\gamma_\nu\right]_{34}^{-}\left[\gamma_\rho\right]_{56}^{-} &= -2\langle p_1p_2\rangle\langle p_3p_5\rangle\langle p_1p_4\rangle^*\langle p_1p_6\rangle^*\,. \qquad \text{(A.0.8)}
\end{aligned}$$

Finally, the relevant SMEs (3.2.12) read in the WvdW formalism

$$\begin{aligned}
\hat{\mathcal{M}}^{---} &= \langle p_1p_3\rangle\langle p_2p_3\rangle^*\langle p_1p_3\rangle\langle p_1p_4\rangle^*\langle p_1p_5\rangle\langle p_1p_6\rangle^*,\\
\hat{\mathcal{M}}^{+--} &= \langle p_1p_3\rangle^*\langle p_2p_3\rangle\langle p_1p_3\rangle\langle p_1p_4\rangle^*\langle p_1p_5\rangle\langle p_1p_6\rangle^*. \qquad \text{(A.0.9)}
\end{aligned}$$

Of course, it would have been possible to translate each spinor chain into WvdW spinor products directly after performing the loop integration, i.e. skipping the steps described in Section 3.2. However, it would have been hard to perform all the manipulations with WvdW objects made there in terms of Lorentz products. For instance, it is practically impossible to make full use of momentum conservation in very involved expressions in terms of WvdW spinor products. It turned out in many examples given in the literature that no algorithmic recipe has been found yet yielding the most compact expressions in complicated amplitudes. Moreover, the generalization to massive fermions is more complicated in the WvdW formalism than in the method described in Section 3.2. In fact a variant of this method has already been used in Ref. [63] for the process $\mathrm{e}^+\mathrm{e}^- \to \mathrm{t}\bar{\mathrm{t}}\mathrm{H}$.

Bibliography

[1] S. L. Glashow, Nucl. Phys. B **22** (1961) 579.

[2] S. Weinberg, Phys. Rev. Lett. **19** (1967) 1264.

[3] A. Salam, in Elementary Particle Theory, ed. N. Svartholm (Almqvist and Wiksell, Stockholm, 1968), p. 367.

[4] G. 't Hooft, Nucl. Phys. B **33** (1971) 173; B **35** (1971) 167.

[5] The LEP Collaborations ALEPH, DELPHI, L3, OPAL, the LEP EWWG, and the SLD Heavy Flavor and Electroweak Groups, hep-ex/0412015.

[6] J. A. Aguilar-Saavedra *et al.*, TESLA Technical Design Report Part III: Physics at an e^+e^- Linear Collider, hep-ph/0106315.

[7] T. Abe *et al.* [American Linear Collider Working Group Collaboration], in *Proc. of the APS/DPF/DPB Summer Study on the Future of Particle Physics (Snowmass 2001)* ed. R. Davidson and C. Quigg, SLAC-R-570, *Resource book for Snowmass 2001*, [hep-ex/0106055, hep-ex/0106056, hep-ex/0106057, hep-ex/0106058].

[8] K. Abe *et al.* [ACFA Linear Collider Working Group Collaboration], ACFA Linear Collider Working Group report, [hep-ph/0109166].

[9] K. Mönig and A. Tonazzo, talk given by K. Mönig at the *2nd ECFA/DESY Study on Physics and Detectors for a Linear Electron–Positron Collider*, Padova, Italy, 2000.

[10] W. Alles, C. Boyer and A. J. Buras, Nucl. Phys. B **119** (1977) 125;
K. J. F. Gaemers and G. J. Gounaris, Z. Phys. C **1** (1979) 259.

[11] M. Lemoine and M. J. G. Veltman, Nucl. Phys. B **164** (1980) 445;
R. Philippe, Phys. Rev. D **26** (1982) 1588;
J. Fleischer, F. Jegerlehner and M. Zrałek, Z. Phys. C **42** (1989) 409.

[12] M. Böhm *et al.*, Nucl. Phys. B **304** (1988) 463.

[13] W. Beenakker, K. Kołodziej and T. Sack, Phys. Lett. B **258** (1991) 469;
W. Beenakker, F. A. Berends and T. Sack, Nucl. Phys. B **367** (1991) 287;
H. Tanaka, T. Kaneko and Y. Shimizu, Comput. Phys. Commun. **64** (1991) 149;
K. Kołodziej and M. Zralek, Phys. Rev. D **43** (1991) 3619;
J. Fleischer, K. Kołodziej and F. Jegerlehner, Phys. Rev. D **47** (1993) 830.

[14] S. Dittmaier, M. Böhm and A. Denner, Nucl. Phys. B **376** (1992) 29 [Erratum-ibid. B **391** (1993) 483];
M. Kuroda, I. Kuss and D. Schildknecht, Phys. Lett. B **409** (1997) 405 [hep-ph/9705294].

[15] W. Beenakker *et al.*, Nucl. Phys. B **410** (1993) 245; Phys. Lett. B **317** (1993) 622;
M. Kuroda and D. Schildknecht, Nucl. Phys. B **531** (1998) 24 [hep-ph/9807250].

[16] D. Y. Bardin, S. Riemann and T. Riemann, Z. Phys. C **32** (1986) 121;
F. Jegerlehner, Z. Phys. C **32** (1986) 425 [Erratum-ibid. C **38** (1988) 519];
A. Denner and T. Sack, Z. Phys. C **46** (1990) 653.

[17] F. A. Berends, R. Pittau and R. Kleiss, Comput. Phys. Commun. **85** (1995) 437 [hep-ph/9409326];
M. Skrzypek, S. Jadach, W. Płaczek and Z. Wąs, Comput. Phys. Commun. **94** (1996) 216;
G. Passarino, Comput. Phys. Commun. **97** (1996) 261 [hep-ph/9602302];
E. Accomando and A. Ballestrero, Comput. Phys. Commun. **99** (1997) 270 [hep-ph/9607317];
J. Fujimoto *et al.*, Comput. Phys. Commun. **100** (1997) 128 [hep-ph/9605312];
D. Y. Bardin *et al.*, Comput. Phys. Commun. **104** (1997) 161 [hep-ph/9612409];
S. Jadach *et al.*, Comput. Phys. Commun. **119** (1999) 272 [hep-ph/9906277];
F. A. Berends, C. G. Papadopoulos and R. Pittau, Comput. Phys. Commun. **136** (2001) 148 [hep-ph/0011031];
E. Accomando, A. Ballestrero and E. Maina, Comput. Phys. Commun. **150** (2003) 166 [hep-ph/0204052].

[18] W. Beenakker *et al.*, in *Physics at LEP2*, eds. G. Altarelli, T. Sjöstrand and F. Zwirner (CERN 96-01, Geneva, 1996), Vol. 1, p. 79 [hep-ph/9602351].

[19] D. Y. Bardin *et al.*, in *Physics at LEP2*, eds. G. Altarelli, T. Sjöstrand and F. Zwirner (CERN 96-01, Geneva, 1996), Vol. 2, p. 3 [hep-ph/9709270].

[20] M. W. Grünewald *et al.*, in *Reports of the Working Groups on Precision Calculations for LEP2 Physics*, eds. S. Jadach, G. Passarino and R. Pittau (CERN 2000-009, Geneva, 2000), p. 1 [hep-ph/0005309].

[21] V. S. Fadin, V. A. Khoze and A. D. Martin, Phys. Lett. B **311** (1993) 311;
D. Y. Bardin, W. Beenakker and A. Denner, Phys. Lett. B **317** (1993) 213.

[22] W. Beenakker, F. A. Berends and A. P. Chapovsky, Nucl. Phys. B **548** (1999) 3 [hep-ph/9811481].

[23] S. Jadach *et al.*, Phys. Rev. D **61** (2000) 113010 [hep-ph/9907436]; Comput. Phys. Commun. **140** (2001) 432 [hep-ph/0103163]; Comput. Phys. Commun. **140** (2001) 475 [hep-ph/0104049];

[24] Phys. Rev. D **65** (2002) 093010 [hep-ph/0007012].

[25] A. Denner, S. Dittmaier, M. Roth and D. Wackeroth, Phys. Lett. B **475** (2000) 127 [hep-ph/9912261]; Eur. Phys. J. direct C **2** (2000) 4 [hep-ph/9912447];

[26] in *Proc. of the 5th International Symposium on Radiative Corrections (RADCOR 2000)*, ed. H. E. Haber, hep-ph/0101257; Comput. Phys. Commun. **153** (2003) 462 [hep-ph/0209330].

[27] A. Denner, S. Dittmaier, M. Roth and D. Wackeroth, Nucl. Phys. B **587** (2000) 67 [hep-ph/0006307].

[28] Y. Kurihara, M. Kuroda and D. Schildknecht, Phys. Lett. B **509** (2001) 87 [hep-ph/0104201].

[29] A. Denner, S. Dittmaier, M. Roth and D. Wackeroth, Nucl. Phys. B **560** (1999) 33 [hep-ph/9904472].

[30] S. Jadach *et al.*, Phys. Lett. B **523** (2001) 117 [hep-ph/0109072];
F. Cossutti, DELPHI note 2004-050 PHYS 944;

[31] R. Brunelière *et al.*, Phys. Lett. B **533** (2002) 75 [hep-ph/0201304].

[32] A. Vicini, Acta Phys. Polon. B **29** (1998) 2847.

[33] F. A. Berends and G. B. West, Phys. Rev. D **1** (1970) 122;
Y. Kurihara, D. Perret-Gallix and Y. Shimizu, Phys. Lett. B **349** (1995) 367 [hep-ph/9412215].

[34] E. N. Argyres *et al.*, Phys. Lett. B **358**, 339 (1995) [hep-ph/9507216].

[35] A. Aeppli, F. Cuypers and G. J. van Oldenborgh, Phys. Lett. B **314**, 413 (1993) [hep-ph/9303236].

[36] W. Beenakker *et al.*, Nucl. Phys. B **500** (1997) 255 [hep-ph/9612260].

[37] R. G. Stuart, Phys. Lett. B **262** (1991) 113.

[38] A. Aeppli, G. J. van Oldenborgh and D. Wyler, Nucl. Phys. B **428** (1994) 126 [hep-ph/9312212].

[39] U. Baur and D. Zeppenfeld, Phys. Rev. Lett. **75** (1995) 1002 [hep-ph/9503344].

[40] G. Passarino, Nucl. Phys. B **574** (2000) 451 [hep-ph/9911482];
E. Accomando, A. Ballestrero and E. Maina, Phys. Lett. B **479** (2000) 209 [hep-ph/9911489].

[41] W. Beenakker, F. A. Berends and A. P. Chapovsky, Nucl. Phys. B **573**, 503 (2000) [hep-ph/9909472];
W. Beenakker *et al.*, Nucl. Phys. B **667**, 359 (2003) [hep-ph/0303105].

[42] M. Beneke, A. P. Chapovsky, A. Signer and G. Zanderighi, Phys. Rev. Lett. **93** (2004) 011602 [hep-ph/0312331] and Nucl. Phys. B **686** (2004) 205 [hep-ph/0401002].

[43] F. Boudjema *et al.*, Nucl. Phys. Proc. Suppl. **135** (2004) 323 [hep-ph/0407079].

[44] A. Denner, S. Dittmaier, M. Roth and L. H. Wieders, Phys. Lett. B **612** (2005) 223 [hep-ph/0502063].

[45] A. Denner, S. Dittmaier, M. Roth and L. H. Wieders, arXiv:hep-ph/0505042.

[46] S. Dittmaier, Nucl. Phys. B **565** (2000) 69 [hep-ph/9904440];
M. Roth, PhD thesis, ETH Zürich No. 13363 (1999), hep-ph/0008033.

[47] W. F. L. Hollik, Fortschr. Phys. **38** (1990) 165.

[48] A. Denner, S. Dittmaier and G. Weiglein, Nucl. Phys. B **440** (1995) 95 [hep-ph/9410338].

[49] J. Küblbeck, M. Böhm and A. Denner, Comput. Phys. Commun. **60** (1990) 165;
H. Eck and J. Küblbeck, *Guide to FeynArts 1.0*, University of Würzburg, 1992.

[50] T. Hahn, Comput. Phys. Commun. **140** (2001) 418 [hep-ph/0012260].

[51] T. Hahn and M. Perez-Victoria, Comput. Phys. Commun. **118** (1999) 153 [hep-ph/9807565];
T. Hahn, Nucl. Phys. Proc. Suppl. **89** (2000) 231 [hep-ph/0005029].

[52] A. Denner, Fortsch. Phys. **41** (1993) 307.

[53] D. B. Melrose, Nuovo Cimento **XL A** (1965) 181.

[54] A. Denner and S. Dittmaier, Nucl. Phys. B **658** (2003) 175 [hep-ph/0212259].

[55] G. Passarino and M. Veltman, Nucl. Phys. B **160** (1979) 151.

[56] G. 't Hooft and M. Veltman, Nucl. Phys. B **153** (1979) 365.

[57] W. Beenakker and A. Denner, Nucl. Phys. B **338** (1990) 349.

[58] A. Denner, U. Nierste and R. Scharf, Nucl. Phys. B **367** (1991) 637.

[59] G. J. van Oldenborgh, Comput. Phys. Commun. **66** (1991) 1.

[60] A. Vicini, Phys. Lett. B **531** (2002) 83 [hep-ph/0104164].

[61] A. Sirlin, Nucl. Phys. B **192** (1981) 93.

[62] A. Denner, S. Dittmaier, M. Roth and M. M. Weber, Nucl. Phys. B **660** (2003) 289 [hep-ph/0302198].

[63] A. Denner, S. Dittmaier, M. Roth and M. M. Weber, Nucl. Phys. B **680** (2004) 85 [hep-ph/0309274].

[64] A. R. Bohm and Y. Sato, Phys. Rev. D **71** (2005) 085018 [hep-ph/0412106].

[65] R. E. Cutkosky, J. Math. Phys. **1** (1960) 429.

[66] M. J. G. Veltman, Physica **29** (1963) 186.

[67] K. I. Aoki *et al.*, Prog. Theor. Phys. **65** (1981) 1001; Prog. Theor. Phys. Suppl. **73** (1982) 1.

[68] R. G. Stuart, in Proceedings of the XXVth Rencontre de Moriond, Z^0 *physics*, ed. J. Trân Thanh Vân, (Editions Frontières, Gif-sur-Yvette, 1990), p. 41.

[69] A. Sirlin, Phys. Rev. Lett. **67** (1991) 2127; Phys. Lett. B **267** (1991) 240;
R. G. Stuart, Phys. Rev. Lett. **70** (1993) 3193;
P. Gambino and P. A. Grassi, Phys. Rev. D **62** (2000) 076002 [hep-ph/9907254];
P. A. Grassi, B. A. Kniehl and A. Sirlin, Phys. Rev. D **65** (2002) 085001 [hep-ph/0109228];
A. Freitas, W. Hollik, W. Walter and G. Weiglein, Nucl. Phys. B **632** (2002) 189 [Erratum-ibid. B **666** (2003) 305] [hep-ph/0202131].

[70] A. Denner and T. Hahn, Nucl. Phys. B **525** (1998) 27 [hep-ph/9711302];
A. Bredenstein, S. Dittmaier and M. Roth, MPP-2005-24, in preparation.

[71] S. Eidelman *et al.* [Particle Data Group Collaboration], Phys. Lett. B **592** (2004) 1.

[72] P. Azzi *et al.* [CDF and D0 Collaborations, and Tevatron Electroweak Working Group], hep-ex/0404010.

[73] F. Jegerlehner, DESY 01-029, LC-TH-2001-035, hep-ph/0105283.

[74] S. Dittmaier, Phys. Rev. D **59** (1999) 016007 [hep-ph/9805445].

[75] V. S. Fadin, V. A. Khoze, A. D. Martin and W. J. Stirling, Phys. Lett. B **363** (1995) 112 [hep-ph/9507422].

[76] D. Y. Bardin, W. Beenakker and A. Denner, Phys. Lett. B **317**, 213 (1993).

Acknowledgments

In this part I would like to thank all the persons who helped and supported me during my work on this thesis.

- I am very grateful to PD. Dr. Ansgar Denner who suggested the topic of my thesis and guided me during my work. It was a pleasure to work with him and without his major contributions and professional support this work would not have been possible.
- I am grateful to Prof. Daniel Wyler for his patronage.
- I am thankful to Dr. Stefan Dittmaier and Dr. Markus Roth for the effective collaboration and team play.
- I would like to thank all my colleagues at the Paul Scherrer Institut and at the Institute for Theoretical Physics for their support. Especially I am thankful to Dr. Andreas Kaiser and Christoph Meier for all the helpful discussions we had.

This work was supported by the Swiss National Science Foundation.